POLYKETIDE SECONDARY METABOLITES OF THE DOMINICAN SPONGE *PLAKORTIS ANGULOSPICULATUS*

by

JUSTIN M.J. PORTER

H.B.Sc. University of Toronto, 2000
B.Ed. OISE/University of Toronto, 2001

A THESIS SUBMITTED IN PARTIAL FULFILLMENT OF
THE REQUIREMENTS FOR THE DEGREE OF

MASTERS OF SCIENCE

in

THE FACULTY OF GRADUATE STUDIES

Department of Chemistry

We accept this thesis as conforming
to the required standard

THE UNIVERSITY OF BRITISH COLUMBIA
September 2004

Library Authorization

Justin Michael James Porter
Name of Author *(please print)*

21/09/2004
Date (dd/mm/yyyy)

Title of Thesis: Polyketide Secondary Metabolites of the Dominican Sponge *Plakortis angulospiculatus*

Degree: Master of Science Year: 2004

Department of Chemistry
The University of British Columbia
Vancouver, BC Canada

ABSTRACT

As part of a search for new antifungal agents, the polyketide cyclic peroxides, compounds **32** and **33,** were isolated from the Dominican sponge *Plakortis angulospiculatus*. Both compounds showed potent *in vitro* activity against *Candida albicans*. Chemical genetic profiling of the crude sponge extract and compound **33** indicated a non-specific mode of action against the yeast, *Saccharomyces cerevisiae.* Further exploration of the sponge extract yielded two furano polyketides, the newly discovered α,β-unsaturated ester, **37**, and the previously isolated compound, glánvillic acid B (**38**). The structures were elucidated by one- and two-dimensional spectroscopic analysis of **32**, **33**, **37**, and **38**.

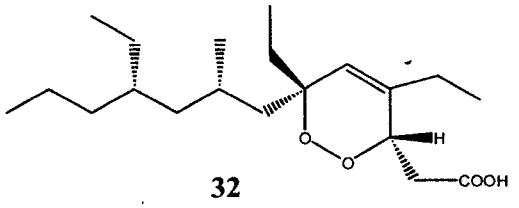

32

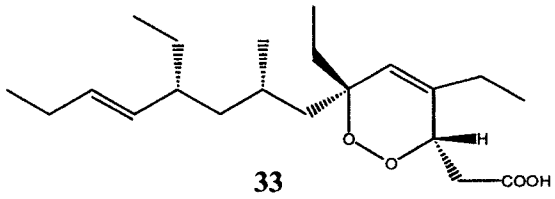

33

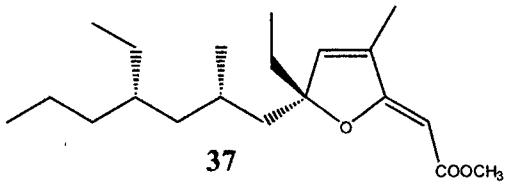

37

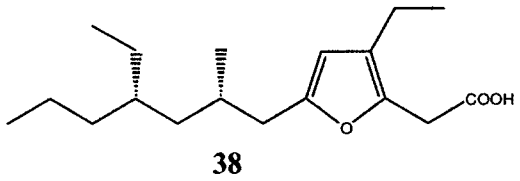

38

TABLE OF CONTENTS

		Page
Abstract		ii
Table of Contents		iii
List of Figures		v
List of Schemes		vii
List of Tables		vii
List of Abbreviations		viii
Dedication		ix
Acknowledgements		x
CHAPTER 1	**General Introduction**	
1.1	Natural Product Chemistry	1
1.2	Marine Invertebrates as a Source of Drugs	2
1.3	Chemical Genetics and Drug Discovery	6
1.4	Polyketide Biosynthesis: The *Plakortis* Polyketide	13
1.5	Current Study's Aim	23
CHAPTER 2	**Antifungal Cyclic Peroxide Polyketides from *Plakortis angulospiculatus***	
2.1	Introduction	25
2.2	Isolation	25
2.3	Structure Elucidation of 3,6-epidioxy-8-methyl-4,6,10-triethyltrideca-4-enoic acid (**32**)	26
2.4	Structure Elucidation of 3,6-epidioxy-8-methyl-4,6,10-triethyltetradeca-4,11-dienoic acid (**33**)	36
2.5	Proposed Stereochemistry and Biosynthesis of Structures **32** and **33**	45
2.6	Biological Activity	53
2.7	Conclusion	54

CHAPTER 3 Furano Polyketides from *Plakortis angulospiculatus*

3.1 Introduction..... 55

3.2 Isolation..... 55

3.3 Structure Elucidation of
methyl-6,10-diethyl-4,8-dimethyl-3,6-epoxytrideca-2,4-dienoate (**37**)..... 56

3.4 Structure Elucidation of Glánvillic Acid B (**38**)..... 69

3.5 Proposed Stereochemistry and Biosynthesis of Structures **37** and **38**..... 78

3.6 Conclusion..... 80

CHAPTER 4 General Conclusions

4.1 Comparison of the Polyketide Biosynthesis for Compounds **32, 33, 37,** and **38**.... 81

4.2 Chemical Genetic Profiling of Marine Invertebrate Extracts..... 84

EXPERIMENTAL SECTION

General Experimental Procedures..... 90

Animal Material..... 91

Extraction of *P.angulospiculatus* and Isolation of Compounds **32, 33, 37,** and **38**..... 92

Bibliography..... 93

LIST OF FIGURES

		Page
Figure 1.3.1	Classical versus Chemical Genetics	7
Figure 1.3.2	Reverse- versus Forward-Chemical Genetics	8
Figure 1.3.3	Drug-Induced Haploinsufficiency Assay	10
Figure 1.3.4	Chemical Genetic Profile of Twelve Inhibitory Compounds of *S. cerevisiae*	12
Figure 1.4.1	*Plakortis* Cyclic Peroxide Polyketides	16
Figure 1.4.2	*Plakortis* Furan Polyketides	20
Figure 1.4.3	*Plakortis* Lactone, Cyclic Ether, Spiculane-Type Polyketides	22
Figure 2.3.1	^{13}C Spectrum (100 MHz, $CDCl_3$) of **32**	28
Figure 2.3.2	^{1}H Spectrum (500MHz, $CDCl_3$) of **32**	29
Figure 2.3.3	HSQC Spectrum (400 MHz, $CDCl_3$) of **32**	30
Figure 2.3.4	COSY Spectrum (500 MHz, $CDCl_3$) of **32**	31
Figure 2.3.5	HMBC Spectrum (500 MHz, $CDCl_3$) of **32**	32
Figure 2.3.6	Methine HMBC Correlations for Compound **32**: Fragment A	33
Figure 2.3.7	Methyl HMBC Correlations for Compound **32**: Fragment A	34
Figure 2.3.8	Methyl HMBC Correlations for Compound **32**: Fragment B	35
Figure 2.4.1	^{13}C Spectrum (100 MHz, $CDCl_3$) of **33**	38
Figure 2.4.2	^{1}H Spectrum (500MHz, $CDCl_3$) of **33**	39
Figure 2.4.3	HSQC Spectrum (400 MHz, $CDCl_3$) of **33**	40
Figure 2.4.4	COSY Spectrum (500 MHz, $CDCl_3$) of **33**	41
Figure 2.4.5	HMBC Spectrum (500 MHz, $CDCl_3$) of **33**	42
Figure 2.4.6	Expanded HSQC Spectrum (400 MHz, $CDCl_3$) of **33**	44
Figure 2.4.7	Selected COSY and HMBC Correlations of **33**	45
Figure 2.5.1	Selected Coupling Constants for **32** and **33**	46
Figure 2.5.2	Selected NOE Correlations of **32**	47
Figure 2.5.3	Selected NOE Correlations of **33**	47
Figure 2.5.4	ROESY Expanded Spectrum (400 MHz, $CDCl_3$) of **32**	48
Figure 2.5.5	ROESY Expanded Spectrum (500 MHz, $CDCl_3$) of **33**	49
Figure 3.3.1	^{13}C Spectrum (100 MHz, $CDCl_3$) of **37**	58

Figure 3.3.2 ^{1}H Spectrum (500MHz, $CDCl_3$) of **37** 59
Figure 3.3.3 HSQC Spectrum (400 MHz, $CDCl_3$) of **37** 60
Figure 3.3.4 COSY Spectrum (500 MHz, $CDCl_3$) of **37** 61
Figure 3.3.5 HMBC Spectrum (500 MHz, $CDCl_3$) of **37** 62
Figure 3.3.6 Selected HMBC Correlations for Compound **37**: Fragment A 63
Figure 3.3.7 Selected HMBC Correlations for Compound **37**: Fragment A 64
Figure 3.3.8 Selective Gradient 1-D NOE (400 MHz, $CDCl_3$) of **37** 65
Figure 3.3.9 Resonance structures for Fragment A (**37**) 66
Figure 3.3.10 Methyl HMBC Correlations for Compound **37**: Fragment B 67
Figure 3.3.11 Selected HMBC and COSY Correlations for Compound **37**: Fragment B 68
Figure 3.3.12 Selected HMBC Correlations for Compound **37** 68
Figure 3.4.1 ^{13}C Spectrum (100 MHz, $CDCl_3$) of **32** 71
Figure 3.4.2 ^{1}H Spectrum (500MHz, $CDCl_3$) of **32** 72
Figure 3.4.3 HSQC Spectrum (400 MHz, $CDCl_3$) of **32** 73
Figure 3.4.4 COSY Spectrum (500 MHz, $CDCl_3$) of **32** 74
Figure 3.4.5 HMBC Spectrum (500 MHz, $CDCl_3$) of **32** 75
Figure 3.4.6 Selected HMBC Correlations for Compound **38**: Fragment A 76
Figure 3.4.7 Selected HMBC Correlations for Compound **38**: Fragment B 77
Figure 4.2.1 Haploid Deletion Mutant Fitness Test Profile 85
Figure 4.2.2 Scatterplot and Fitness Test Profile Expansion for Clotrimazole and Fluconazole 86
Figure 4.2.3 Scatterplot and Fitness Test Profile Expansion for Fluconazole and Camptothecin 87
Figure 4.2.4 Scatterplot and Fitness Test Profile Expansion for Extracts 00-132 and 00-192 89

LIST OF SCHEMES

		Page
Scheme 1.4.1	Chain Extension in Polyketide Biosynthesis	14
Scheme 1.4.2	Biosynthesis of Amphotericin B	15
Scheme 1.4.3	Biosynthesis of Triophamine: Butyrate Incorporation	18
Scheme 1.4.4	Proposed Biosynthesis for Monotriajaponide A: Cyclic Peroxide Precursor	19
Scheme 1.4.5	Proposed Formation of the Cyclic Peroxide Moiety	19
Scheme 1.4.6	Proposed Cyclic Peroxide to Furano Conversion	20
Scheme 1.4.7	Production of Glánvillic Acid A from a Hypothetical Precursor	21
Scheme 2.5.1	Proposed Biosynthesis of Compounds **32** and **33**	51
Scheme 2.5.2	Proposed Biosynthesis of the Cyclic Peroxide Moiety in Compounds **32** and **33**	52
Scheme 3.5.1	Proposed Biosynthesis of Compounds **37** and **38** from Cyclic Peroxides	79
Scheme 4.1.1	Polyketide Linear Chain Representations for **32, 33, 37,** and **38**	82
Scheme 4.1.2	Proposed Biosynthetic Schemes for Compounds **32, 33, 37,** and **38**	83

LIST OF TABLES

		Page
Table 2.3.1	^{13}C and ^{1}H NMR Data for **32**	27
Table 2.4.1	^{13}C and ^{1}H NMR Data for **33**	37
Table 2.4.2	^{13}C and ^{1}H NMR Chemical Shift Comparison for **33**	43
Table 2.6.1	Minimum Inhibitory Concentration of **32** and **33**	53
Table 3.3.1	^{13}C and ^{1}H NMR Data for **37**	57
Table 3.4.1	^{13}C and ^{1}H NMR Data for **38**	70
Table 4.2.1	Drugs in Fitness Test Profile	84
Table 4.2.2	Marine Invertebrate Extracts in Fitness Test Profile	86

LIST OF ABBREVIATIONS

AcN	acetonitrile, CH_3CN
amu	atomic mass unit
br s	broad singlet
$[\alpha]^{23}_D$	specific optical rotation at wavelength of sodium D line (23°C)
COSY	homonuclear correlation spectroscopy
d	doublet
dd	double doublet
δ	chemical shift (ppm)
DNA	deoxyribonucleic acid
EtOAc	ethyl acetate, $CH_3COOCH_2CH_3$
HEX	hexanes
HMBC	heteronuclear multiple bond correlation
HMQC	heteronuclear multiple quantum coherence
HPLC	high performance liquid chromatography
HRESIMS	high resolution electrospray ionization mass spectrometry
HSQC	heteronuclear single quantum coherence
m	multiplet
MeOH	methanol, CH_3OH
MTT	methylthiazolyldiphenyl tetrazolium bromide
NMR	nuclear magnetic resonance
NOE	nuclear Overhauser enhancement
ODS	octadecyl silyl
q	quartet
ROESY	rotating frame nuclear overhauser enhancement spectroscopy
PCR	polymerase chain reaction
R_f	retardation factor
s	singlet
S	solvent signal
SCUBA	self-contained underwater breathing apparatus
sp.	species (singular)
t	triplet
TLC	thin-layer chromatography
TFA	trifluoroacetic acid
UV	ultraviolet
w	water signal

DEDICATION

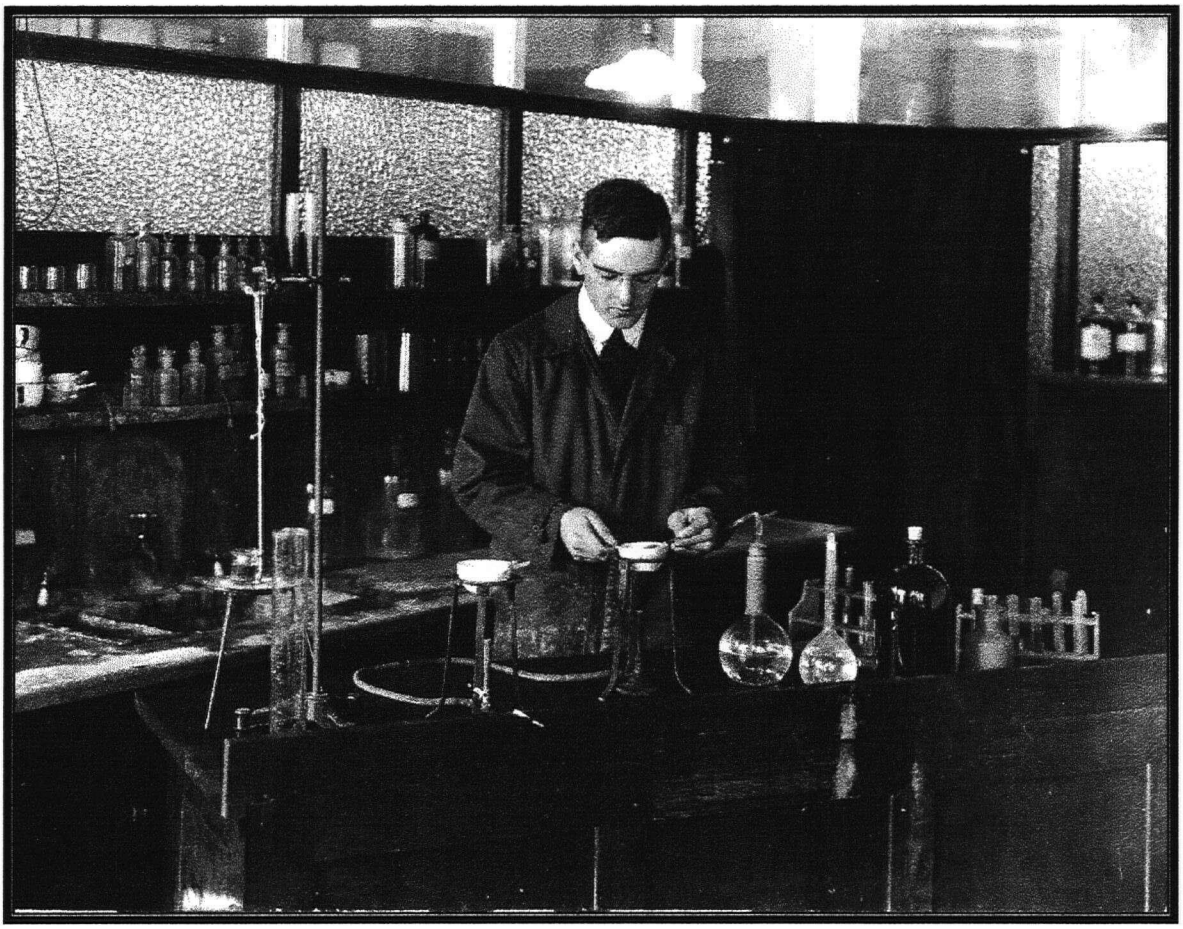

I must have gotten the chemistry bug from this fellow, my great-grandfather, William Alexander Brackley. He graduated from Central Technical School (Toronto) as a chemist. I understand he first worked for a paint and varnish company before going to the T. Eaton Company. He is shown above in the quality testing labs of the T. Eaton Co. during the late 1920s. I would like to dedicate this thesis to his son, my grandfather, William James Brackley (1932-2004) and to my grandmother Margaret Porter (1919-2003). Both were very influential people in my life.

ACKNOWLEDGEMENTS

I would like to acknowledge my supervisor, Dr. Raymond Andersen, for the opportunity to do this research. Also, I would like to thank him for his patience and many ideas from which I have learned a great deal. I would also like to acknowledge the following people: Helen Wright for the countless biological assays. Ainslie Parsons for her chemical genetic work out at the University of Toronto. Rob Van Soest for identifying the sponge at the core of this study. Mike LeBlanc for all the gear and stuff. Dave Williams for his invaluable insight into marine natural product chemistry. Xin-Hui Huang for his technical expertise and friendly nature. Dr. Burlinson and the NMR staff for helping to tame temperamental NMR machines. Starbucks coffee® for keeping me awake... too awake. Fellow grad students Alban, Kate, Kelsey and Roger for anytime dive buddies and for always being open to discussing new ideas. Also, Harry and Lu for their advice on a wide array of topics. Mom, Dad and, my lil'sis, Araby who have continued to support me throughout my degree and my life. And, of course, where would I be without Louise.

CHAPTER 1 General Introduction

1.1 Natural Product Chemistry

One of the primary goals of natural product chemistry is to isolate and characterize secondary metabolites. Secondary metabolites are small molecular weight compounds (<1500 amu) that are not essential for the development, growth, or reproduction of the producing organism. Indeed, biosynthetic pathways yielding secondary metabolites are specific to certain cell types. By comparison, primary metabolites (e.g. nucleic acids, amino acids, polysaccharides, etc.) are common to all cells and are essential for the existence of the organism. Although one might consider any chemical of biological origin a natural product, the term "natural product" usually implies a secondary metabolite.[1]

Three penchants spur on the discovery and isolation of a natural product:

1) The secondary metabolite is of novel origin or structure, possibly indicating a unique biogenesis leading to a previously undescribed carbon skeleton or functional group array.

2) The secondary metabolite plays an important role in the producing organism, such as protecting the organism against predation (i.e. the study of Chemical Ecology.)

3) The secondary metabolite displays *in vitro* biological activity (i.e. the source of lead compounds for drug discovery.)

The third penchant provides one of the strongest motivations to discover new molecules from nature. Roughly half of all papers published for new marine natural products contain biological activity data.[2] Furthermore, the majority of natural product chemists use a

"bioassay-guided fractionation" scheme, in conjunction with a purification regiment and spectroscopic data, to discover new, relatively complex chemical entities that, in some cases, become drugs in human therapeutics.

1.2 Marine Invertebrates as a Source of Drugs

Approximately half of the best selling drugs in clinical use are natural products or their synthetic derivatives.[3] Given the great chemical diversity of natural products and the likelihood that many natural products have evolved to target specific proteins, they remain a rich source of lead compounds for drug development.[4] One of the best known examples of a natural product turned drug is Taxol (**1**, paclitaxel), a tricyclic diterpene, originally isolated from the bark of the Pacific Yew tree, *Taxus brevifolia.*[5] By stabilizing microtubules during

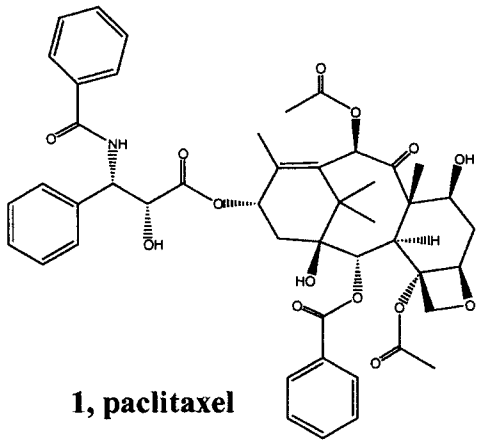

1, paclitaxel

cell division, paclitaxel has a mode of action against cancer cell lines that was previously unknown. Today, Taxol has become one of the best-selling drugs in the treatment of breast and ovarian cancers, reaching sales of 1.5 billion USD in 2000.[6] From this example we can see how a natural product not only has the potential to add to the scientific pool of knowledge, but how it may also bear great therapeutic and commercial rewards.

The marine environment, covering over 70% of the earth's surface and presenting a much larger volume of inhabitable space than terrestrial surfaces, provides a wealth of biodiversity. There are roughly 100,000 species of invertebrates in the world's oceans, with possibly more yet to be discovered. Representative invertebrate phyla including Bryozoa, Coelenterata, Porifera, and Echinodermata only exist in aquatic regions and have adapted their metabolism to survive the uniqueness of their saline environments. A great number of the organisms in these phyla lack any form of physical protection, such as shells or spines, but they do make use of biologically active secondary metabolites to defend against predation.[7] These are the chemicals that marine natural product chemists have sought after for the past three and a half decades. Such compounds isolated from organisms in areas of high biodiversity represent an ideal source of new secondary metabolites with diverse chemical structures and potent biological activity.

Many novel bioactive molecules have already been discovered from marine invertebrates, some of which are promising drug leads. One compound, the diterpene glycoside, eleutherobin (**2**), from the Australian soft-coral *Eleutherobia* sp., works by a similar mode of action as Taxol, in that it is microtubule stabilizing. Eleutherobin is 100 times more potent than Taxol against a number of different cancer cell lines *in vitro*.[8] Other exciting new natural products with strong potential as drug leads have been discovered from the extracts of marine invertebrates. Some examples include bryostatin 1 (**3**), a macrolide isolated from extracts of the bryozoan, *Bugula neritina*, now in phase II clinical trials[9], and discodermolide (**4**), an anticancer polyketide from Caribbean sponge *Discodermia dissoluta*.[10] These marine natural products, or one of their synthetic derivatives, may one day represent viable candidates for medicinal use.

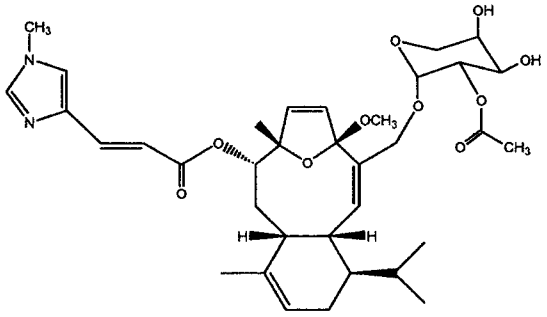

2, eleutherobin

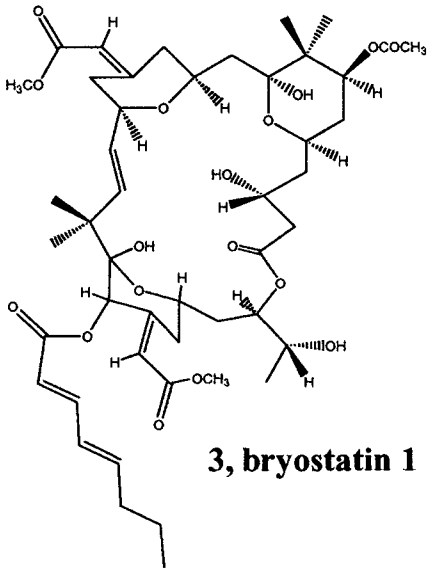

3, bryostatin 1

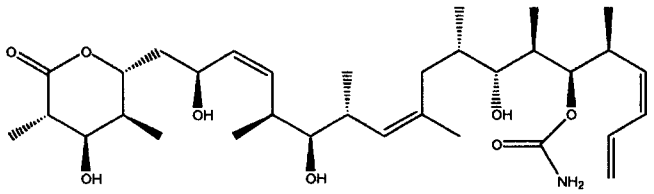

4, discodermolide

Although the majority of compounds isolated are directed towards finding anticancer agents, in part due to societal demand and funding concerns, there is a pressing need to find lead compounds for other therapeutics. With the rise in immunocompromised individuals (e.g. AIDS, cancer chemotherapy, transplant recipients, etc.) there exists a great necessity to add to the limited arsenal of current antifungal drugs. Over the past two decades there has been a 400% increase in the cases of systemic mycoses, echoed by a 10-fold increase in the frequency of candidiasis from the infection of *Candida albicans.*[11] The two major classes of antifungal drugs, polyenes (e.g. amphotericin B) and azoles (e.g. fluconazole), are problematic in that the polyenes can be toxic and the azoles aren't always very effective.[12]

Part of the difficulty in finding effective antifungal agents is that fungi are eukaryotic and possess a metabolism with similarities to mammals, thus limiting the number of viable cellular targets. Targets for antifungal agents are usually focused on the cell envelope and the fungal membrane sterol ergosterol and its biosynthesis.[13] The search for antifungal lead compounds must seek out agents which are selective to fungal targets and yet remain broad-spectrum in the treatment of different fungal pathogens.

Once again we see examples of marine natural products as potential lead compounds for drug discovery, specifically in the treatment of fungal infections. One antifungal compound is 15G256γ (**5**), a cyclic lipopeptide isolated from a mangrove-derived fungus, *Hypoxylon oceanicum.*[14] This compound appears to inhibit cell wall biosynthesis and is currently being evaluated in preclinical trials for its usefulness as an antifungal drug. Another compound, spongistatin 1 (**6**), purified from the Eastern Indian Ocean sponge *Spongia* sp. was originally isolated for its strong growth inhibition of a subset of the National Cancer Institute's (NCI) 60 human cancer cell lines.[15] Spongistatin 1, a macrocyclic lactone polyether, has also displayed broad-spectrum antifungal activitiy.[16] It is proposed that spongistatin 1 works by a similar mode of action against cancer cells and fungi, in that it is an antimicrotubule agent.[17] Although there are many other examples of other invertebrate-derived antifungal agents, **5** and **6** are interesting as the respective activity studies seem to indicate they act in specific ways against fungi. However, to become lead compounds for drug development, these compounds must also be selective in their cellular targeting, avoiding the toxic effects that would limit their therapeutic benefits for humans.

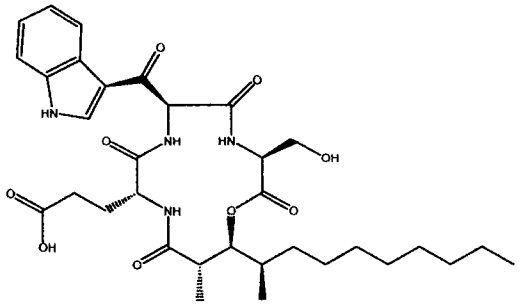

5, 15G256γ

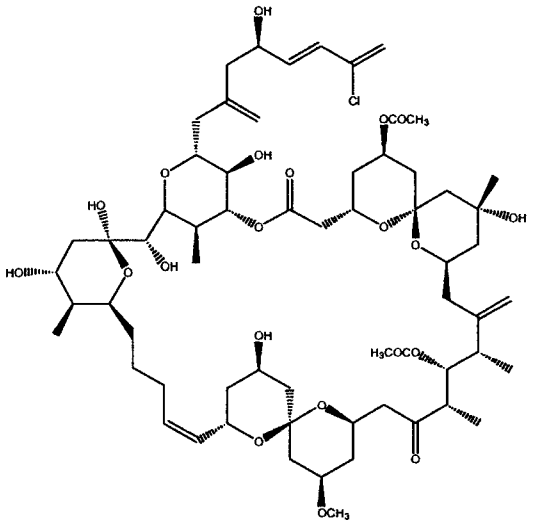

6, spongistatin 1

1.3 Chemical Genetics and Drug Discovery

Chemical genetics employs small molecules to probe the function of proteins, thereby allowing scientists to understand and govern the physiological and cellular function of such gene products. By binding to protein targets, small molecules either activate (e.g. nuclear hormone receptors are steroid hormone-activated transcription factors) or inactivate the proteins (e.g. colchicines inactivate tubulin) giving information about the function of the gene product.[18] This chemical genetic approach mimics classical genetics in which biochemists activate genes by mutations or inactivate genes (e.g. a deletion or "knock-out" mutant) to explore the function of a particular gene product[19] (**Figure 1.3.1**). Chemical genetics has the advantage over the classical genetic approach in that the small molecules act as conditional mutations, either inducing or suppressing the formation of a specific phenotype. Since the small molecules act quickly and reversibly, they act as provisional mutations that can be turned on and off, thus imparting the ability to study dynamic cellular

processes.[20] By linking the phenotype, caused by a small compound, to a specific target (or not), chemical genetics purports to be of invaluable utility in the drug discovery process.

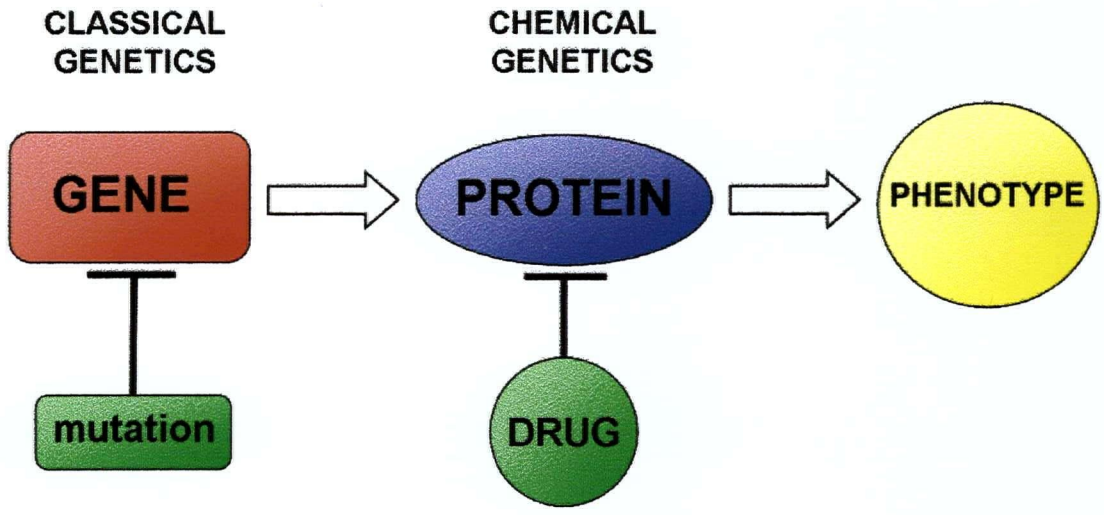

Figure 1.3.1 Classical versus Chemical Genetics

There are two different types of chemical genetic screens: forward and reverse (**Figure 1.3.2**). Reverse-chemical genetic screens test a large number of small molecules against a protein of interest until an appropriate bioactive ligand is found. The forward-chemical genetic approach takes place in three steps. In analogy to creating random genetic mutations, the first step of forward-chemical genetics involves treating the organism or cell type of interest with a varied collection of small molecules. In turn, the next step involves identifying the phenotype, or observable effect, within the collection of compound-treated cells and finally identifying the actual drug target in the screening organism.[21] Given that fewer than 5% of employable human proteins have been utilized as drug targets,[22] forward-chemical genetics is an advantageous means of finding new protein targets for drug discovery.

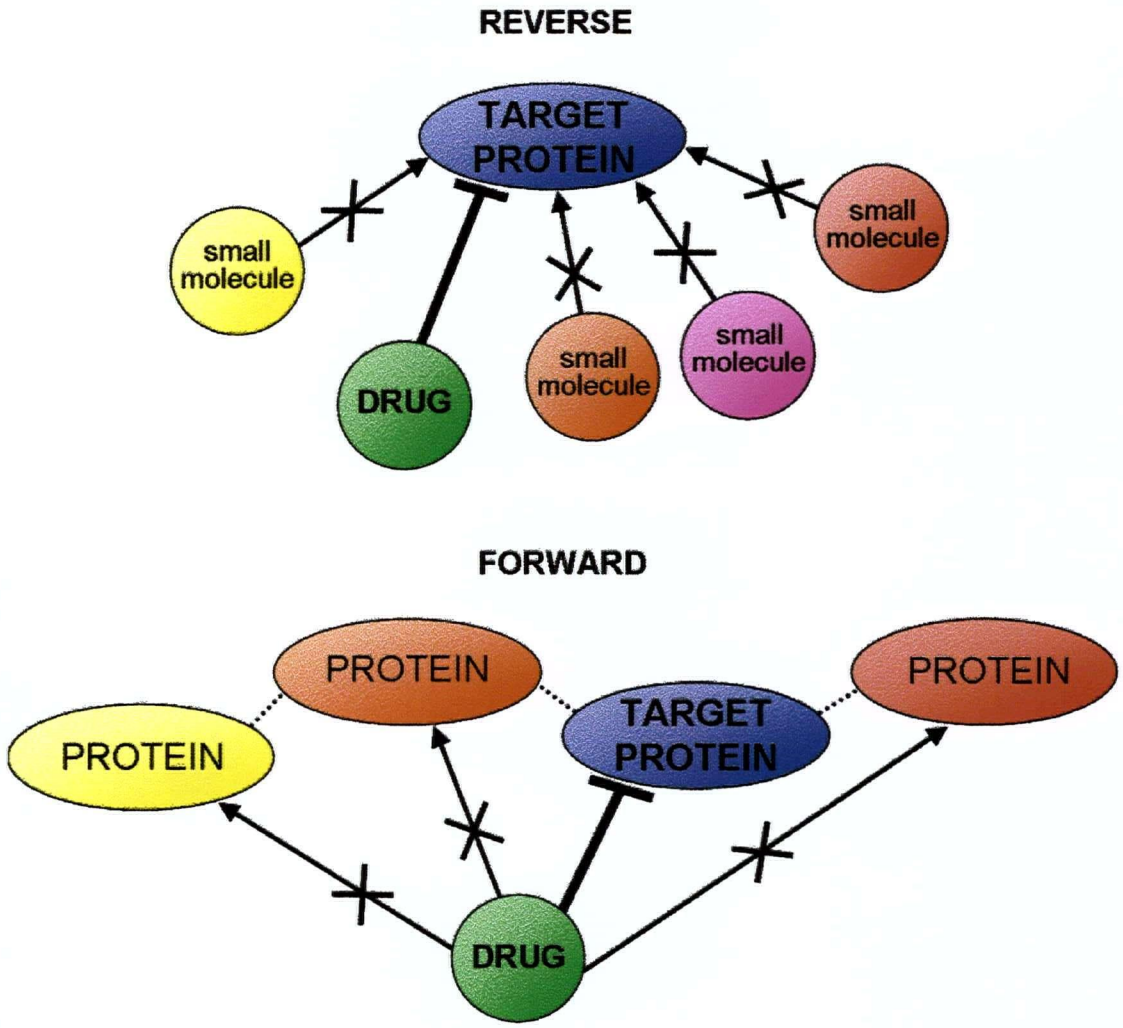

Figure 1.3.2 Reverse- versus Forward-Chemical Genetics

Sharing a high degree of gene conservation with the human genome, the yeast, *Saccharomyces cerevisiae*, is a model organism for drug discovery using chemical genetic screens. Amongst the ~6000 genes found from sequencing of the *S. cerevisiae* genome, there are several hundred gene products with similar sequences to proteins implicated in many human diseases.[23] In addition, a number of drugs used against human targets, such as lovastatin,[24] will specifically inhibit the related yeast protein. In the search for antifungal

drugs, researchers seek viable protein targets from genes conserved in *S. cerevisiae* and other fungi, but absent from humans. Inherent within the ~1100 essential genes of *S. cerevisiae* are ~350 genes that do not match sequences found in the human genome. A portion of these ~350 genes are thought to be highly conserved with other fungi and are important for immediate viability (i.e. inhibiting the gene product would prove fungicidal).[25] Hence, small molecules that would target the products of this subset of the ~350 genes would have the potential to be ideal antifungal compounds.

Recently, a yeast haploinsufficiency profiling assay has been gaining widespread acceptance as an invaluable tool to determine the exact cellular target of a molecular inhibitor. This phenotype-based assay lowers the amount of a gene encoding a drug target by transforming a wild-type diploid cell into a heterozygous diploid cell. This effectively leaves one copy of the gene encoding the cellular target (we began with two) often leaving the heterozygote mutant hypersensitive to a normally sublethal concentration of the drug – this is called "drug-induced haploinsufficiency" (**Figure 1.3.3**). Molecular barcodes, unique oglionucleotides surrounded by common PCR primers, are integrated at the site of each gene deletion allowing for detection and quantification of each strain. The abundance of each strain is quantified with respect to time and the heterozygotes showing hypersensitivity to the drug are detected by a DNA microarray analysis of the PCR-amplified barcode pool. By this methodology, haploinsufficiency profiling is advantageous as it may indicate the cellular target of the drug as sensitive strains drop out of the pool. Furthermore, many of the targets for drugs are the products of essential genes, such that, by assaying strains that retain one copy of a given gene, haploinsufficiency profiling can examine all ~6000 potential genes in the *S. cerevisiae* genome.[26]

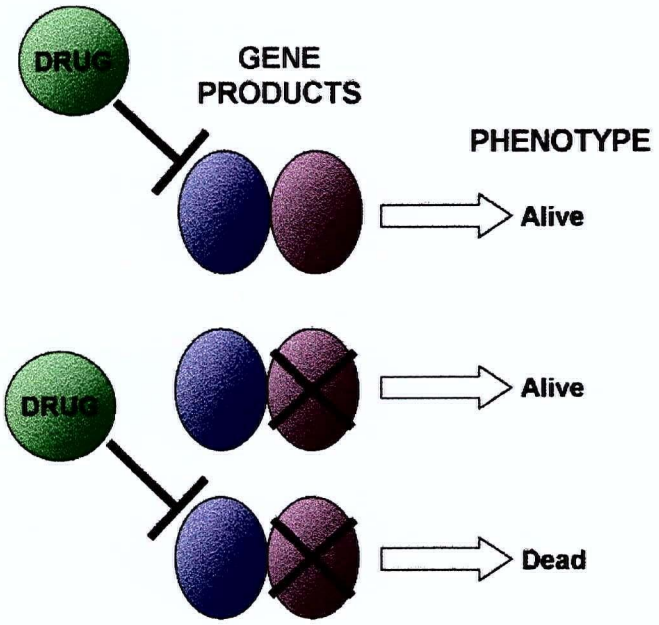

Figure 1.3.3 Drug-Induced Haploinsufficiency Assay

A complementary assay to haploinsufficiency profiling uses chemical genetic and genetic interaction data to connect bioactive compounds to cellular pathways. The main difference between the two assays is the gene copy number. Whereas the haploinsufficiency assay makes use of heterozygote deletion mutants, missing one of two copies of a particular gene, the other assay uses haploid deletion mutants that are missing the one and only copy of a particular gene. This chemical genetic, haploid deletion assay can only produce strains based upon the ~5000 non-essential genes of *S. cerevisiae*. Furthermore, this screen reveals information about the general pathways and cellular processes affected by the drug, instead of finding a specific target. To make sense of chemical genetic profiles generated from haploid deletion mutants, genetic interaction profiles are generated for the targets of known compounds by synthetic genetic array (SGA) analysis. Basically, if two genes are deleted and

cell death occurs, when neither deletion by itself is lethal to the organism, the cell death is referred to as a "synthetic lethal" interaction. These relationships can occur for genes within a single biochemical pathway or for genes acting in two distinct pathways. Similarly, when a drug inhibits a gene product, combined with the deletion of a different gene, a "synthetic lethal" interaction may occur. This allows for comparison between the chemical genetic profiles of compounds and genetic interaction data for the haploid deletions of *S. cerevisiae*.[27]

Inhibitory compounds with characterized targets are used to construct chemical genetic profiles to test if a set of haploid deletion mutants will not only show hypersensitivity to the drug, but also indicate the correct pathway in the chemical-genetic interaction. **Figure 1.3.4** shows the chemical-genetic profiles for twelve inhibitory compounds of *S. cerevisiae*: cyclosporine A, FK506, fluconazole, sulfometuron methyl, wortmannin, tunicamycin, caffeine, rapamycin, camptothecin, hydroxyurea, cycloheximide, and benomyl. The rows of the cluster plot display the individual profiles for each compound. Red bars within the rows indicate the sensitive genes, 647 different genes in total for all 12 compounds. Of interest, the compound benomyl (bottom row, **Figure 1.3.4**) is the only compound shown enriched for mitosis, chromosome structure, and cell structure. Benomyl showed chemical-genetic interactions with genes involved in the structure of tubulin (*TUB3*), the prefoldin actin/tubulin chaperone complex (*GIM3, GIM4, GIM5, PAC2, PAC10, PFD1, YKE2*), tubulin folding (*CIN1, CIN2, CIN4*), and the mitotic spindle checkpoint (*MAD1, MAD2, BUB3*). These interactions are consistent with the fact that benomyl is a microtubule depolymerizing agent. Two compounds with similar profiles are cyclosporin A and FK506 (top two rows, **Figure 1.3.4**). Their chemical genetic interaction profiles are enriched for

vacuolar structure and function as well as genes involved in cell wall organization. Indeed, both compounds are calcineurin inhibitors and calcineurin plays an established role in vacuolar function and cell wall homeostasis. Based upon these drug signatures it is possible to characterize the cellular targets for varying compounds. Most importantly, such chemical-genetic profiles give researchers an efficacious tool to find the target of new compounds, by comparing profiles or by directly characterizing the genes and pathways inhibited by the compound.[28]

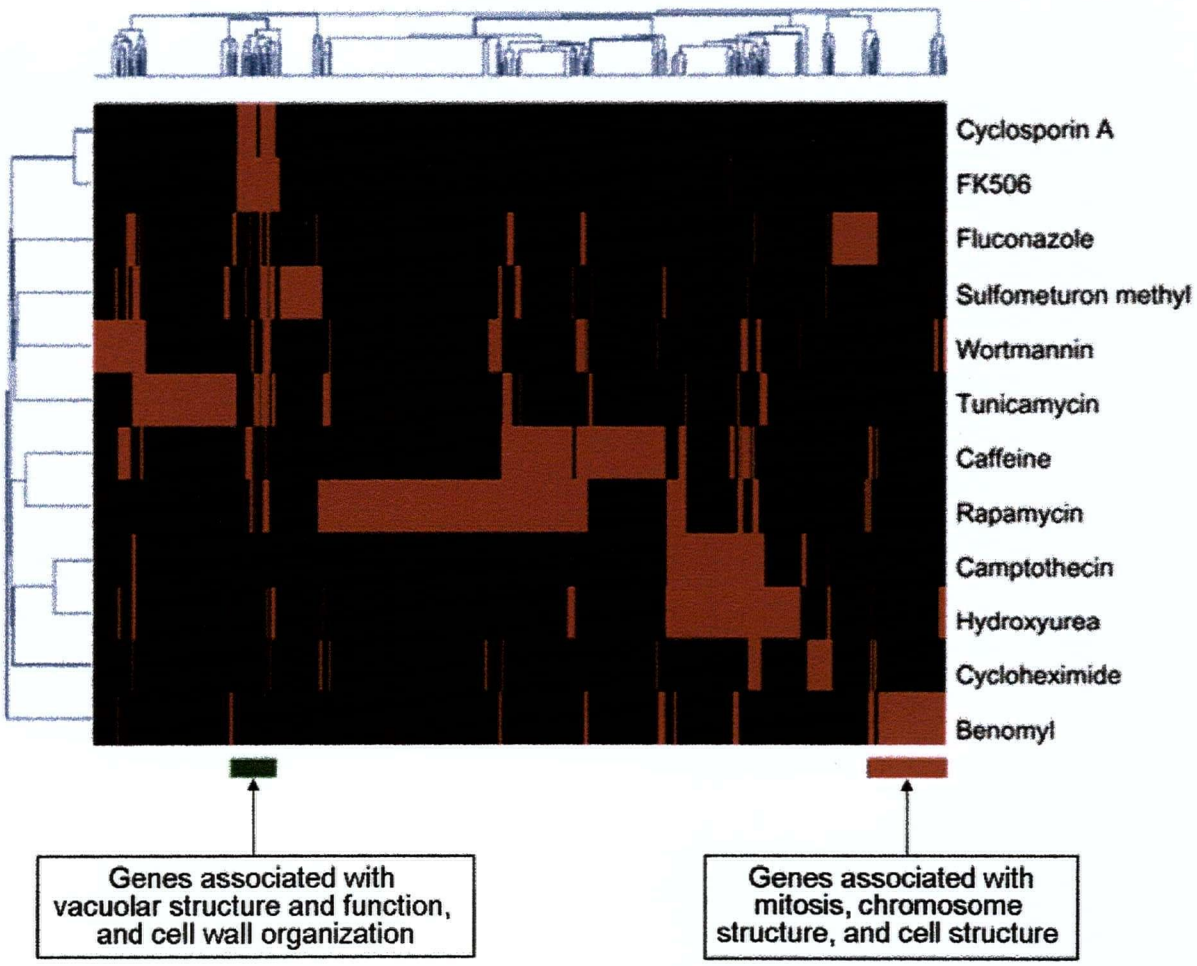

Figure 1.3.4 Chemical-Genetic Profile of Twelve Inhibitory Compounds of *S. cerevisiae*

Natural products make ideal small molecules to be used in such chemical genetic profiling. By prescreening crude extracts from marine based organisms in this manner, one is in effect screening hundreds of compounds not only for a desired phenotypic response, but for biological activity that acts in a specific way. This focuses the search for *lead compounds* in drug discovery.[29]

1.4 Polyketide Biosynthesis: The *Plakortis* Polyketide

Polyketides are a class of secondary metabolites with a wide range of functional, structural, and biological diversity. Biological activities found for this class include antibacterial, anticancer, antifungal, antiparasitic and immunosuppressive, making for a medicinally important group of compounds. The main building block of a polyketide is acetate in the form of acetyl Coenzyme A. A collection of enzymes known as the Polyketide Synthases (PKS) act in an assembly-line fashion (**Scheme 1.4.1**) to construct polyketide chains of varying length in a manner similar to fatty acid biosyntheis. First, a starter unit, usually acetyl CoA, is loaded onto the keto synthase (KS) by acyltransferase (AT). Malonyl CoA, formed from the carboxylation of acetyl CoA, is loaded onto an acyl carrier protein (ACP), again by acyltransferase (AT), where it undergoes a carbon-carbon bond forming Claisen ester condensation with the acyl residue bound to the KS. This results in an elongated chain in the form of a β–keto ester bound to the ACP. The chain extension is followed by several steps including reduction by keto reductase (KR), dehydration by dehydratase (DH), and reduction by enoyl reductase (ER). The cycle then repeats after transfer of the chain from the ACP to the KS. Finally the polyketide chain is transferred to a thioesterase (TE) and is cleaved off the enzyme as a free acid or an acyl ester. Post-PKS modifications, including the

formation of rings and the addition of various functional groups, produces polyketides with the diverse set of structures found in nature.[30]

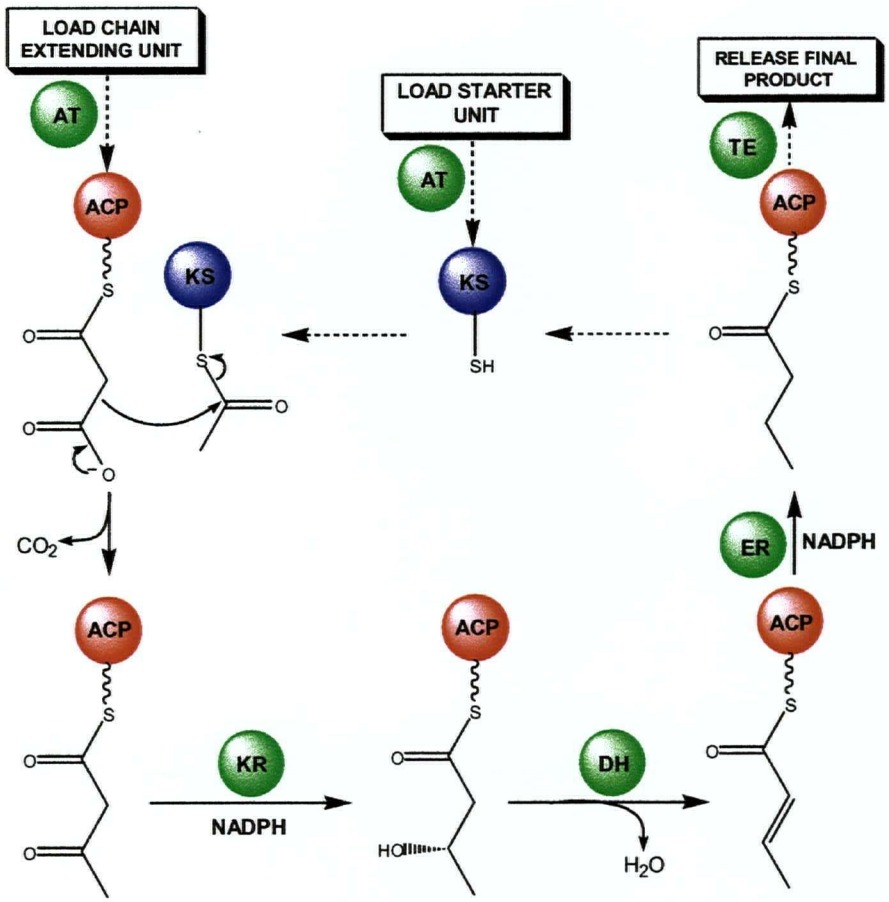

Scheme 1.4.1 Chain Extension in Polyketide Biosynthesis

Originally isolated in 1955, the polyketide amphotericin B (**8**) is today the most commonly used antifungal drug in human therapeutics. An isolate of the soil bacterium *Streptomyces nodosus*, from the bed of the Orinoco river in South America, produced amphotericin B (**8**). Elucidation of its full structure in the 1970s by X-ray crystallography hinted at its polyketide origin. In 1997 the polyketide biogenesis of amphotericin B was supported by a Double Quantum Filtered (DQF)-HSQC experiment. Labeled precursors

sodium [$^{13}C_2$]acetate, sodium [1-^{13}C]proprionate and sodium [3-^{13}C]proprionate were fed to *S. nodosus* . Sixteen acetates and three propionate units were incorporated into amphotericin B (**8**) (**Scheme 1.4.2**) by the PKS at the expected positions. The chain was released from the enzyme complex to give the polyene intermediate **7**. Further oxidations and glycosylations result in the final product of amphotericin B (**8**).[31] Of note in the biosynthesis of amphotericin B is the inclusion of propionate units, leading to methyl branches in the gross structure. As will be seen momentarily, the polyketide building blocks include, not only acetate and propionate residues, but also butyrate.

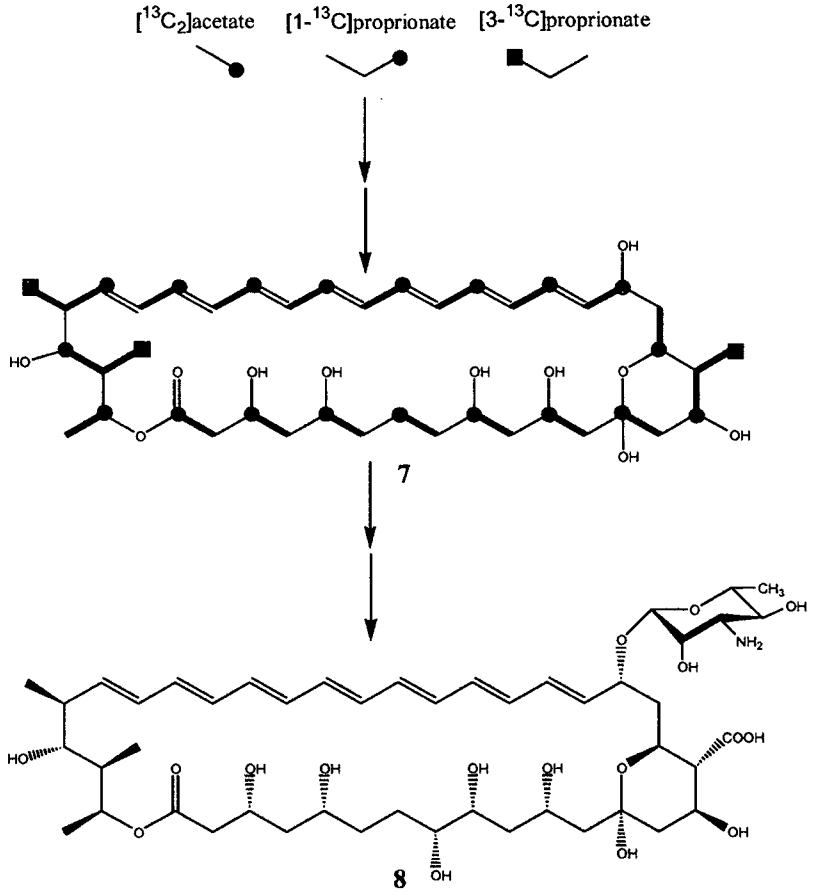

Scheme 1.4.2 Biosynthesis of Amphotericin B

Sponges of the family Plakinidae, specifically within the genus *Plakortis*, produce many novel polyketides with potent biological activities. Representative polyketide structural classes include cyclic peroxides, furans, lactones, cyclic ethers, and spiculane-type compounds. Many of these compounds are biosynthetically related and, at first glance, there appears to be a great deal of similarities between the polyketide synthases that make them. However, one must use caution in using these compounds as chemotaxonomic markers. Structures previously isolated from *Plakortis* sponges have been found in sponges of different genera. Time may tell whether or not the original producer of these polyketides is a sponge or a bacterial symbiont, an occurrence that does not go without precedence.

Cyclic peroxide polyketides are the most prevalent structures isolated from *Plakortis* sponges. A few representative polyketides are shown in **Figure 1.4.1**. Plakortide M (**9**)[32] and haterumadioxin A (**10**),[33] isolated from *Plakortis halichondrioides* and *Plakortis lita*, respectively, represent two of the most common types of cyclic peroxide polyketides.

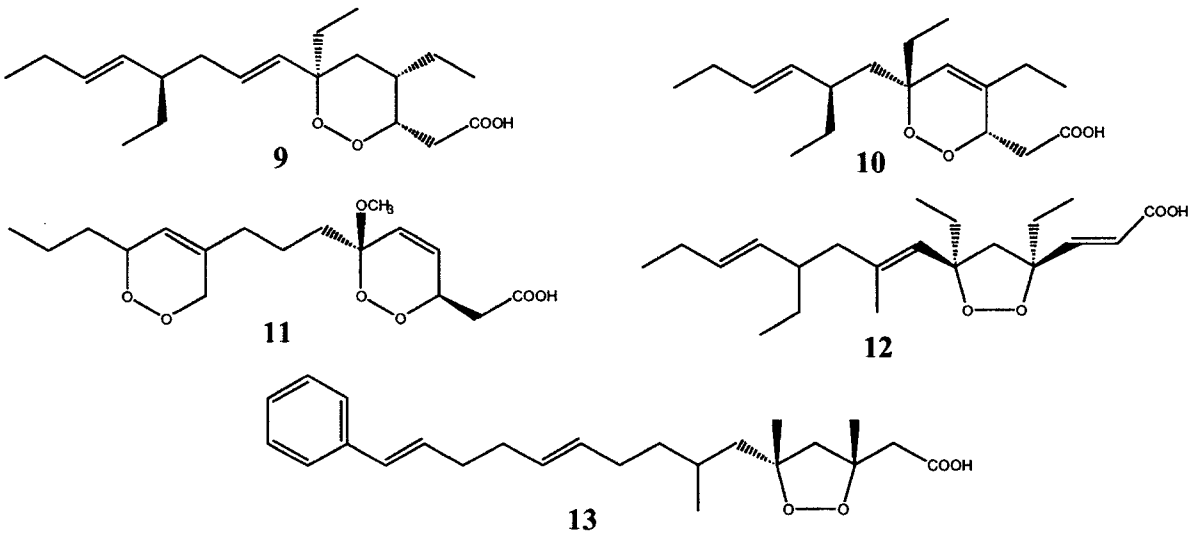

Figure 1.4.1 *Plakortis* Cyclic Peroxide Polyketides

Both compounds were shown to possess potent cytotoxic activity against numerous cancer cell lines, with the authors of the plakortide M paper noting that this compound did not appear to be selective against the different cell lines. Structurally, **9** and **10** are typical of *Plakortis* polyketides with either a saturated or unsaturated six-membered peroxide ring and ethyl group substitutions on the ring and chain. Usually methyl or ethyl esters are serendipitously discovered with the free acid as artifacts of the extraction process. In terms of structure activity relationships, the esters appear to show weaker levels of biological activity than do the free acids. Compound **11** from the sponge *Plakortis simplex*, contains two 1,2-dioxene rings and its methyl ester had an IC_{50} of <0.1μg/ml against P388 murine leukemia cells (the authors of this paper speculated that the unstable free acid would have had a lower IC_{50} had it been available for testing).[34] Two five-membered cyclic peroxides plakinic acid D (**12**)[35] and plakortide E (**13**)[36] are both from *Plakortis* sp.. Plakinic acid D was cytotoxic against certain cancer cell lines, while no activity data was listed for plakortide E. The structures do bear similarities to the six-membered cyclic peroxides, however, one striking difference is the phenyl acetate starter unit of **13**.

Biosynthetic studies of *Triopha catalinae* were the first to show *de novo* polyketide biosynthesis in a dorid nudibranch and the first demonstration of biosynthesis involving butyrate units in a marine invertebrate. Skin extracts of *T. catalinae* produced triophamine (**14**), a symmetrical diacylguanidine. The existence of ethyl branches in triophamine hinted at the possibility of butyrate incorporation in a processive polyketide biosynthetic scheme. A biosynthetic feeding experiment of *T. catalinae* used [2,3-$^{13}C_2$]butyrate and [2,3-$^{13}C_2$]ethyl malonate (**Scheme 1.4.3**). It was found that butyrate was incorporated via the commonly

accepted intermediate 2-ethylmalonate. This study was important as it showed that butyrate units are used to form ethyl branches in the polyketide biosynthesis of marine invertebrates.[37]

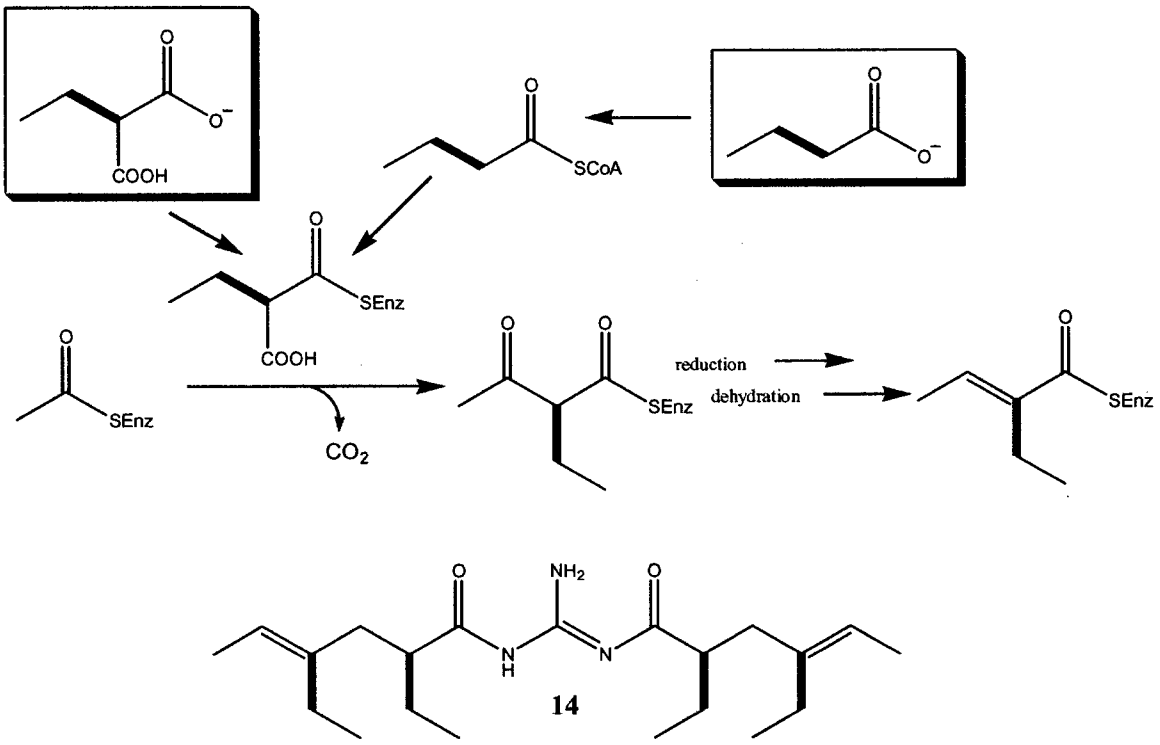

Scheme 1.4.3 Biosynthesis of Triophamine: Butyrate Incorporation

Although feeding experiments, involving labeled precursors, have not been performed on sponges to demonstrate polyketide biosynthesis, one can envision a biosynthetic proposal for the cyclic peroxide polyketides from sponges. For example, Monotriajaponide A (**15**) was discovered from the sponge, *Monotria japonica*, along with other *Plakortis*-type cyclic peroxides.[38] Monotriajaponide A (**15**), although from a sponge of a different genus, could be the precursor to a compound such as haterumadioxin A (**10**). **Scheme 1.4.4** shows the possible polyketide biogenesis that would lead to **15**.

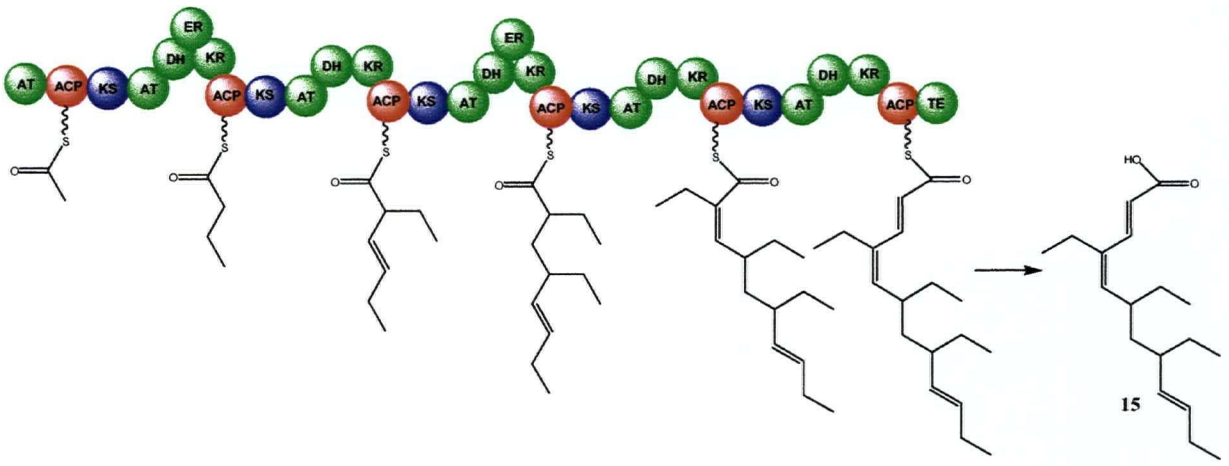

Scheme 1.4.4 Proposed Biosynthesis for Monotriajaponide A: Cyclic Peroxide Precursor

Monotriajaponide A (**15**) could then be converted to a radical by abstraction of a hydrogen by triplet oxygen as shown in **Scheme 1.4.5**. This would form a resonance stabilized radical intermediate. An enzymatic intramolecular Michael type addition would form the six-membered peroxide similar to the mechanism described for norterpene cyclic peroxides,[39] thus yielding haterumadioxin A (**10**).

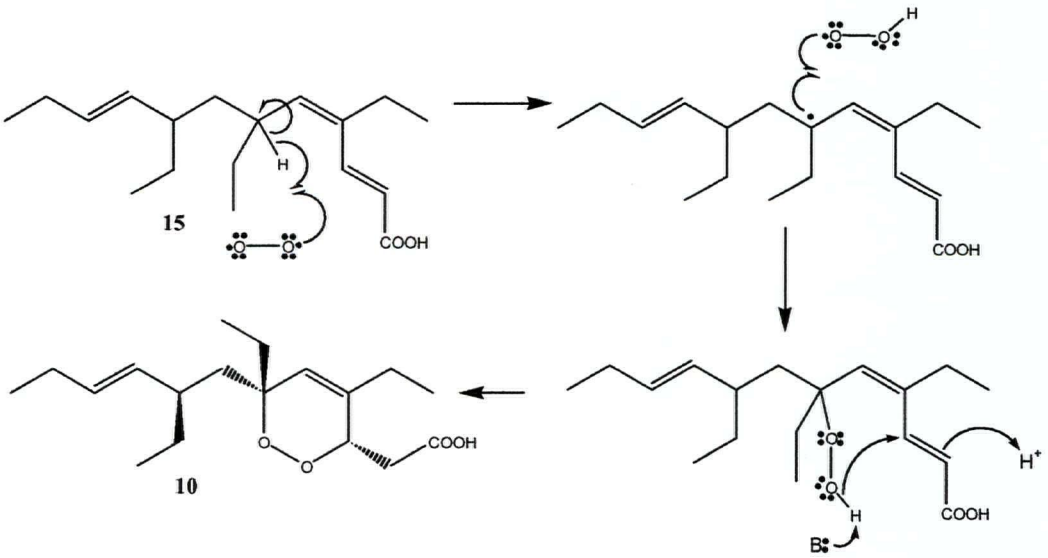

Scheme 1.4.5 Proposed Formation of the Cyclic Peroxide Moiety

A smaller, but related class of compounds are the furano polyketides from *Plakortis* sponges (**Figure 1.4.2**). These compounds are most likely biosynthetically derived from the cyclic peroxides. Two representative examples are glánvillic acid A (**16**)[40] and the methyl ester (**17**).[41] Both were isolated from *Plakortis halichondrioides* and no *in vitro* biological activity was reported for either compound.

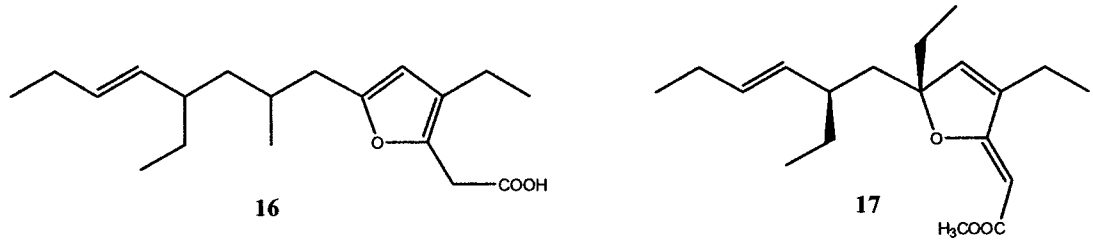

Figure 1.4.2 *Plakortis* Furan Polyketides

As just mentioned, it is believed that furano-type polyketides are derived from the cyclic peroxides (**Scheme 1.4.6**). Abstraction of an α-proton from the cyclic peroxide **18** opens the ring and forms an epoxide intermediate. Intramolecular attack on the epoxide would form the furano type ring system shown for **19**. Loss of H_2O would produce the final conjugated structure of the furano polyketide, **20**.[42]

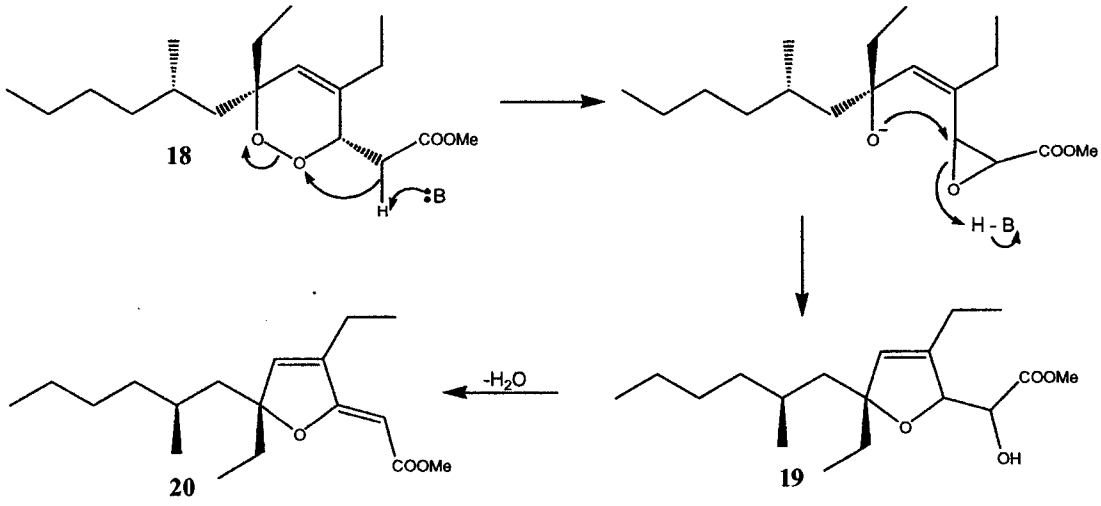

Scheme 1.4.6 Proposed Cyclic Peroxide to Furano Conversion

Furthermore, the *true* furans, the glánvillic acids are thought to be created via a proton-initiated reaction (**Scheme 1.4.7**). However, to this point in time, there have been no reports in the literature of such a precursor as **21**. In most cases, analogs of the hypothetical precursor **21** would be a methyl ester and have ethyl or methyl substitution at carbon six, instead of an abstractable proton.

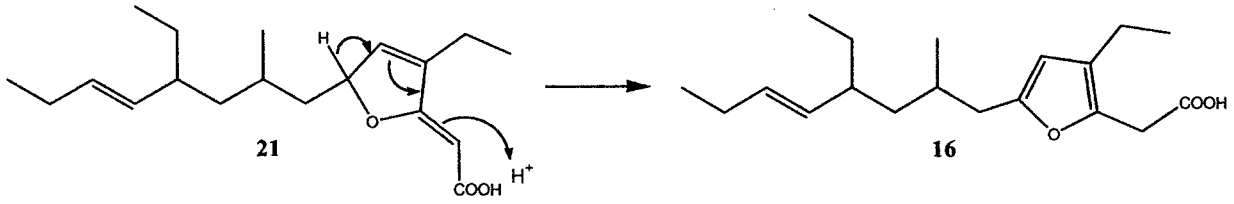

Scheme 1.4.7 Production of Glánvillic Acid A from a Hypothetical Precursor

In brief, other polyketides from Plakortis sponges include lactones, cyclic ethers and spiculane-type structures (**Figure 1.4.3**). Plakortone D (**22**) was discovered from the Carribean sponge, *Plakortis halichondrioides*. Compound **22** was shown to be an activator of cardiac SR-Ca^{2+}-pumping ATPase.[43] The lactone (**23**),[41] γ-lactone (**24**), δ-lactone (**25**)[44] were also discovered from *Plakortis halichondrioides*. The 1,2-dioxane peroxylactone, plakortolide H (**26**), was isolated from *Plakortis simplex*.[45] Only one article reports finding cyclic ethers, as shown by plakortethers C, E, F (**27**,**28**,**29**) from *Plakortis simplex*. These compounds are, once again, derived from cyclic peroxides and plakortether E (**28**) exhibits selective cytotoxicity against the RAW 264-7 cell line (murine macrophage).[46] A specimen of *Plakortis lita* yielded homo-plakotenin (**30**) which was found to reduce the proliferation of rheumatoid synovial fibroblasts.[47] Spiculoic Acid A (**31**) was discovered from a sample of the Caribbean sponge *Plakortis angulospiculatus*. Its central ring system is proposed to be

formed by a Diels Alderase catalyzed intramolecular [4+2] cycloaddition reaction.

Furthermore, **31** displayed *in vitro* cytotoxicity against human breast cancer MCF-7 cells.[48]

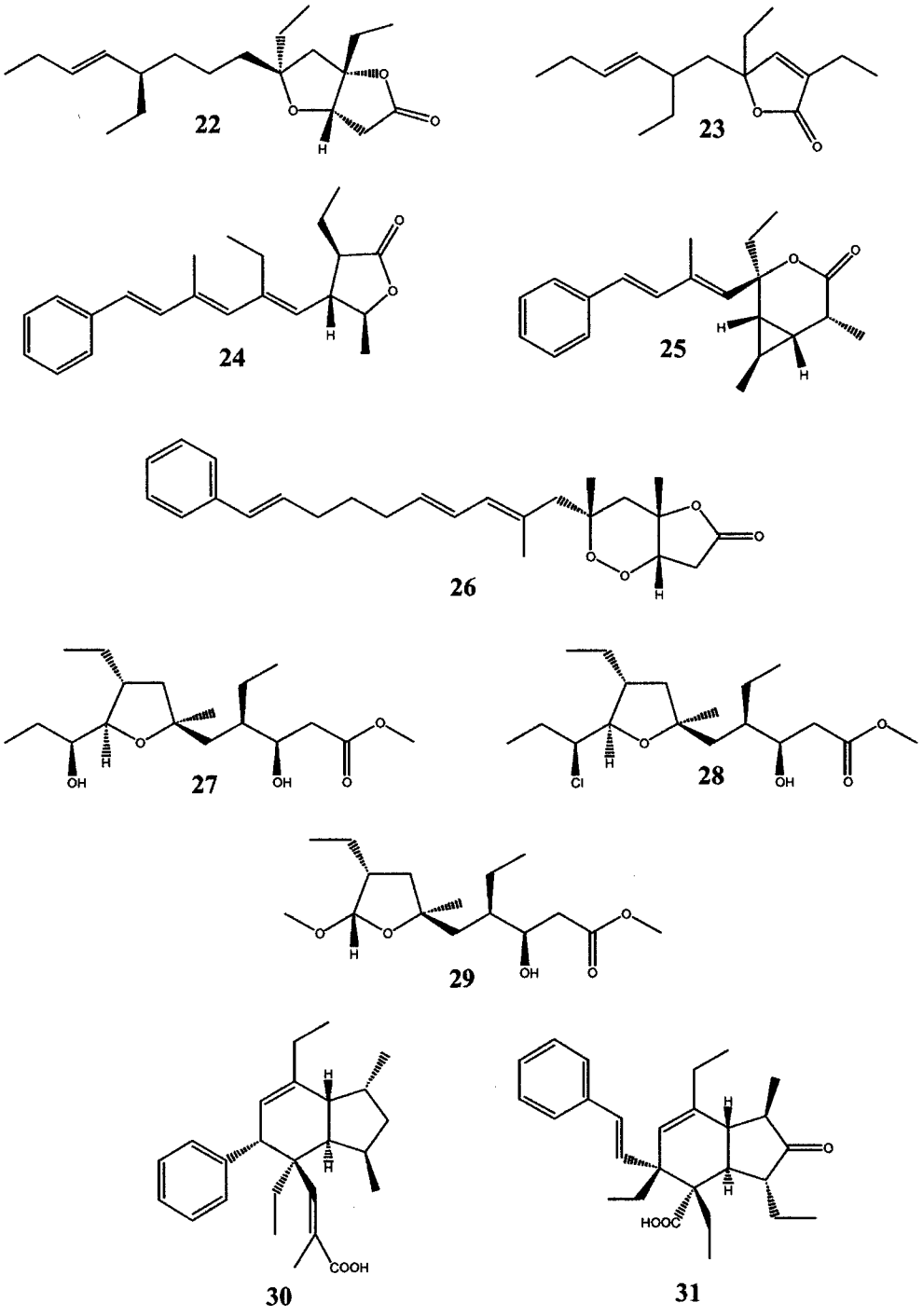

Figure 1.4.3 *Plakortis* Lactone, Cyclic Ether, Spiculane-Type Polyketides

As can be seen from the preceding examples, sponges of the genus *Plakortis* have evolved to produce a varied selection of polyketide structures. Possibly *Plakortis* sponges make these compounds as chemical defenses to discourage predation in the wild. As a result, *Plakortis* polyketides not only display a wealth of structural diversity, but, also, demonstrate a wide-range of potent *in vitro* bioactivity that has prompted many scientists to study them.

1.5 Current Study's Aim

The main goal of this study was to isolate novel antifungal agents. To accomplish this, a total of 64 marine invertebrate and 24 bacterial extracts were screened against *Candida albicans* for antifungal activity. The extract with the most potent antifungal activity, a Dominican sponge (collection number 00-303) was chosen as an isolation project.

In collaboration with Dr. Charlie Boone, a sample of the crude extract (00-303) was sent to his lab in the Banting and Best Department of Medical Research, University of Toronto. Our intent was to send other fractions throughout the purification process for Dr. Boone's lab to test against their *S. cerevisiae* haploid and heterozygote deletion mutant arrays. It was hoped that by using this chemical genetic screen the biological target of the active metabolite would be revealed. In addition, by sending samples of increasing purity throughout the isolation, we wished to assess the viability of screening crude extracts by the *S. cerevisiae* deletion mutant arrays. Such screens would allow our group to focus future research on discovering antifungal agents that target specific proteins of interest. The results of this study are discussed in the following chapters.

CHAPTER 2 Antifungal Cyclic Peroxide Polyketides from *Plakortis angulospiculatus*

2.1 Introduction

The most prolific class of biologically active compounds from *Plakortis sp.* is the cyclic peroxides. Herein, the isolation and structural elucidation is described for two cyclic peroxides, **32** and **33**. Compound **32** has not been previously isolated, however, the related cyclic peroxide **33**, differing by one degree of unsaturation and an extra carbon in the chain, was previously reported. The absolute configuration of both compounds is suggested as it has been deduced via spectroscopic data and a survey of the literature. Both compounds were pursued for their potent activity against the yeast, *Candida albicans*.

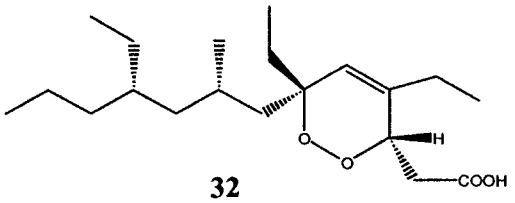

32

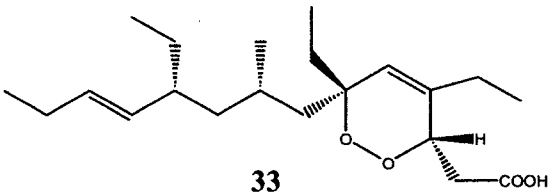

33

2.2 Isolation

A portion of the collected *Plakortis angulospiculatus* (50 g, wet weight) was immersed in and extracted twice with MeOH. The methanol extract was concentrated and reduced to dryness *in vacuo*, leaving a brown gum (1.76 g) that was partitioned between EtOAc (5 x 100 mL) and H_2O (200 mL.) The EtOAc layer was dried over $MgSO_4$, filtered, and reduced to dryness *in vacuo* (yellow-brown oil, 366 mg). Alamar Blue® assays against *Candida albicans* placed the activity in the organic layer residue (6.3 μg/mL) and no activity at 100μg/mL in the aqueous layer residue. Bioautographic assay of the organic layer residue

displayed a zone of inhibition corresponding to an R_f of 0.21 (10 μg, 1:1 EtOAc/HEX). Consequently, the EtOAc residue was chromatographed on Sephadex LH-20® (4:1 MeOH/CH_2Cl_2). Active fractions displaying the characteristic R_f were pooled (yellow oil, 156 mg, 3.3 μg/mL against *C.albicans*) and further separated by normal phase silica gradient flash column chromatography (7:93 EtOAC/CH_2Cl_2 → EtOAc). Final purification of the pooled active fractions (31 mg) by reversed-phase HPLC (3:2 AcN/H_2O, 0.1% TFA) yielded two pure compounds **32** (6 mg) and **33** (6 mg) as clear oils.

2.3 Structure Elucidation of 3,6-epidioxy-8-methyl-4,6,10-triethyltrideca-4-enoic acid (32)

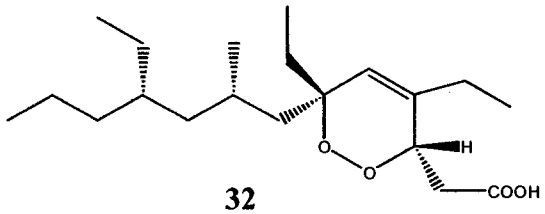

32

Compound **32** was isolated as an optically active, clear oil, that gave a positive mode HRESIMS $[M+Na]^+$ peak at m/z 363.2505 appropriate for a molecular formula of $C_{20}H_{36}O_4$ (calc'd 363.2511 for $C_{20}H_{36}O_4Na$). Accordingly, **32** had three degrees of unsaturation. The ^{13}C NMR (**Figure 2.3.1**), ^1H NMR (**Figure 2.3.2**), and HSQC (**Figure 2.3.3**) spectra revealed five methyl carbons, eight methylene carbons, three methine carbons (δ_C 26.0, 36.1, 76.2), one quarternary carbon (δ_C 83.8), two olefinic carbons (δ_C 125.3, 137.5) and one carbonyl carbon (δ_C 175.2). Two fragments, a peroxide ring and a carbon chain, were constructed and connected based upon COSY (**Figure 2.3.4**) and HMBC (**Figure 2.3.5**) spectra to provide the gross structure of **32**. A detailed summary of the 1- and 2-D NMR spectroscopic data is listed in **Table 2.3.1**.

Table 2.3.1 ^{13}C and ^{1}H NMR Data for **32**

C#	^{13}C δ, ppm[a]	^{1}H δ, ppm (Int., m, J(Hz))[b]	COSY	HMBC
1	175.2			H2, H2', H3
2	36.9	2.93 (1, dd, 16.2, 9.6)	H2', H3	H3
2'		2.61 (1, dd, 16.3, 2.8)	H2, H3	
3	76.2	4.57 (1, br d, 8.3)	H2, H2', H5	H2, H2', H5, H14
4	137.5			H2, H3, H5, H7, H14, H15
5	125.3	5.49 (1, br, s)	H3, H14	H3, H7, H14, H16, H16'
6	83.8			H5, H7, H8, H16, H16', H17
7	42.9	1.40 (2, m)	H8	H5, H8, H9', H16, H16', H18
8	26.0	1.52 (1, m)	H7, H9', H18	H7, H18
9	43.3	1.08 (1, m)	H8, H9', H10	H7, H18
9'		1.00 (1, m)	H8, H9	
10	36.1	1.23 (1, m)	H9	H8, H9, H9', H20
11	35.4	1.15 (2, m)		H9, H9', H13
12	19.5	1.23 (2, m)	H13	H10, H11, H13
13	14.6	0.86 (3, t, 7.3)	H12	H11, H12
14	24.9	2.01 (2, m)	H5, H15	H5, H15
15	11.6	1.07 (3, t, 7.4)	H14	H14
16	31.0	1.75 (1, dq, 14.1, 7.5)	H16', H17	H7, H17
16'		1.63 (1, dq, 14.1, 7.4)	H16, H17	
17	8.2	0.88 (3, t, 7.5)	H16, H16'	H16, H16'
18	22.4	0.87 (3, d, 6.7)	H8	H7, H8, H9
19	26.4	1.23 (2, m)	H20	H9, H9', H10, H11, H20
20	10.8	0.81 (3, t, 7.0)	H19	H19

[a]Recorded at 100 MHz, calibrated to the $CDCl_3$ ^{13}C δ of 77.0 ppm
[b]Recorded at 500 MHz, calibrated to the $CDCl_3$ ^{1}H δ of 7.24 ppm

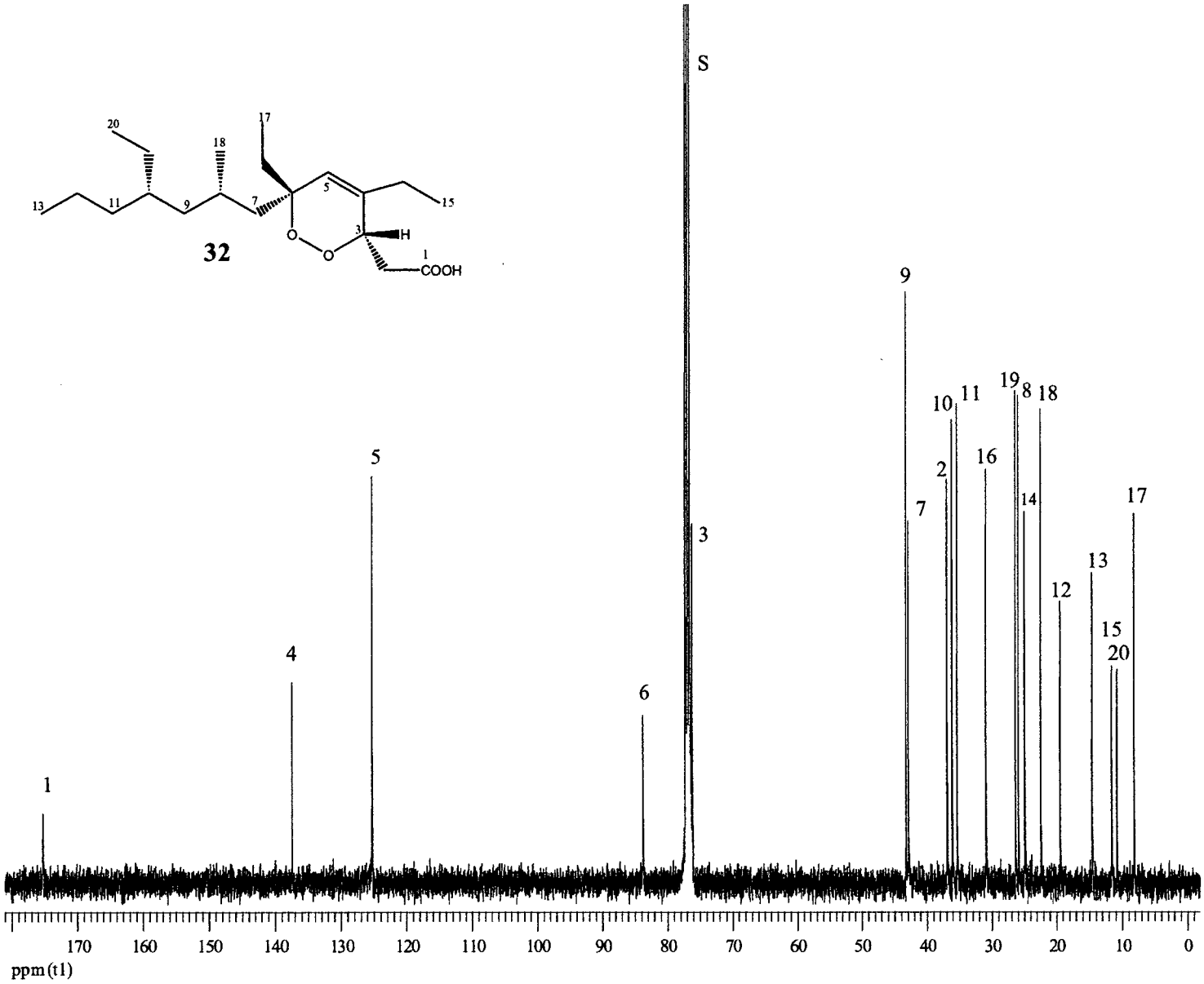

Figure 2.3.1 ^{13}C Spectrum (100 MHz, $CDCl_3$) of **32**

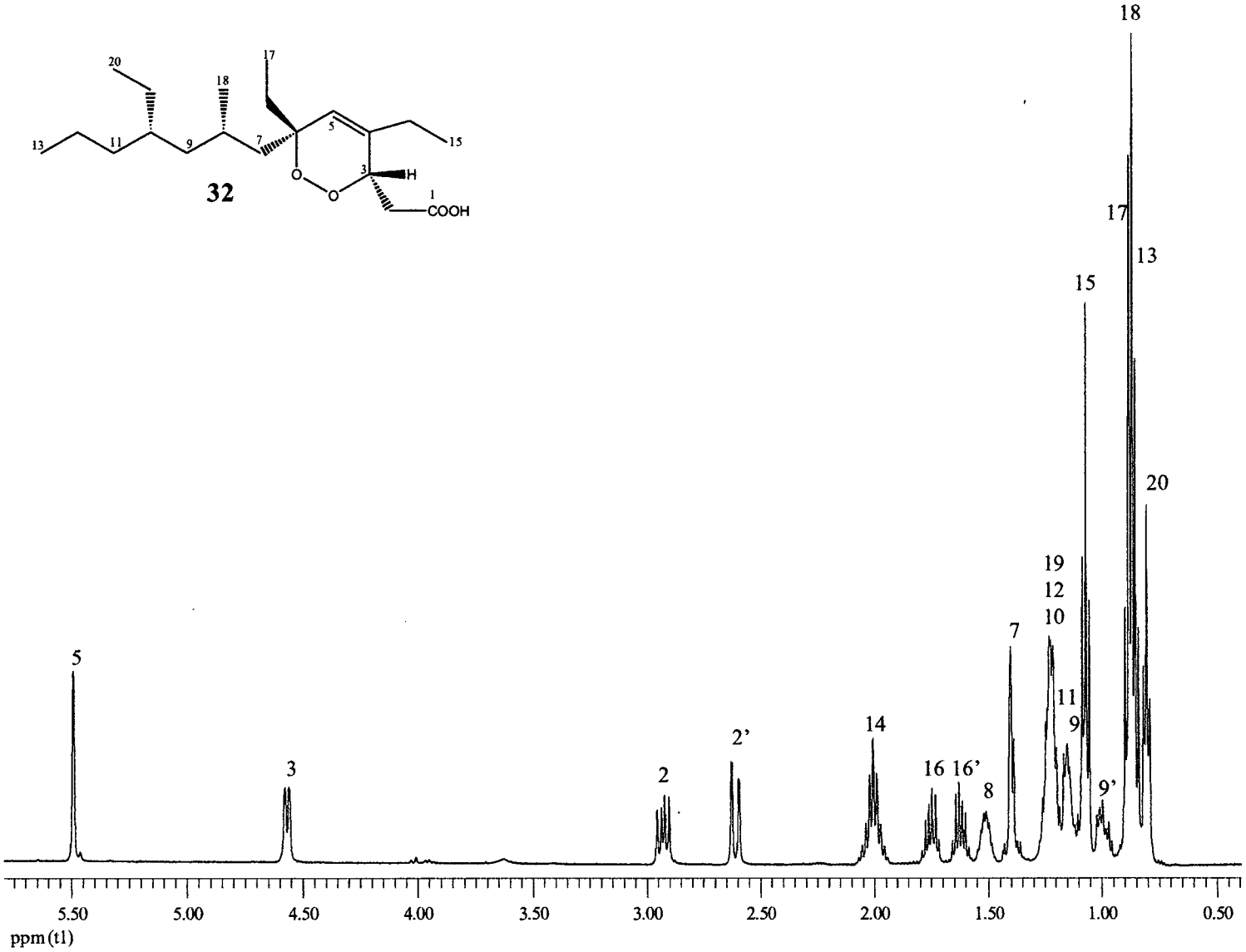

Figure 2.3.2 ^{1}H Spectrum (500 MHz, $CDCl_3$) of **32**

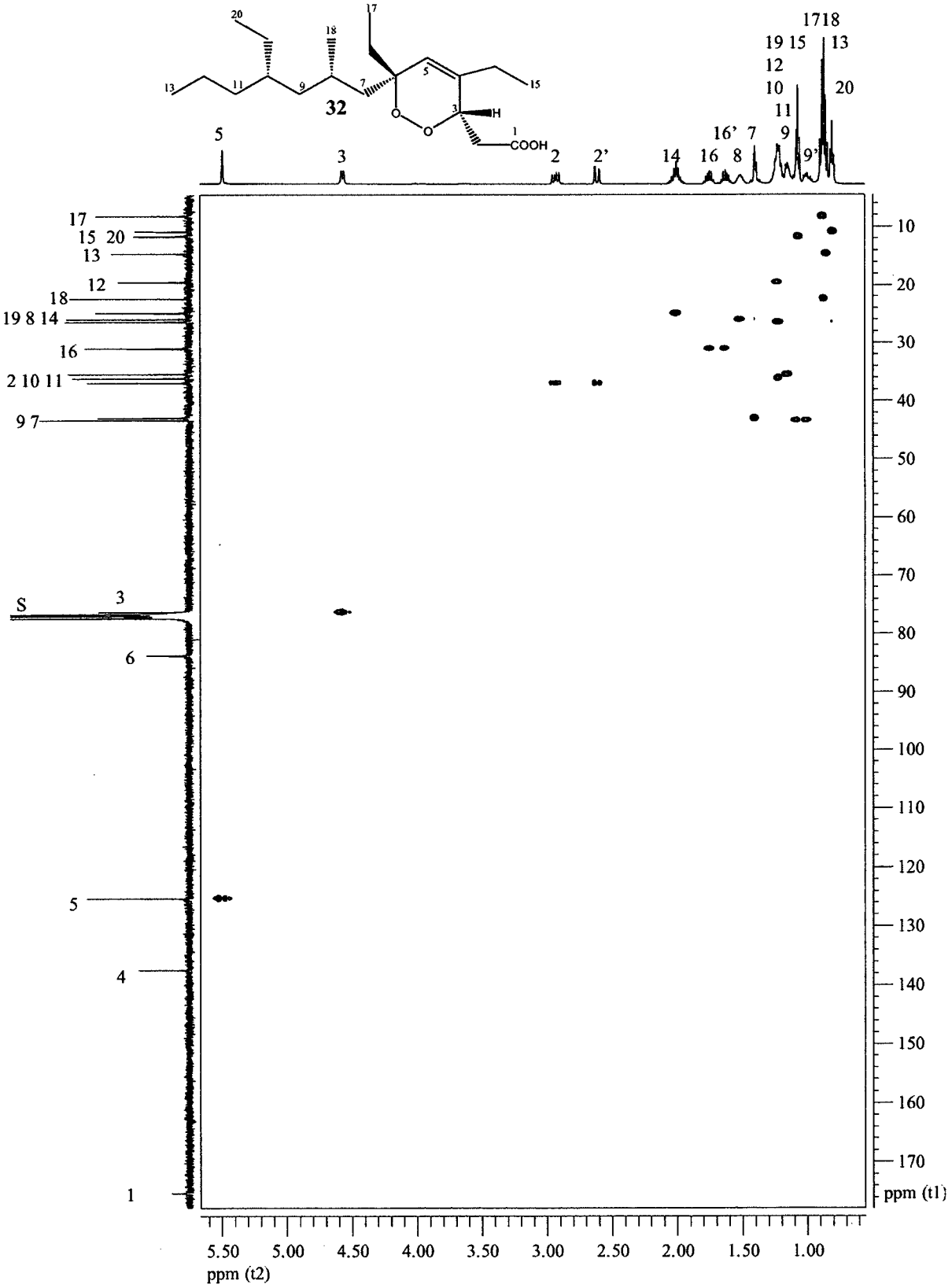

Figure 2.3.3 HSQC Spectrum (400 MHz, $CDCl_3$) of **32**

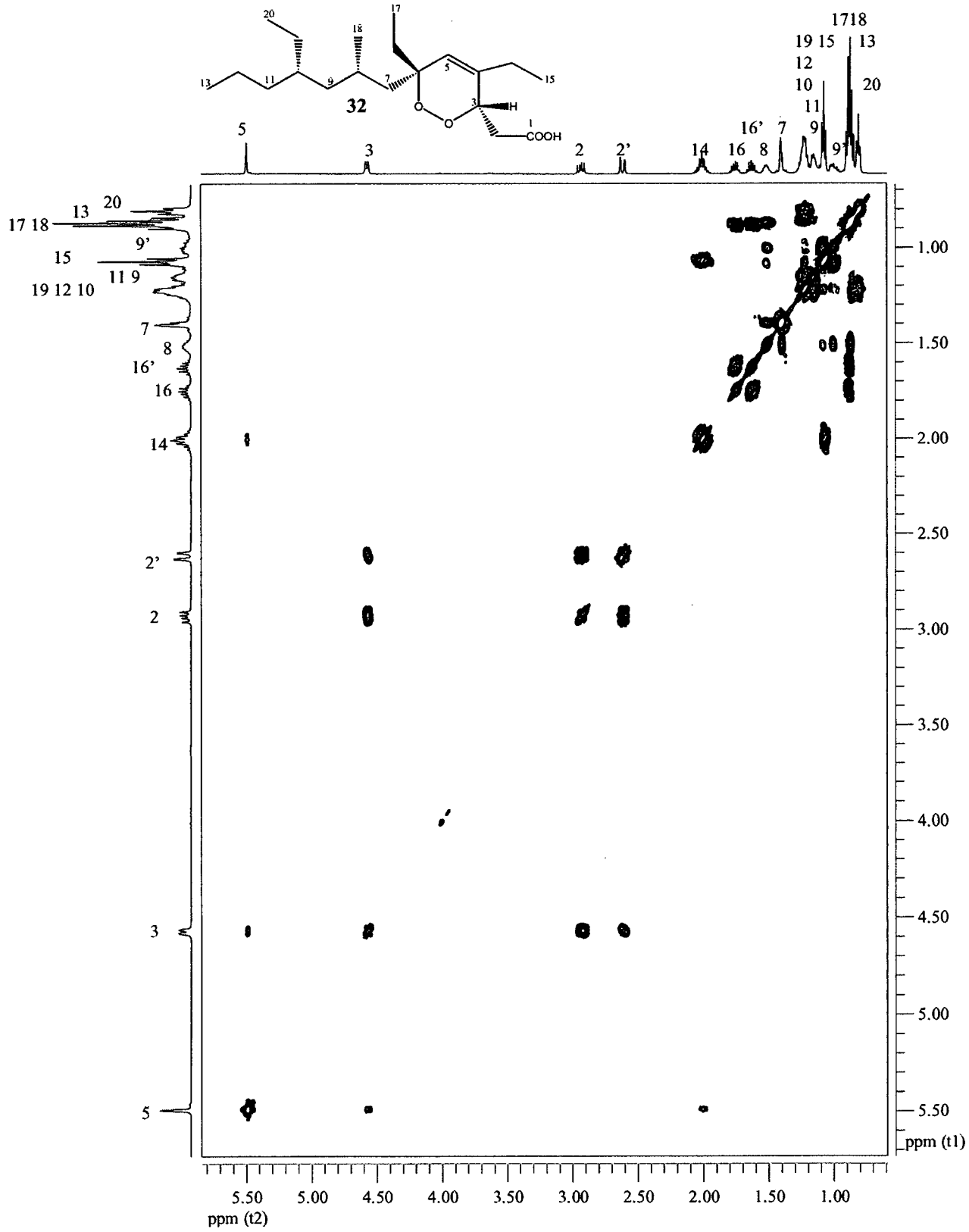

Figure 2.3.5 COSY Spectrum (500 MHz, $CDCl_3$) of **32**

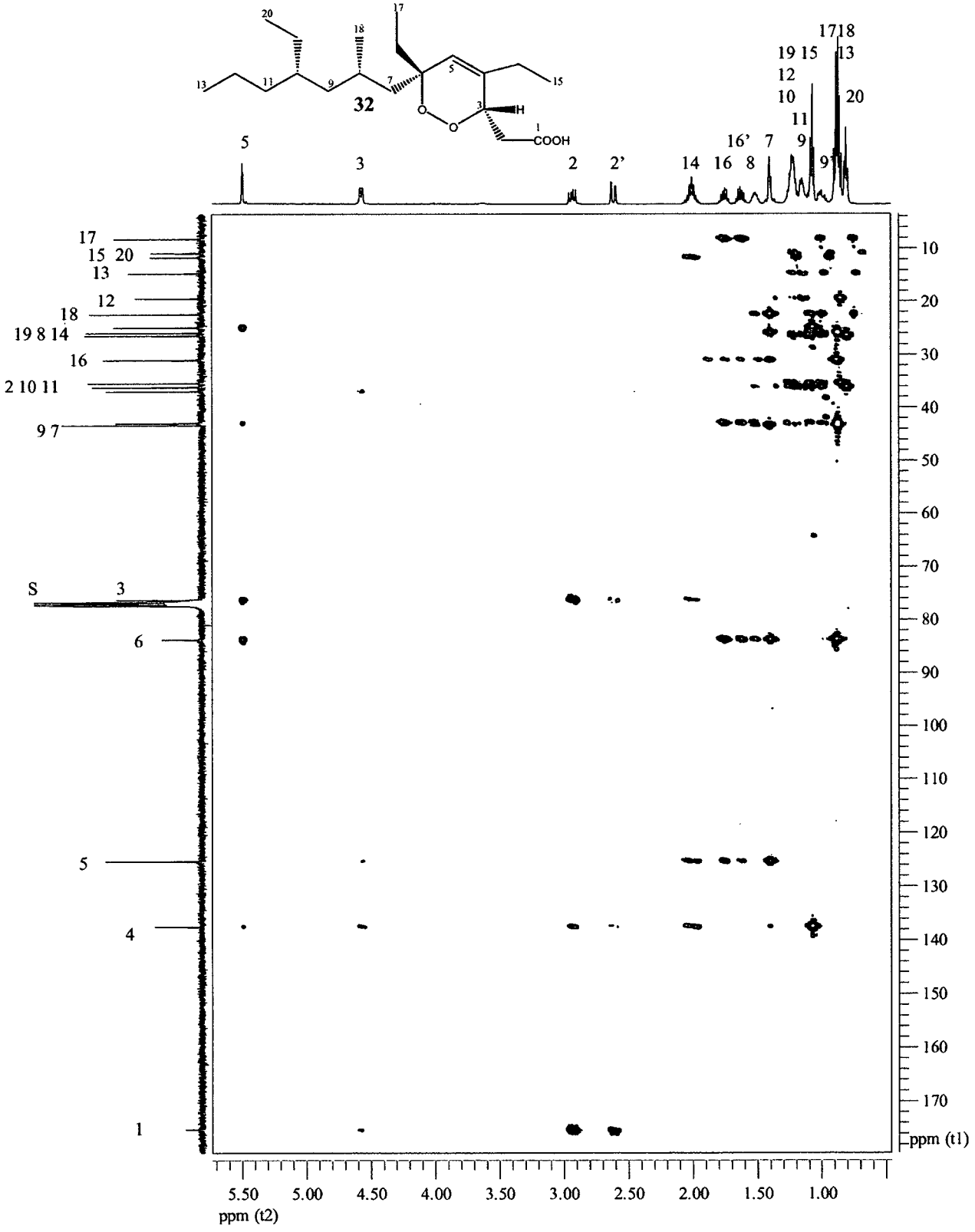

Figure 2.3.5 HMBC Spectrum (500 MHz, $CDCl_3$) of **32**

One carbonyl carbon and two olefinic carbons accounted for 2 out of 3 degrees of unsaturation. Based upon the molecular formula, the lack of any other olefinic or carbonyl carbons, and the unaccounted for degree of unsaturation, compound **32** had to contain a ring. Two characteristic hydrogen signals, the olefinic proton at δ_H 5.49 (H5) and the methinic proton at δ_H 4.57 (H3), gave HMBC correlations to C1 through C7 allowing for the assignment of the unsaturated peroxide ring, Fragment A (**Figure 2.3.6**).

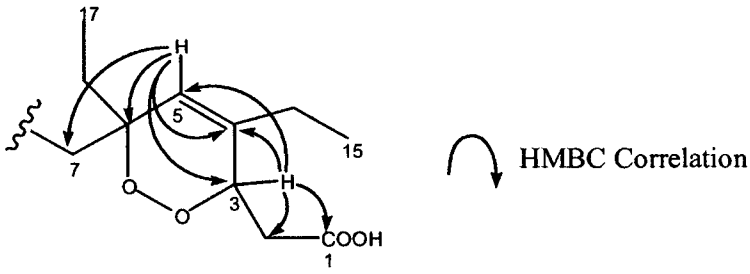

Figure 2.3.6 Methine HMBC Correlations for Compound **32**: Fragment **A**

A pair of two-bond correlations from δ_H 5.49 (H5) and δ_H 4.57 (H3) to the olefinic carbon at δ_C 137.5 (C4), established the C3/C4/C5 connectivity and positioned the double bond between C4 and C5 (δ_C 125.3.) Further HMBC correlations from δ_H 4.57 (H3) to the carbon at δ_C 36.9 (C2) and the carboxylic carbon, δ_C 175.2 (C1), established the connectivity C1/C2/C3. The C3/C2 bond was confirmed by COSY correlations between H3 and H2/2'. As one would expect, the geminally coupled α-methylene protons, H2/2', were deshielded and appear downfield at δ_H 2.61 and δ_H 2.93. The signal at δ_H 5.49 (H5) also showed HMBC correlations to δ_C 83.8 (C6) and δ_C 42.9 (C7). The more deshielded quarternary carbon, C6 (δ_c 83.8), was appropriate for an oxygen bearing carbon directly attached to the olefinic carbon at δ_C 125.3 (C5). The lack of an HMBC correlation between H3 and C6 is consistent

with a peroxide linkage forming a six-membered ring. Both C3 (δ_c 76.2) and C6 (δ_c 83.8) possess chemical shifts appropriate for oxygen bearing carbons. Based upon the molecular formula and the chemical shift data, it is suggested that Fragment A is an unsaturated 6-membered peroxide ring.

Two triplet ^{1}H NMR signals at δ_H 0.88 (H17) and δ_H 1.07 (H15) were evident in the one-dimensional spectrum. HMBC correlations from the two methyls established the connectivity of C17/C16 and C15/C14, allowing for the placement of two ethyl branch substituents on the ring at C6 (δ_c 83.8) and C4 (δ_C 137.5) (**Figure 2.3.7**), respectively.

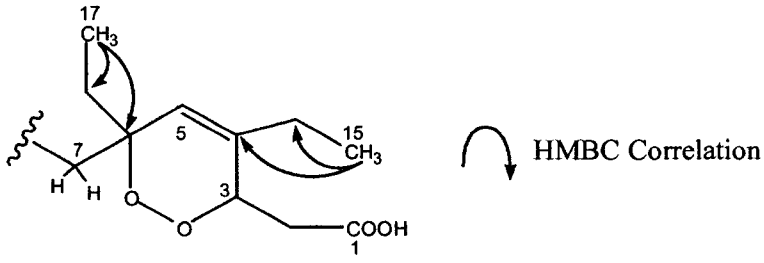

Figure 2.3.7 Methyl HMBC Correlations for Compound **32**: Fragment **A**

The key to constructing Fragment B resided in the strong HMBC correlations between the three remaining methyl group resonances and the chain carbons (**Figure 2.3.8**). Two triplet signals (δ_H 0.81, 0.86) and one doublet (δ_H 0.87) in the ^{1}H NMR spectrum indicated chain branching as two ethyls and one methyl, respectively. Two of the branching points were located at the remaining methine carbons δ_c 26.0 (C8) and δ_c 36.1 (C10). HMBC correlations showed the connectivity to be C8/C18, for the methyl branch, and C10/C19/C20, for the ethyl branch.

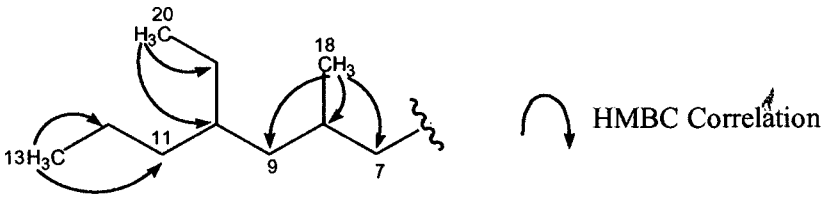

Figure 2.3.8 Methyl HMBC Correlations for Compound **32**: Fragment **B**

The final ethyl group (δ_H 0.86, H13) correlated into a methylene carbon (δ_C 35.4, C11) to form the fragment C11/C12/C13. This fragment was found to be the terminus of the main carbon chain backbone. As the protons of the C8/C18 fragment had three-bond HMBC correlations into C7 (δ_C 42.9) and C9 (δ_C 43.3), C8/C18 was connected through C7 directly to the ring moiety. Thus, the C10/C19/C20 fragment was central to the chain and attached to the C11/C12/C13 terminus.

COSY correlations supported the assignment of Fragment B. The signal at δ_H 1.52 (H8) was found to have three key COSY signals to δ_H 1.40 (H7), δ_H 1.00 (H9') and δ_H 0.87 (H18.) Also, δ_H 1.08 (H9) correlated into the methinic proton at δ_H 1.23 (H10), further extending the chain. The placement of the two methylene carbons, C11 and C12, was confirmed by a COSY correlation between H12 (δ_H 1.23) and H13 (δ_H 0.86), but not H11 (δ_H1.15) and H13 (δ_H 0.86).

All assignments were consistent with unsaturated cyclic peroxides possessing polyketide chains similar to those that have been reported in the literature.

2.4 Structure Elucidation of 3,6-epidioxy-8-methyl-4,6,10-triethyltetradeca-4,11-dienoic acid (33)

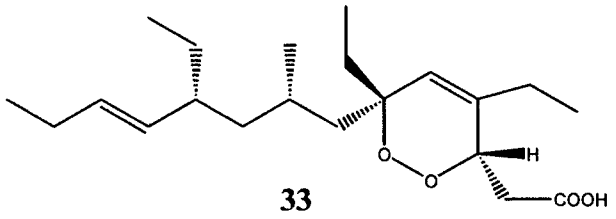

33

Compound **33** was isolated as an optically active, clear oil, that gave an HRESIMS $[M+Na]^+$ peak at m/z 375.2502 appropriate for a molecular formula of $C_{21}H_{36}O_4$ (calc'd 375.2511 for $C_{21}H_{36}O_4Na$). Accordingly, **33** had four degrees of unsaturation. The ^{13}C NMR (**Figure 2.4.1**), ^1H NMR (**Figure 2.4.2**), and HSQC (**Figure 2.4.3**) spectra revealed five methyl carbons, seven methylene carbons, three methine carbons (δ_C 25.9, 42.3, 76.3), one quarternary carbon (δ_C 83.7), four olefinic carbons (δ_C 125.3, 132.2, 133.2, 137.2) and one carbonyl carbon (δ_C 175.4). The ^{13}C NMR and ^1H NMR spectra for **32** and **33** were similar, the major difference being two extra olefinic signals in both the ^{13}C NMR (δ_C 132.2, 133.2) and the ^1H NMR (δ_H 4.95, 5.36) spectra of **33**. This accounted for the extra degree of unsaturation of **33** in comparison to the related structure, **32**. A detailed analysis of COSY (**Figure 2.4.4**) and HMBC (**Figure 2.4.5**) spectroscopic data (**Table 2.4.1**) afforded the assignment of the gross structure, **33**. Comparison of NMR chemical shift values reported in the literature (**Table 2.4.2**) supported this structure with the exception of two inappropriately assigned carbons (C9 and C20).

Table 2.4.1 ^{13}C and ^{1}H NMR Data for **33**

C#	^{13}C δ, ppm[a]	^{1}H δ, ppm (Int., m, J(Hz))[b]	COSY	HMBC
1	175.4			H2, H2'
2	36.8	2.92 (1, dd, 16.3, 9.6)	H2', H3	H3
2'		2.58 (1, dd, 16.3, 2.8)	H2, H3	
3	76.3	4.55(1, br d, 8.5)	H2, H2'	H2, H5, H15
4	137.2			H2, H5, H15, H16
5	125.3	5.49(1, br s)		H7, H15, H17
6	83.7			H5, H7, H8, H17, H17', H18
7	43.3	1.40 (2, m)	H8	H5, H8, H9, H9', H17, H17', H19
8	25.9	1.52 (1, m)	H7, H9', H19	H7, H9, H9'H10, H19
9	44.5	1.19 (1, m)	H9', H10	H7, H8, H10, H19, H20
9'		1.05 (1, m)	H8, H9	
10	42.3	1.81 (1, m)	H11, H9	H9, H9', H11, H12, H20, H21
11	133.2	4.95(1, dd, 15.3, 9.2)	H10, H12	H9, H9', H10, H13, H20, H20'
12	132.2	5.36(1, dt, 15.2, 6.4)	H11, H13	H10, H13, H14
13	25.7	1.97 (2, m)	H12, H14	H11, H12, H14
14	14.3	0.94 (3, t, 7.5)	H13	H12, H13
15	24.9	1.99 (2, m)	H16	H5, H16
16	11.6	1.07 (3, t, 7.4)	H15	H15
17	30.9	1.73 (1, dq, 14.1, 7.5)	H17', H18	H7, H18
17'		1.62 (1, dq, 14.1, 7.5)	H17, H18	
18	8.1	0.87 (3, t, 7.5)	H17, H17'	H17, H17'
19	21.3	0.83 (3, d, 6.5)	H8	H7, H8, H9, H9'
20	28.9	1.28 (1, m)	H20', H21	H9, H9', H10, H11, H21
20'		1.14 (1, m)	H20, H21	
21	11.7	0.80 (3, t, 7.4)	H20, H20'	H10, H20, H20'

[a]Recorded at 100 MHz, calibrated to the $CDCl_3$ ^{13}C δ of 77.0 ppm
[b]Recorded at 500 MHz, calibrated to the $CDCl_3$ ^{1}H δ of 7.24 ppm

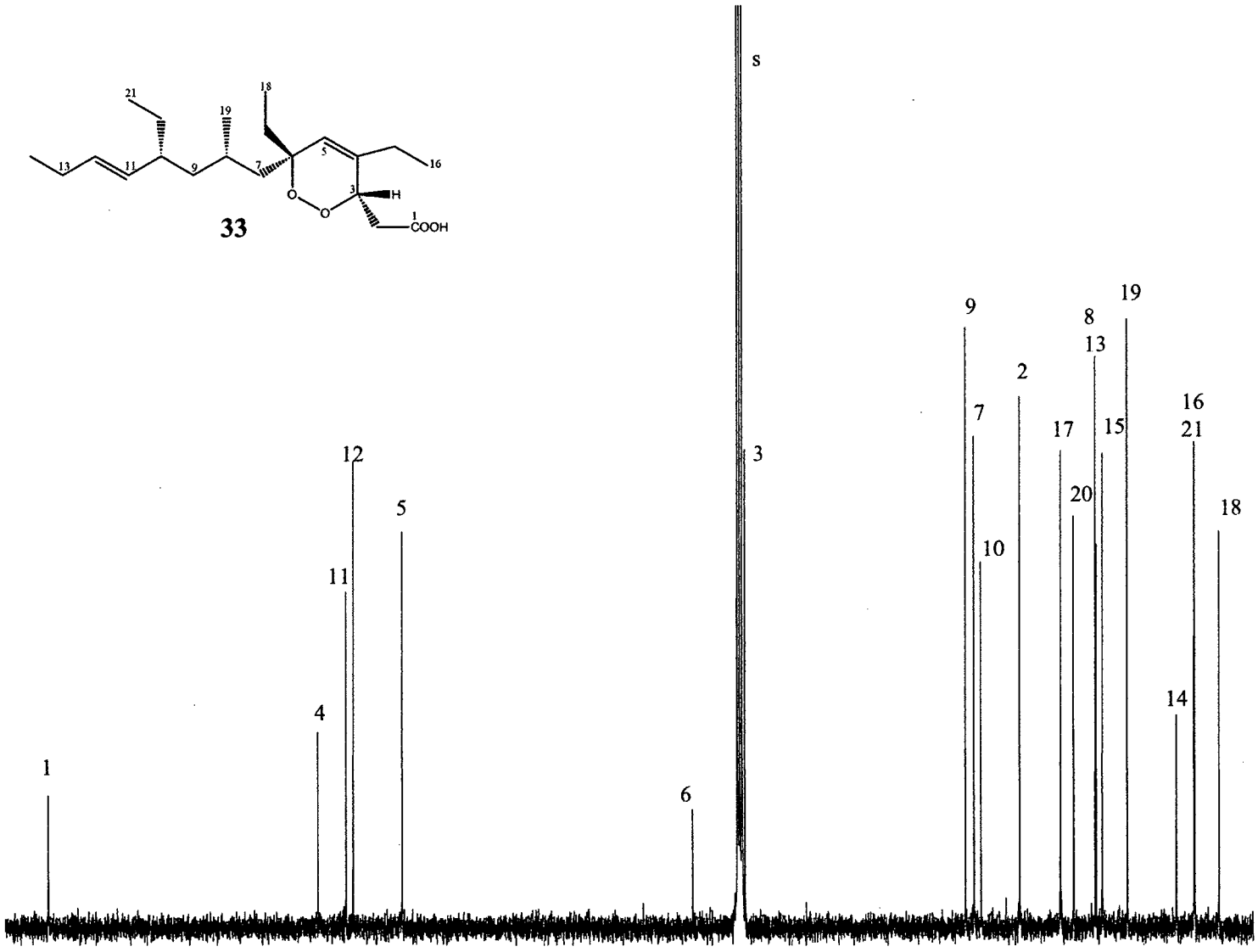

Figure 2.4.1 ^{13}C Spectrum (100 MHz, $CDCl_3$) of **33**

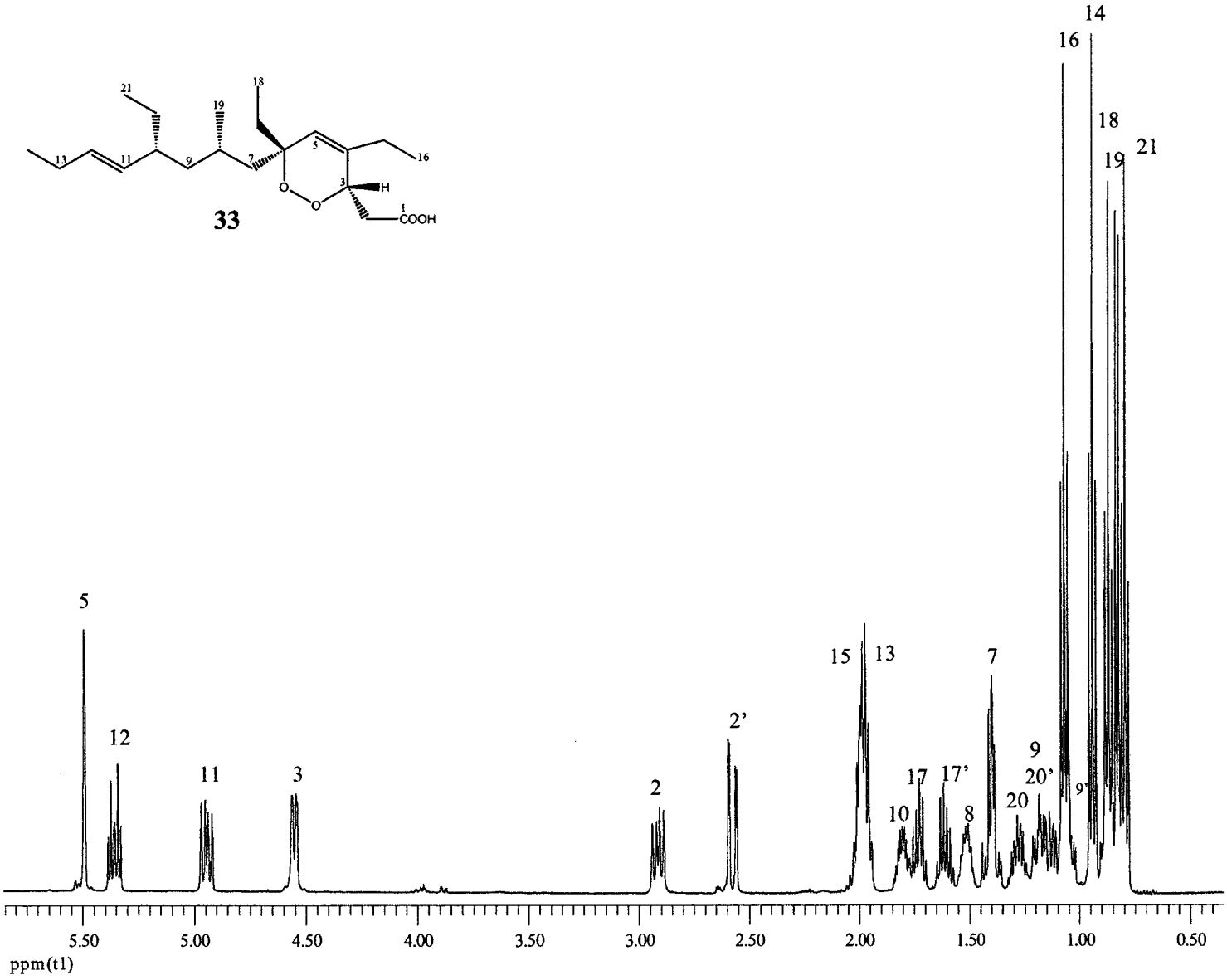

Figure 2.4.2 ^{1}H Spectrum (500 MHz, $CDCl_3$) of **33**

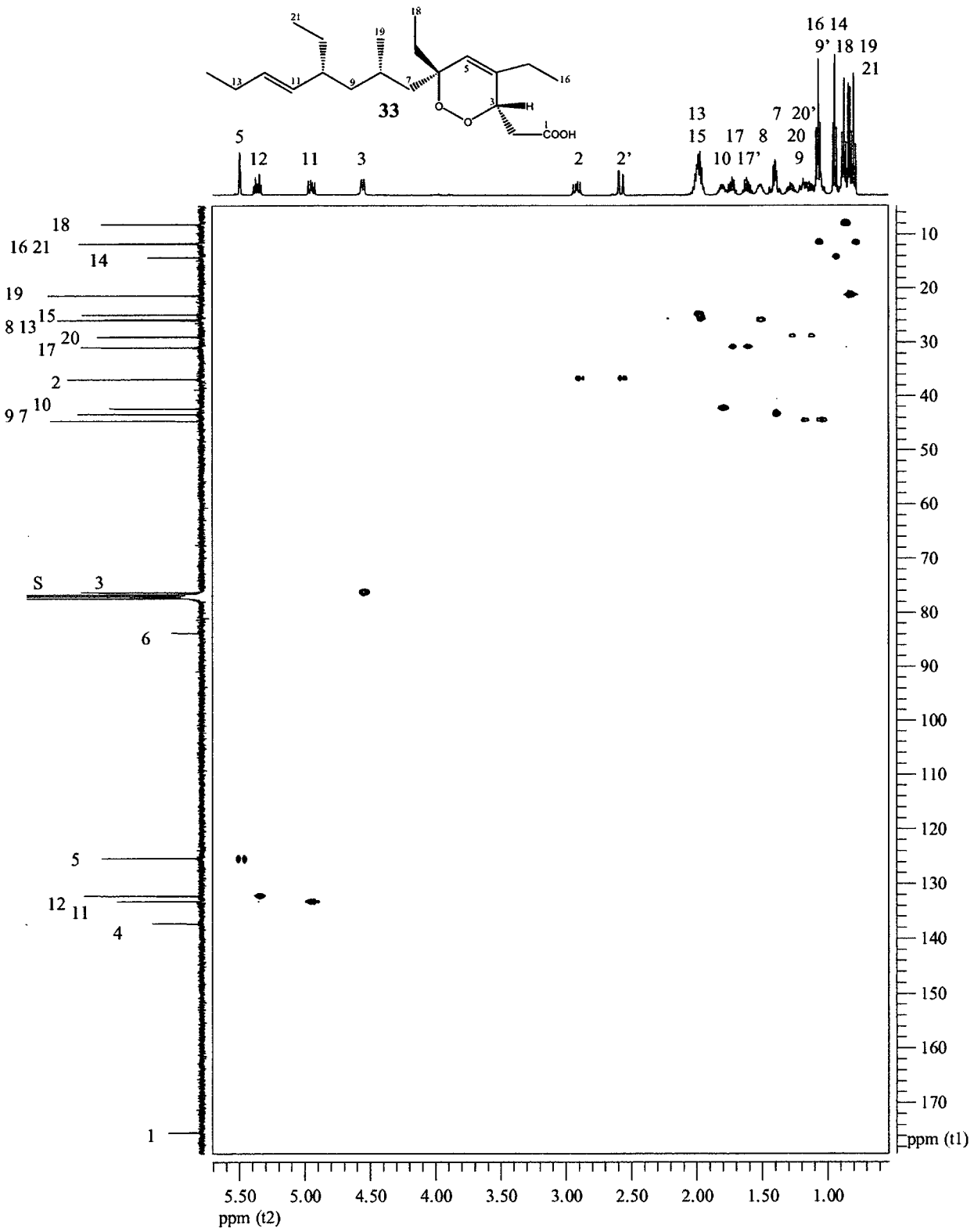

Figure 2.4.3 HSQC Spectrum (400 MHz, $CDCl_3$) of **33**

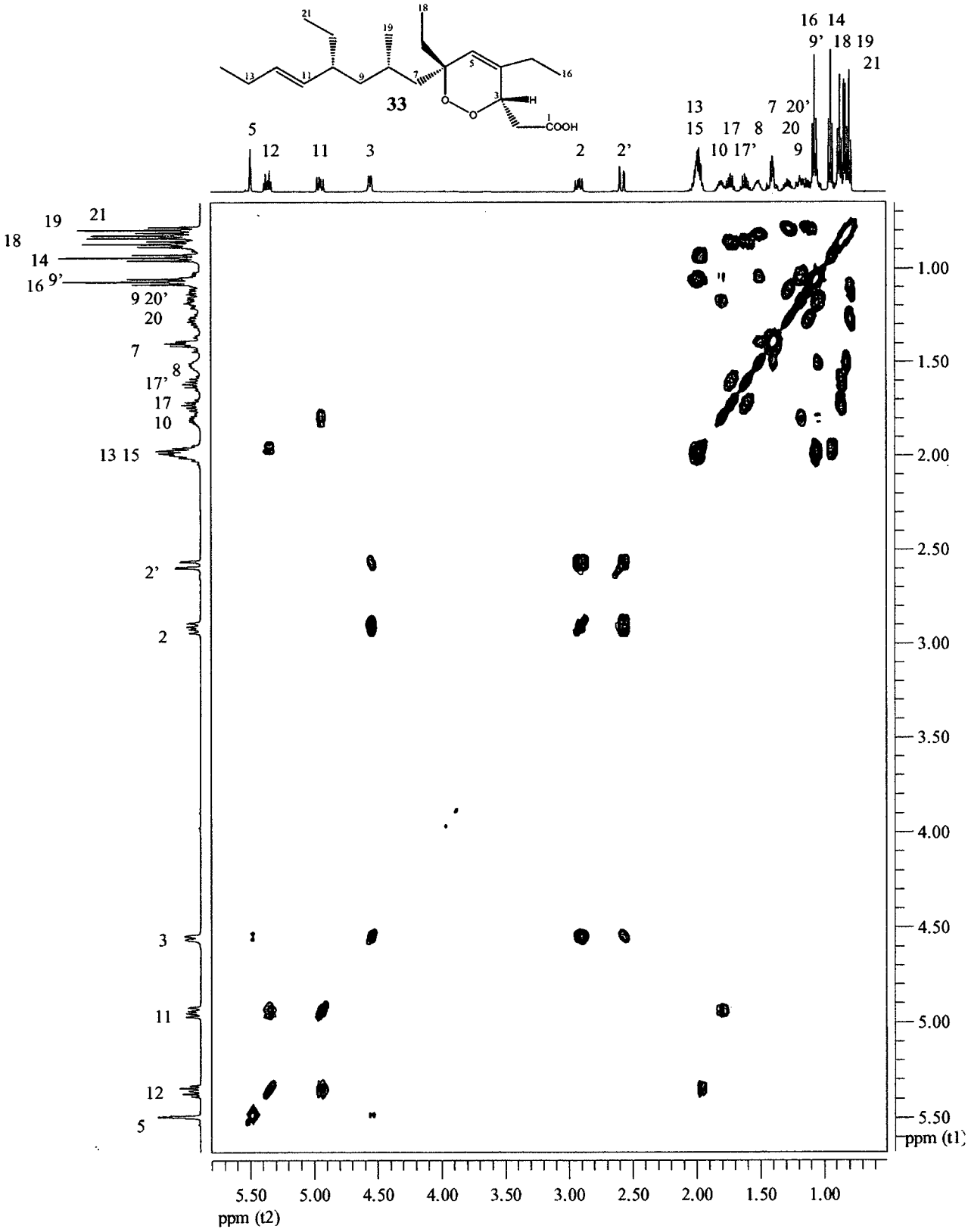

Figure 2.4.4 COSY Spectrum (500 MHz, $CDCl_3$) of **33**

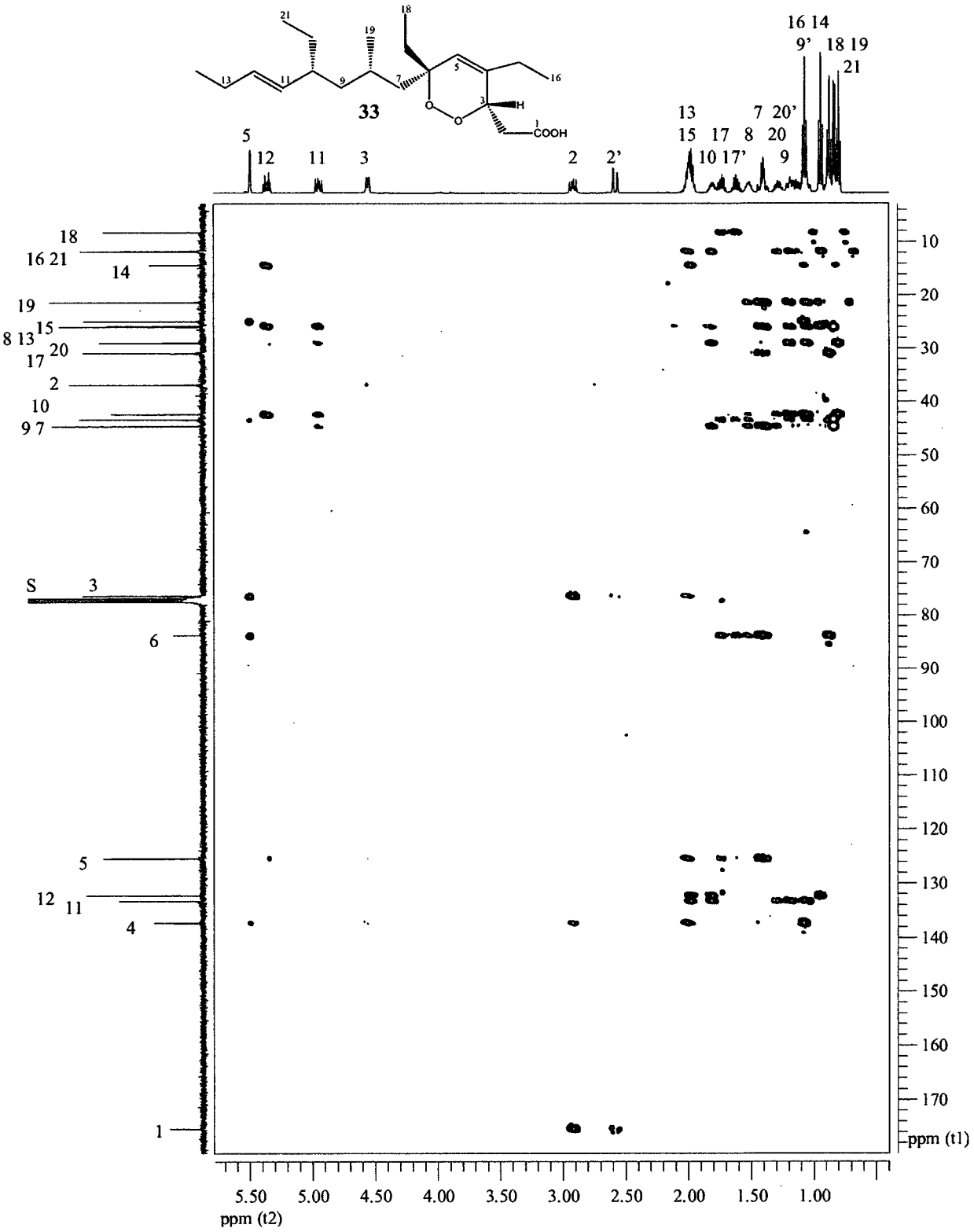

Figure 2.4.5 HMBC Spectrum (500 MHz, $CDCl_3$) of **33**

The cyclic peroxide moieties of both **32** and **33** are identical. The ^{13}C and ^{1}H NMR chemical shifts for both rings were nearly identical. COSY and HMBC correlations confirmed the nature of the ring. However, the carbon chain connected to the ring of **33** was found to be extended by one carbon and contain a double bond. The double bond was placed between C11 (δ_C 133.2, δ_H 4.95) and C12 (δ_C 132.2, δ_H 5.36). Coupling constants of 15 Hz for both protons indicated an E stereochemistry across the double bond. Structural assignments for **33** were consistent with, but not in complete concurrence with the values reported in the literature (**Table 2.4.2**).

Table 2.4.2 ^{13}C and ^{1}H NMR Chemical Shift Comparisons for **33**

C#	Found Values		Literature Values	
	^{13}C δ, ppm[a]	^{1}H δ, ppm	^{13}C δ, ppm[a]	^{1}H δ, ppm
1	175.4		176.6	
2	36.8	2.92	35.3	2.86
2'		2.58		2.53
3	76.3	4.55	76.5	4.55
4	137.2		137.5	
5	125.3	5.49	124.9	5.46
6	83.7		83.6	
7	43.3	1.40	43.3	1.38
8	25.9	1.52	25.9	1.50
9	44.5	1.19	28.9	1.39
9'		1.05		1.15
10	42.3	1.81	42.3	1.80
11	133.2	4.95	133.2	4.95
12	132.3	5.36	132.1	5.35
13	25.7	1.97	25.7	1.98
14	14.3	0.94	14.2	0.94
15	24.9	1.99	24.8	1.98
16	11.6	1.07	11.7	1.06
17	30.9	1.73	30.9	1.69
17'		1.62		1.58
18	8.1	0.87	8.1	0.86
19	21.3	0.83	21.3	0.83
20	28.9	1.28	44.5	1.28
20'		1.14		1.13
21	11.7	0.80	11.6	0.79

As found in the current study, Gunasekera *et al.* who were the first to isolate **33**, have switched the values of C9 and C20.[49] In addition, the chemical shift values of H9 (δ_H 1.19) and H9' (δ_H 1.05) do not correspond to those chemical shift values reported in the literature (δ_H 1.39 and 1.15, respectively). Also, the chemical shift of H20 and H20' do match the chemical shift values found in the current study. In the expanded HSQC spectrum (**Figure 2.4.6**) it is evident that the protons with δ_H 1.19 (H9) and δ_H 1.05 (H9') are attached to the carbon with a chemical shift of δ_C 44.5 (C9). Again, in the expanded HSQC the protons with

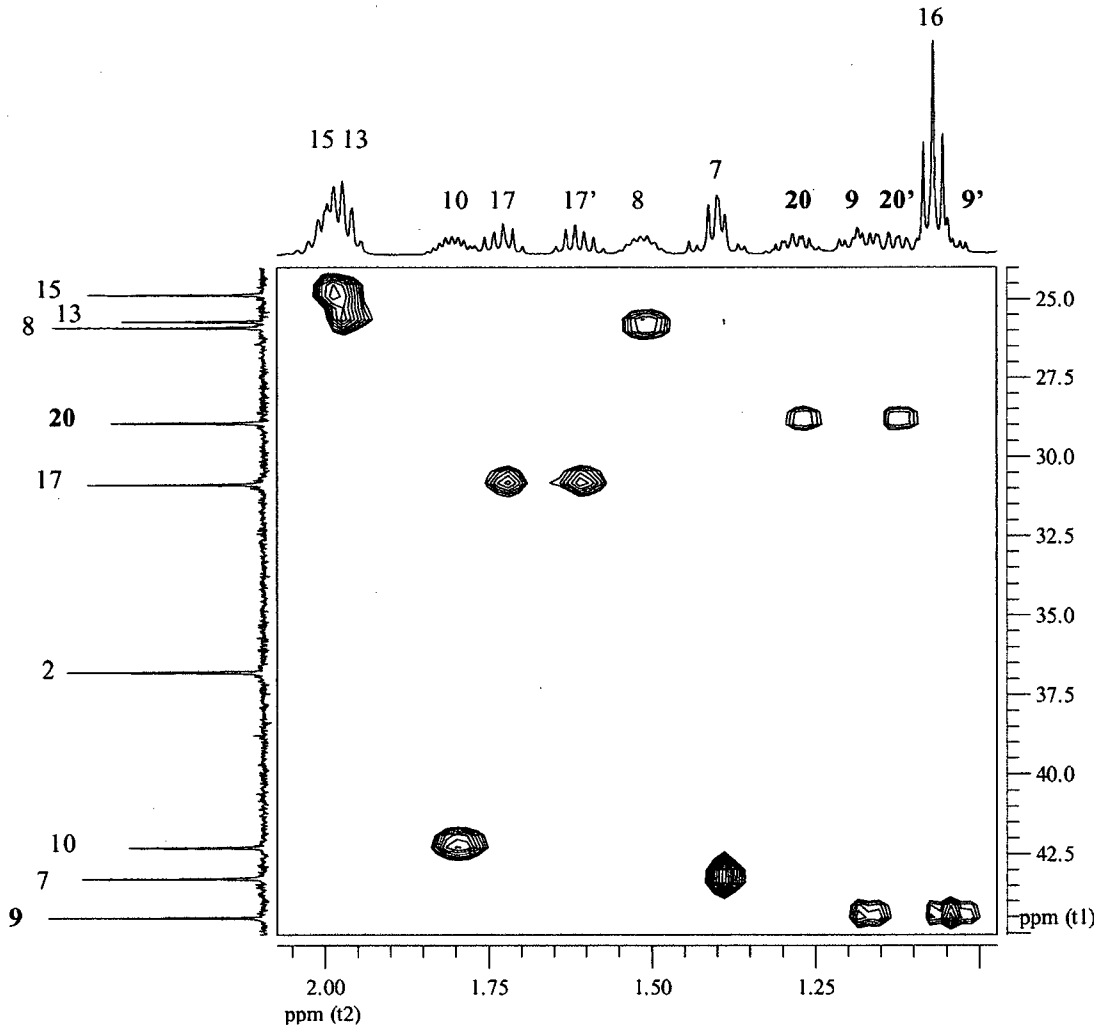

Figure 2.4.6 Expanded HSQC Spectrum (400 MHz, $CDCl_3$) of **33**

δ_H 1.28 (H20) and δ_H 1.14 (H20') are clearly bonded to the carbon with a chemical shift of 28.9 ppm (C20). Furthermore, the assignments in the current study correspond to the integration of the peaks in the ^{1}H NMR spectrum. It is impossible to have H9 with a chemical shift of δ_H 1.39 as there is an isolated multiplet at δ_H 1.40 which integrates to only two protons – not three. Inspection of the ^{1}H NMR spectrum of **33** from Gunasekera *et al.* we see a similar integration pattern.[50] **Figure 2.4.7** displays the observed H20/H21, H8/H9 COSY correlations, and the H19/C9, H7/C9 HMBC correlations that are impossible if C9 and C20 are switched.

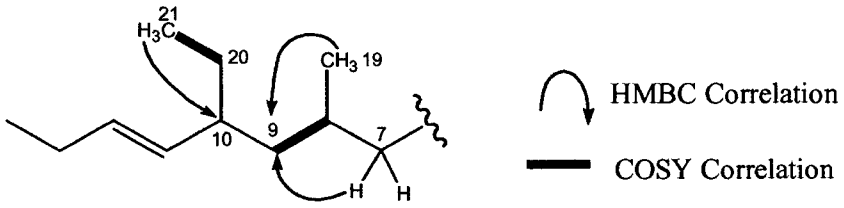

Figure 2.4.7 Selected COSY and HMBC Correlations of **33**

Finally, the trend in the carbon chemical shifts found in **32** and the assignments of other *Plakortis* polyketides with similar chains reported in the literature are consistent with the current analysis of **33**.

2.5 Proposed Stereochemistry and Biosynthesis of Structures 32 and 33

It is proposed here that the absolute configuration of both **32** and **33** is (3S,6R,8S,10S) and (3S,6R,8S,10R), respectively. This stereochemical assignment is largely based upon the study by Gang Yao and Kosta Steilou in which they synthesized two methyl ester diastereomers of **33** (**34** and **35**).[51] Based upon similarities in the ^{13}C and ^{1}H NMR data

from the methyl ester natural product derivative (**36**), isolated by Gunasekera and co-workers, Yao and Steilou proposed that the free acid, identical to **33**, would have the same absolute configuration as the methyl ester, **36**.

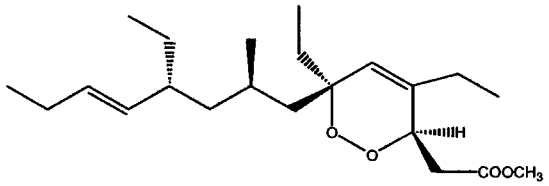

34 (3R,6S,8R,10R)

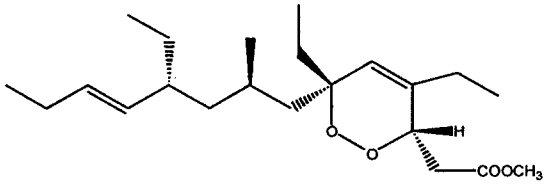

35 (3S,6R,8R,10R)

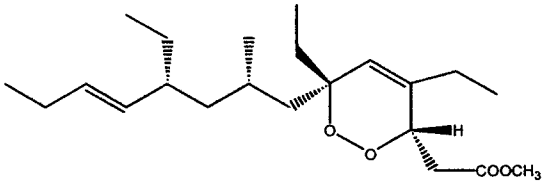

36 (3S,6R,8S,10R)

Experimental data supports the suggestion that **32** and **33** have the same relative stereochemistry as **36**. As shown in **Figure 2.5.1**, the coupling constants between H2/H2' and H3 are the same for both **32** and **33**. Based upon these couplings there is a preferred staggered conformation across the C2/C3 bond. H2 couples to H3 with a constant of 9.6 Hz making these two protons *anti* to each other. H2' and H3 are *gauche* with a coupling constant of 2.8 Hz. This is consistent with the Karplus curve.

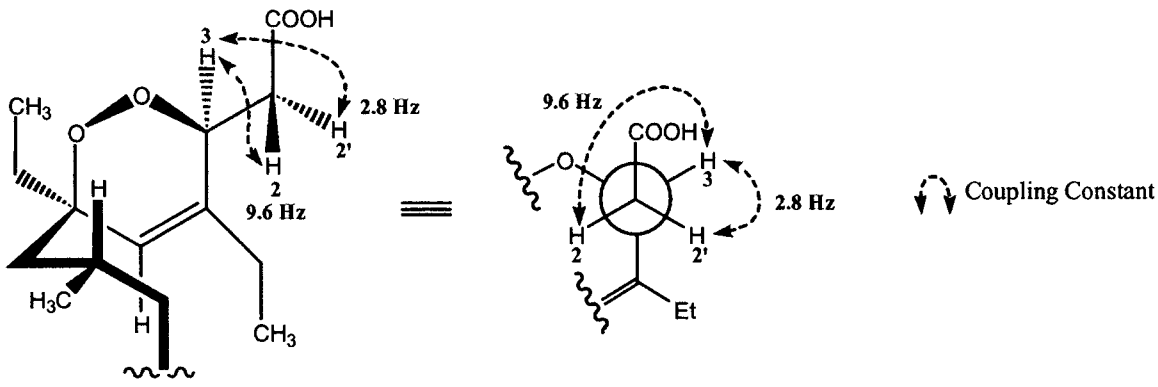

Figure 2.5.1 Selected Coupling Constants for **32** and **33**

Given the preferred conformation of C2/C3, the relative stereochemistry at positions 3 and 6 of the ring is supported by nuclear Overhauser correlations for both compounds **32** and **33**. **Figure 2.5.2** shows the NOE correlations from the ROESY spectrum (**Figure 2.5.4**) of compound **32**. Of note are the correlations of H2 to H8 and H18 on the *top-side* of the ring. Furthermore, H3 and H17 correlate indicating that this ethyl branch and the methine proton both exist on the *bottom side* of the ring.

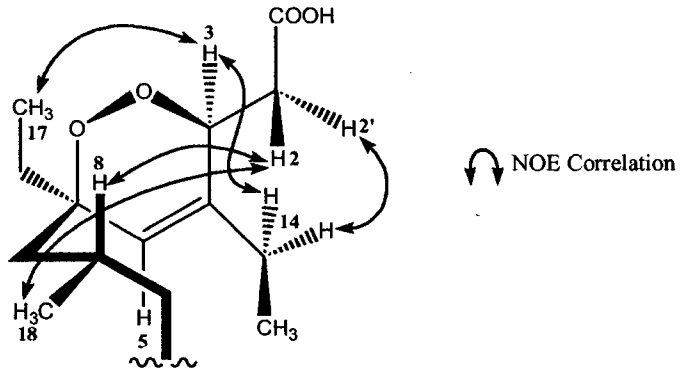

Figure 2.5.2 Selected NOE Correlations of **32**

A similar pattern is repeated in the ROESY spectrum of **33** (**Figure 2.5.5**). However, here there are only nuclear overhauser correlations on the *top-side* of the ring (**Figure 2.5.3**). These correlations are found between H2 and H7, H8, and H19.

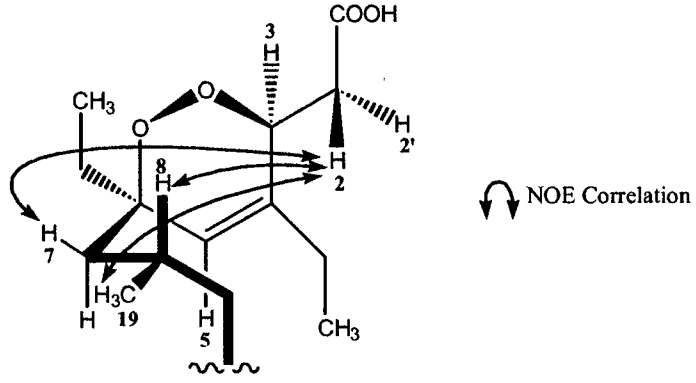

Figure 2.5.3 Selected NOE Correlations of **33**

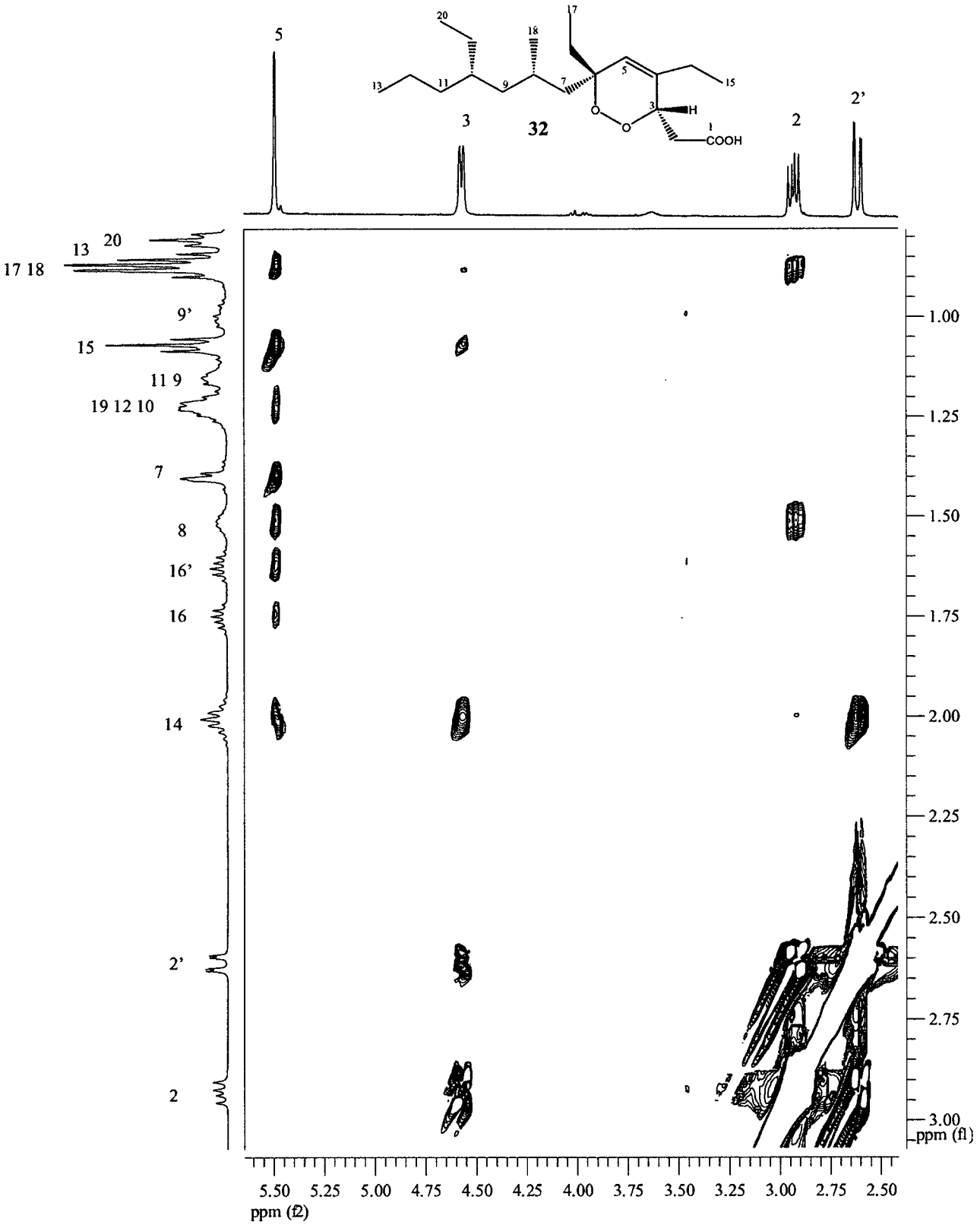

Figure 2.5.4 ROESY Expanded Spectrum (400 MHz, $CDCl_3$) of **32**

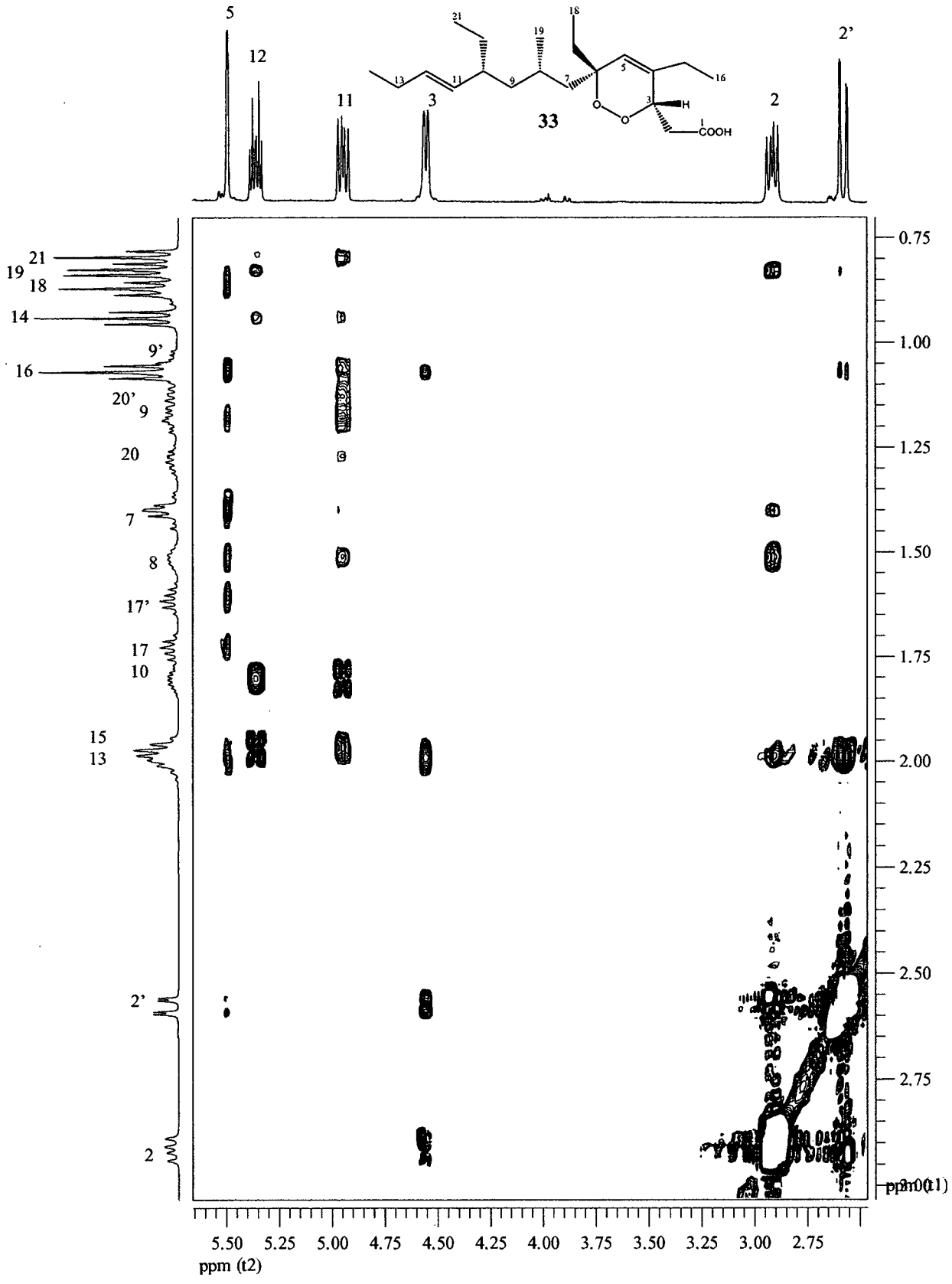

Figure 2.5.5 ROESY Expanded Spectrum (500 MHz, $CDCl_3$) of **33**

Given the preferred conformation across C2/C3 and the NOE correlations of both **32** and **33**, the relative stereochemistry of the ring moiety is (3S,6R)*. Furthermore both compounds had negative optical rotations (**32**: $[\alpha]^{23}_D = -37.8^\circ$ (c 0.26, $CHCl_3$); **33**: $[\alpha]^{23}_D = -30.7^\circ$ (c 0.25, $CHCl_3$)) and it has been noted for such compounds that the sign of the optical rotation tends to be governed by the peroxide ring moiety.[52] It is then quite possible that the rings in **32** and **33** have the same absolute configuration as that of **36** ($[\alpha]_D = -89^\circ$ (c 0.1, $CHCl_3$)). That is, both **32** and **33** have an absolute configuration of (3S,6R) for the ring moiety.

As it was already proposed, **33** has the same absolute configuration as that of the methyl ester **36**. It is very likely that **32** has the same spatial orientation as **33** since they were isolated from the same sponge and the chain branching is identical. One can envision a similar biosynthetic origin for **32** and **33**, employing a related polyketide synthase to construct both compounds. The difference in both pathways would occur during the initial step, with the two pathways converging, thereafter. Biosynthetically, that is, **32** would most likely have a propionate starter unit and **33** would begin with either an intact butyrate starter unit or with the combination of two acetates (**Scheme 2.5.1**). The remainder of both compounds would be constructed from three butyrates, one propionate, and an acetate residue with the stereochemistry determined enzymatically. Furthermore, the methyl and ethyl substituents at positions 8* and 10*, respectively, would remain *syn* to one another in both compounds. This would result in **33** having an absolute configuration of (8S,10R) in the chain and compound **32** existing as (8S,10S), as the assignment of priority groups about C10 is reversed without the double bond. The final step in the biosynthesis of **32** and **33** would

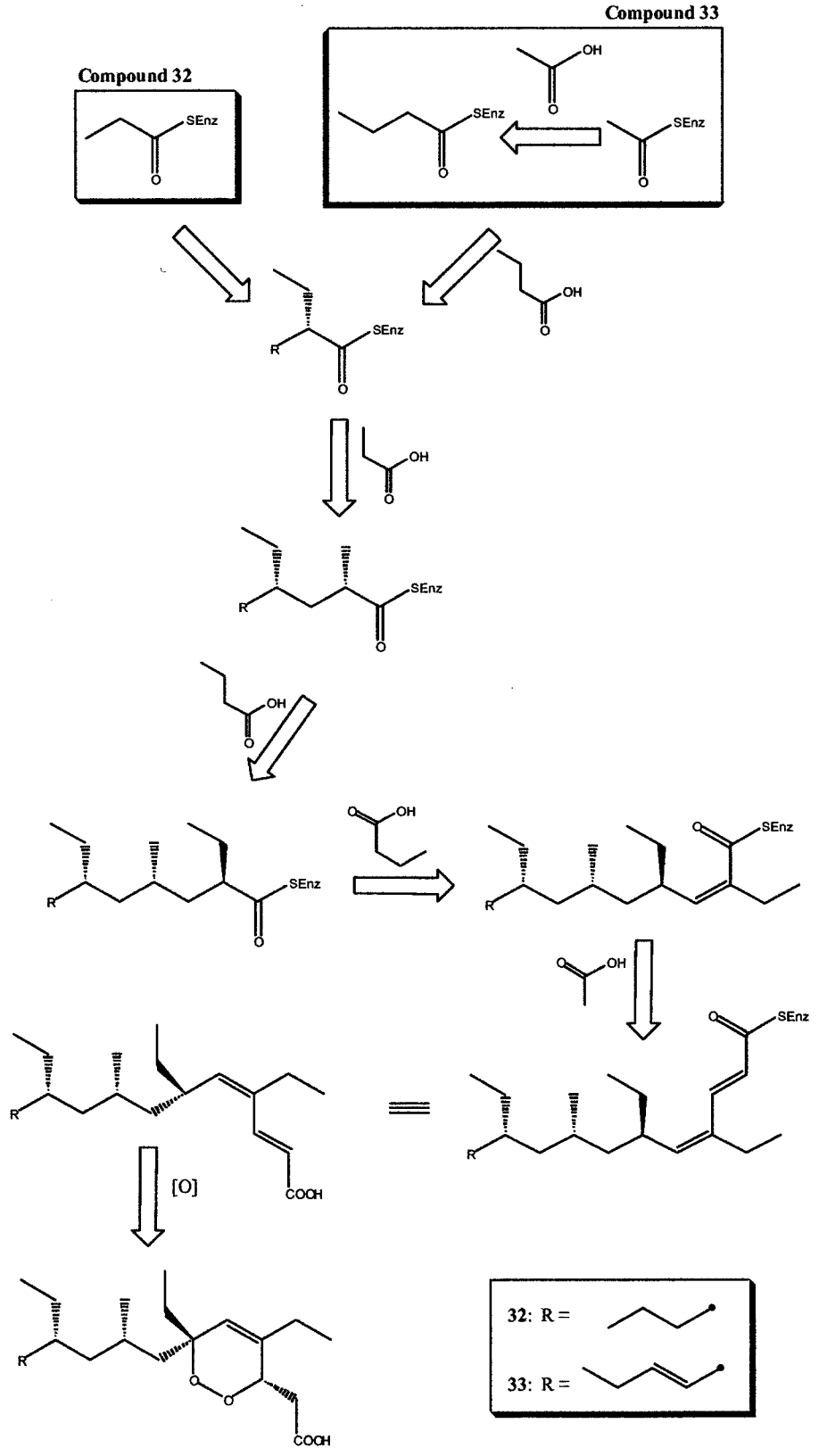

Scheme 2.5.1 Proposed Biosynthesis of Compounds **32** and **33**

involve the enzymatic addition of oxygen and cyclization, possibly via an intramolecular Michael addition of the peroxide (**Scheme 2.5.2**).

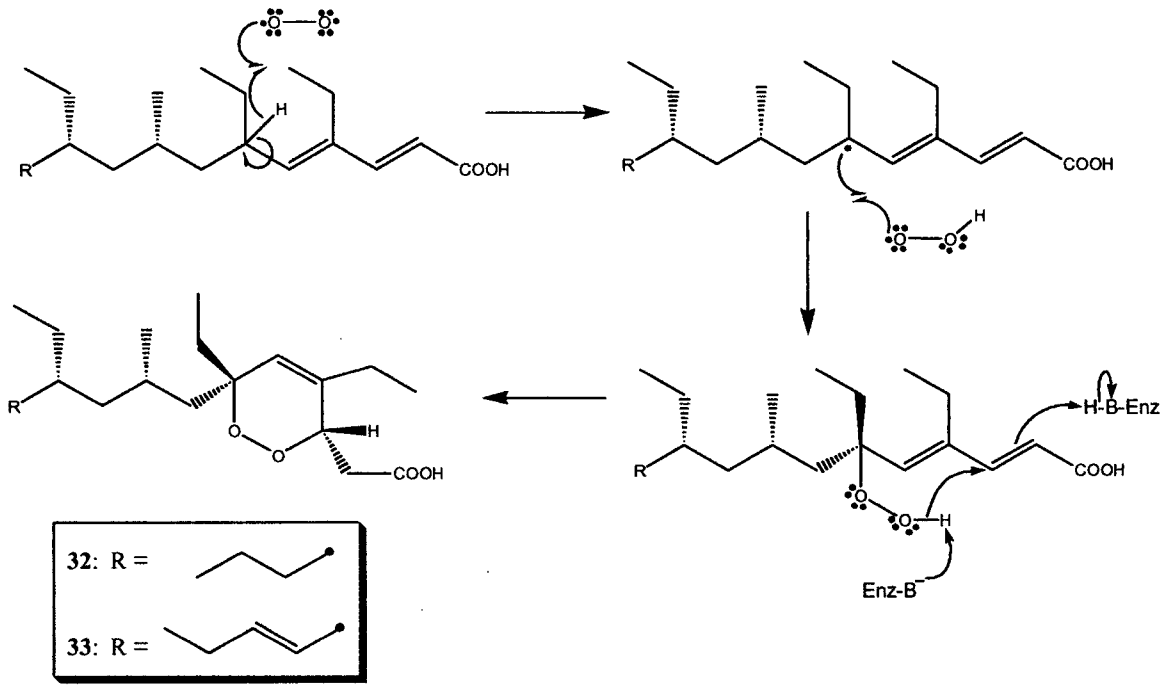

Scheme 2.5.2 Proposed Biosynthesis of the Cyclic Peroxide Moiety in Compounds **32** and **33**

The absolute stereochemistry of **33** is proposed to be (3S,6R,8S,10R) based upon the aforementioned synthetic study by Yao and Steilou. It is tentatively proposed here that the absolute stereochemistry of **32** is most likely (3S,6R,8S,10S) as it appears to share a similar biosynthetic origin with **33**. Mosher's empirical method could be used to confirm the absolute configuration of **32** and **33**, however, this would be dependent upon the relative configuration determined in the previously mentioned synthetic study. Therefore, the two cyclic peroxide polyketides are proposed as: (3S,6R,8S,10S)-3,6-epidioxy-8-methyl-4,6,10-triethyltrideca-4-enoic acid (**32**) and (3S,6R,8S,10R)-3,6-epidioxy-8-methyl-4,6,10-triethyltetradeca-4,11-dienoic acid (**33**).

2.6 Biological Activity

The minimum inhibitory concentrations (MIC) for compounds **32** and **33** (**Table 2.6.1**) were established by an Alamar Blue® microdilution assay. Both compounds showed potent activity against *Candida albicans* and, to a lesser extent, activity against various bacterial pathogens. Interestingly, compounds **32** and **33** have the greatest activity against yeast (*C. albicans*), gram-positive bacteria (MRSA, VRE), and gram-negative bacteria (*E.coli, P.cepacia*), in that order. In addition, compound **32** was found to be consistently more active than compound **33**. Possibly, compound **32** is more soluble than **33** in aqueous environments, increasing the availability of **32** to the pathogens in the broth assays. Otherwise, the functionalized end of both molecules, the cyclic peroxide moiety, is identical and cannot account for the difference in activities.

Table 2.6.1 Minimum Inhibitory Concentration of **32** and **33**

Pathogen	**MIC of Compound 32 (μg/mL)**	**MIC of Compound 33 (μg/mL)**
Candida albicans	0.8	1.6
Methicillin Resistant *Staphylococcus aureus*	25	50
Vancomycin Resistant *Enterococcus*	25	100
Pseudomonas cepacia	100	100
Escherichia coli	> 100	> 100

Yeast deletion mutant profiling against the crude extract of *Plakortis angulospiculatus* and compound **33** yielded no clear targets or affected pathways. Both the

profiles appeared similar and only a few strains were identified as sensitive. The strains that were identified as sensitive are strains that often show general, non-specific drug sensitivity.

2.7 Conclusion

Cyclic peroxide polyketides from *Plakortis* sponges constitute the majority of compounds isolated from such organisms and are usually found to be saturated within the ring moiety. Indeed, cyclic peroxides, such as compounds **32** and **33,** with an extra degree of unsaturation in the peroxide ring, form a smaller subset of the body of compounds discovered from *Plakortis* sponges. Compound **32** was new, in that, its carbon chain had one less carbon than a related compound cited in the literature. Both **32** and **33** showed potent activity against *Candida albicans*. However, upon further study, compound **33** did not appear to have a particularly unique or interesting fungal cellular target. It may be possible that most, if not all, *Plakortis*-type cyclic peroxides have general modes of action against fungi that would negate their usefulness as lead compounds for drug discovery.

CHAPTER 3 Furano Polyketides from *Plakortis angulospiculatus*

3.1 Introduction

In addition to the search for the biologically active natural products, this research project was concerned with *chemical prospecting* for new secondary metabolites. By chemical prospecting one searches for new and novel molecular structures based upon *interesting* NMR signatures. Such an approach to isolating natural products has the potential to yield unprecedented carbon skeletons that may be overlooked in a particular bioassay-guided fractionation scheme. In such a manner, by ^{1}H NMR data, two furano polyketides have been isolated: the α,β-unsaturated furano ester, **37**, and the previously discovered furan polyketide, glánvillic acid B (**38**). Compound **37** is the first example of a *Plakortis* type furano ester with a methyl branch attached to the ring at position 4. Glánvillic acid B, **38**, was isolated in its free acid form for the first time and spectroscopic data is reported accordingly.

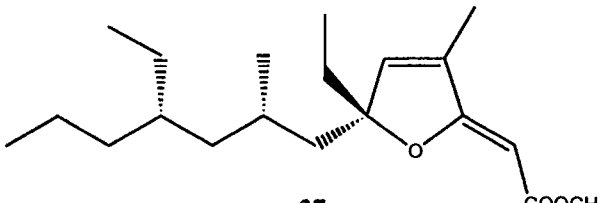

37

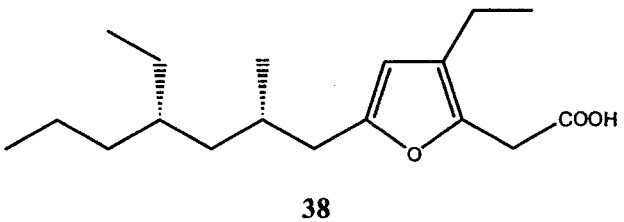

38

3.2 Isolation

A portion of the collected sponge *Plakortis angulospiculatus* (50 g, wet weight) was immersed in and extracted twice with MeOH. The methanol extract was concentrated and reduced to dryness *in vacuo*, leaving a brown gum (1.76 g) that was partitioned between

EtOAc (5 x 100 mL) and H_2O (200 mL). The EtOAc layer was dried over $MgSO_4$, filtered, and reduced to dryness *in vacuo* (yellow-brown oil, 366 mg). Subsequently, the EtOAc residue was chromatographed on Sephadex LH-20® (4:1 MeOH/CH_2Cl_2). One fraction (pale yellow oil, 33 mg) displaying a characteristic ^1H NMR signal of 6.21 ppm (in $CDCl_3$) was chromatographed on a gradient normal phase silica flash column (95:5 HEX/EtOAc → 100%EtOAc). Fractions containing the aforementioned NMR signal were pooled (9.5 mg) and purified by reversed-phase HPLC (78:22 MeOH/H_2O, 0.1% TFA) yielding one pure compound, **37** (colourless oil, 1.2 mg). A separate LH-20 fraction (pale yellow oil, 26 mg) was subjected to a normal phase silica flash column (95:5 HEX/EtOAc → 50:50 HEX/EtOAc). One fraction (clear oil, 4.5 mg) containing a characteristic ^1H NMR signal of 5.85 ppm (in $CDCl_3$) was purified by reverse-phased HPLC (3AcN:2H_2O, 0.1% TFA) to yield one pure compound, **38** (clear oil, 0.5 mg).

3.3 Structure Elucidation of methyl-6,10-diethyl-4,8-dimethyl-3,6-epoxytrideca-2,4-dienoate (37)

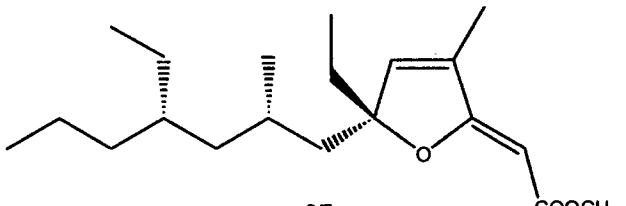

37

Compound **37** was isolated as an optically active, clear oil, that gave a positive mode HRESIMS $[M+Na]^+$ peak at m/z 345.2415 appropriate for a molecular formula of $C_{20}H_{34}O_3$ (calc'd 345.2406 for $C_{20}H_{34}O_3Na$). Accordingly, **37** had four degrees of unsaturation. The ^{13}C NMR (**Figure 3.3.1**), ^1H NMR (**Figure 3.3.2**), and HSQC (**Figure3.3.3**) spectra revealed six methyl carbons, six methylene carbons, two methine carbons (δ_C 26.1, 36.0), one

quarternary carbon (δ_C 98.1), four olefinic carbons (δ_C 84.0, 133.8, 141.6, 172.3) and one carbonyl carbon (δ_C 166.9). Two fragments, a ring and a carbon chain, were constructed and connected based upon COSY (**Figure 3.3.4**) and HMBC (**Figure 3.3.5**) spectra to provide the gross structure of **37**. A detailed summary of the 1- and 2-D NMR spectroscopic data is listed in **Table 3.3.1**.

Table 3.3.1 ^{13}C and ^{1}H NMR Data for **37**

C#	^{13}C δ, ppm[a]	^{1}H δ, ppm (Int., m, J(Hz))[b]	COSY	HMBC
1	166.9			H20
2	84.0	4.79 (1, s)		
3	172.3			H2, H14
4	133.8			H2, H5, H14
5	141.6	6.21 (1, s)	H14	H15, H15'
6	98.1			H8, H15, H15', H16
7	45.1	1.68 (2, d, 5.7)	H8	H8, H9, H9', H17
8	26.1	1.36 (1, m)	H7, H9', H17	H7, H17
9	43.0	1.07 (1, m)	H9'	H7, H8, H17
9'		0.97 (1, m)	H8, H9	
10	36.0	1.19 (1, m)	H11	H8, H9, H9', H11, H18, H19
11	35.4	1.11 (2, m)	H10	H13
12	19.5	1.21 (2, m)	H13	H13
13	14.6	0.84 (3, t, 7.2)	H12	H11
14	11.0	1.83 (3, d, 1)	H5	H5
15	32.0	1.82 (1, m)	H15', H16	H7, H16
15'		1.70 (1, m)	H15, H16	
16	8.0	0.78 (3, t, 7.4)	H15, H15'	H15, H15'
17	21.7	0.84 (3, d, 6.5)	H8	H7, H8, H9
18	26.3	1.19 (2, m)	H19	H9, H9', H10, H11, H19
19	10.7	0.79 (3, t, 7.1)	H18	
20	50.5	3.67 (3, s)		

[a]Recorded at 100 MHz, calibrated to the $CDCl_3$ ^{13}C δ of 77.0 ppm
[b]Recorded at 500 MHz, calibrated to the $CDCl_3$ ^{1}H δ of 7.24 ppm

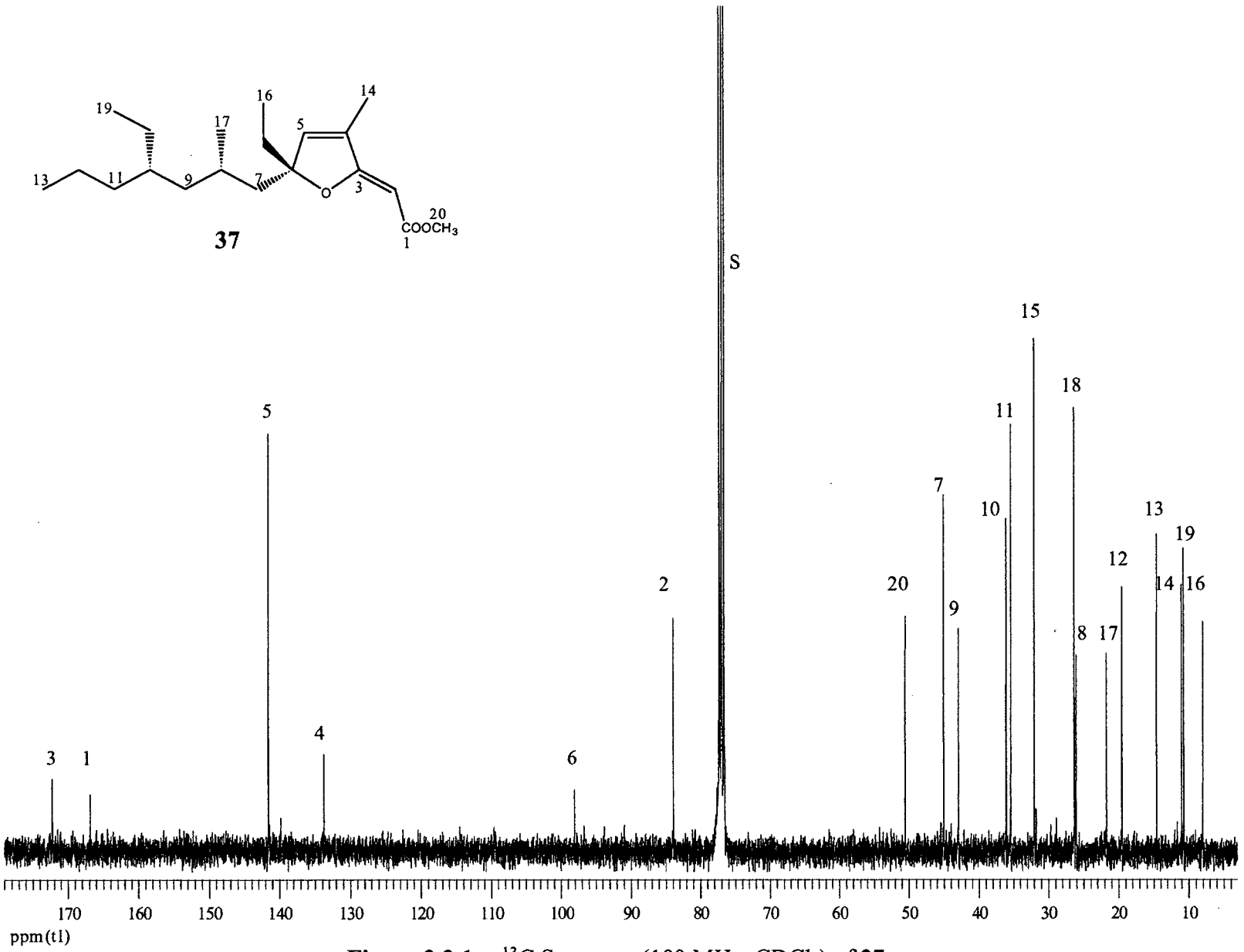

Figure 3.3.1 ^{13}C Spectrum (100 MHz, $CDCl_3$) of **37**

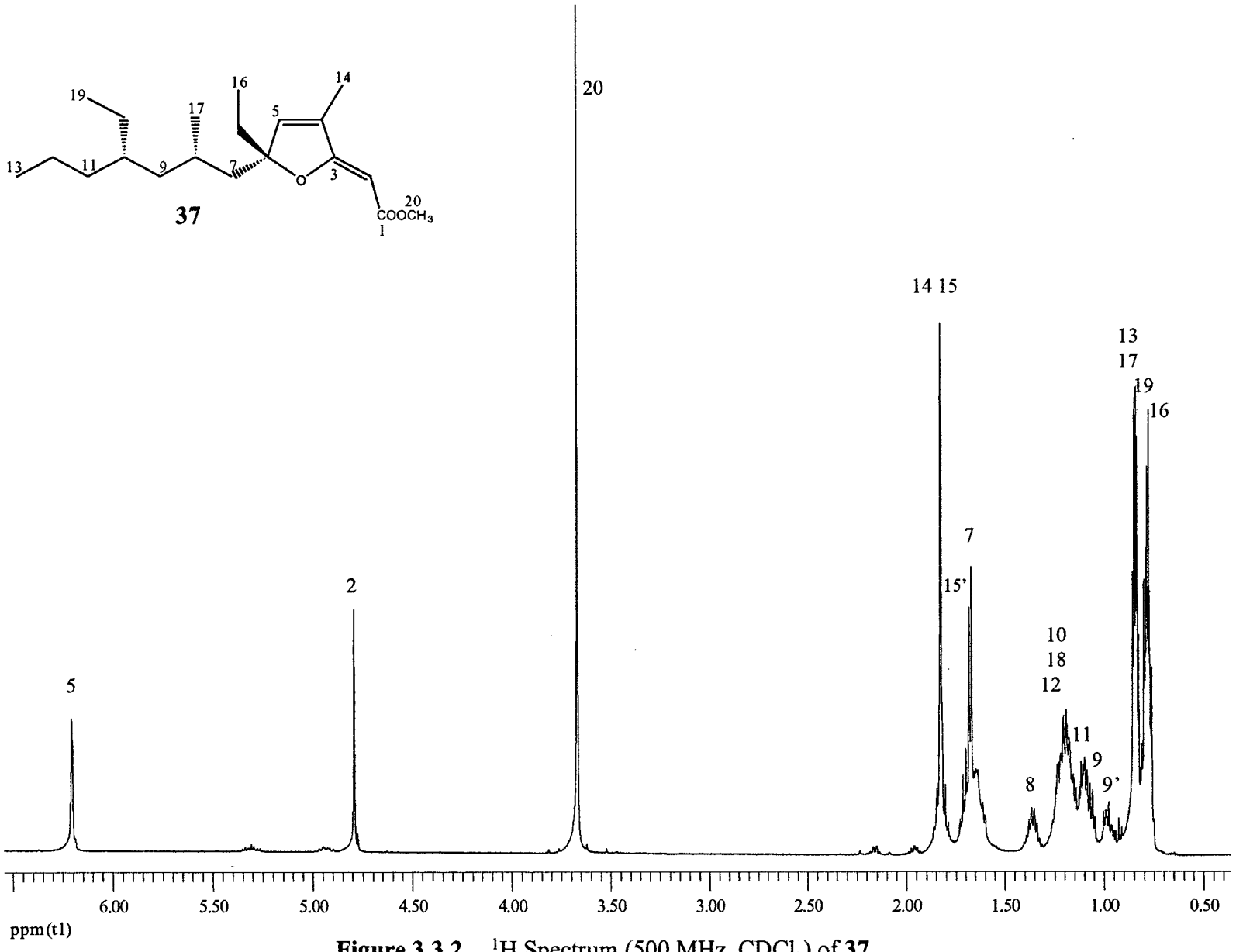

Figure 3.3.2 ^{1}H Spectrum (500 MHz, $CDCl_3$) of **37**

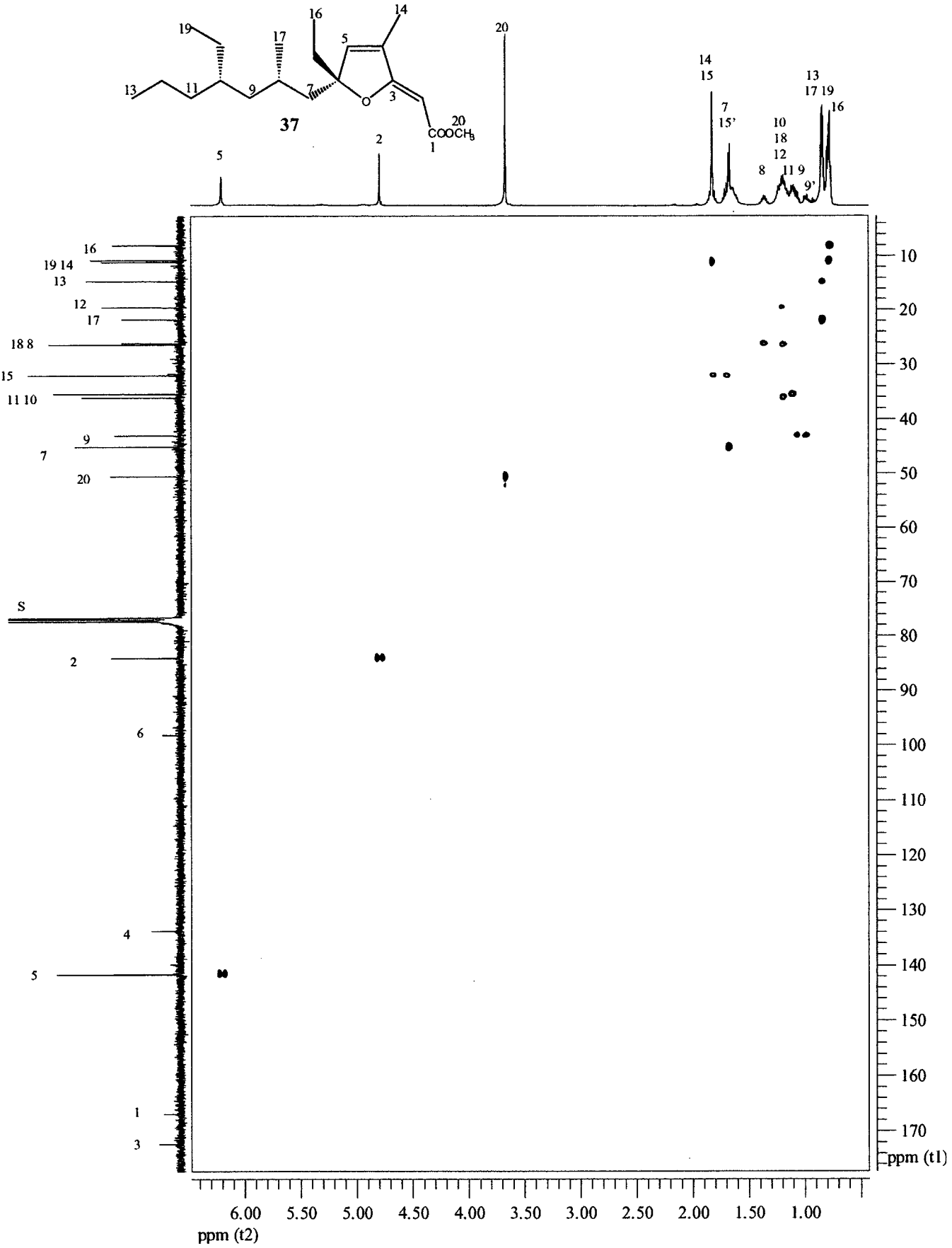

Figure 3.3.3 HSQC Spectrum (400 MHz, $CDCl_3$) of **37**

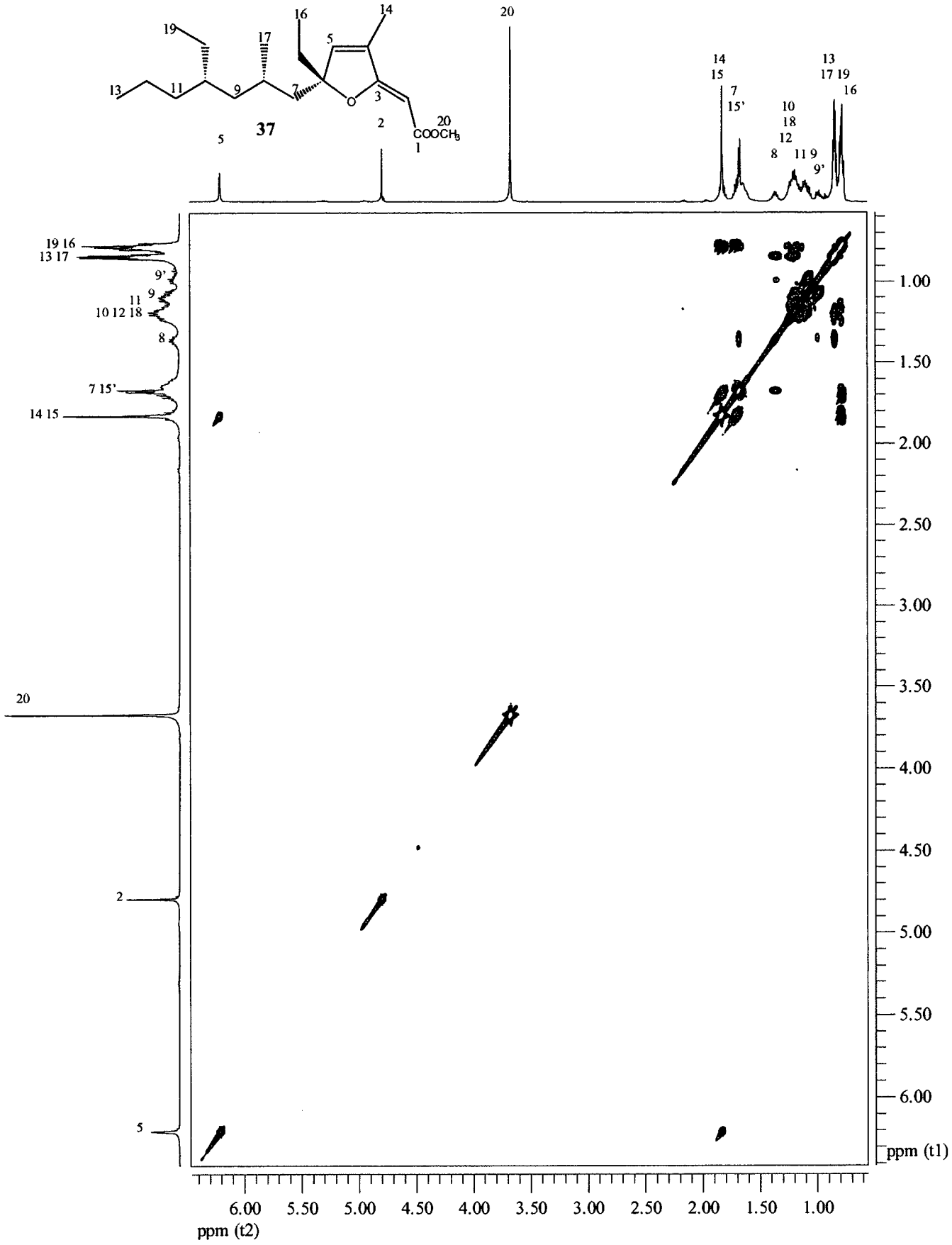

Figure 3.3.4 COSY Spectrum (500 MHz, $CDCl_3$) of **37**

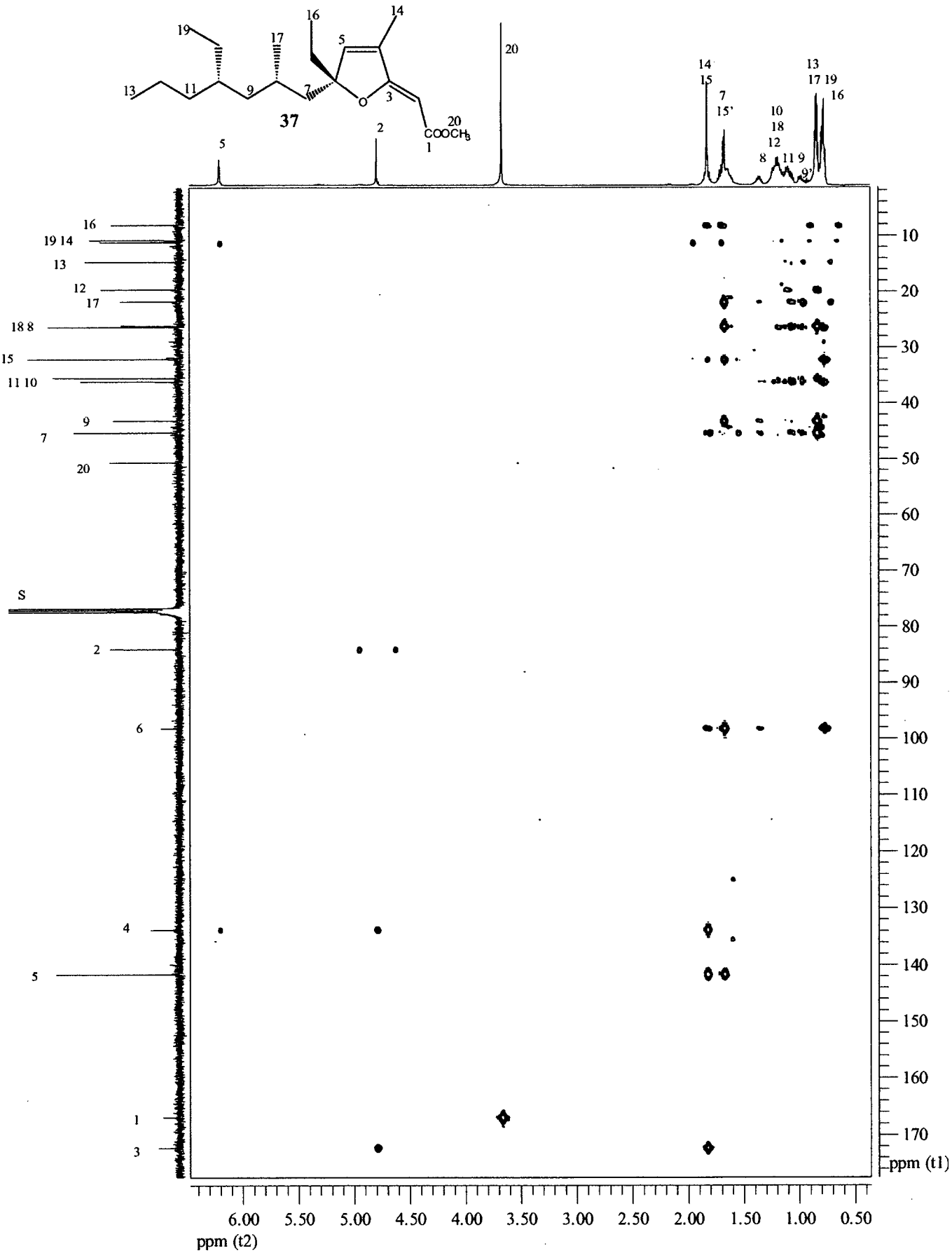

Figure 3.3.5 HMBC Spectrum (500 MHz, $CDCl_3$) of **37**

Two distinctive proton singlets at δ_H 6.21 and δ_H 4.79 were useful in solving the structure of the ring moiety, Fragment A. By HSQC data, the proton at δ_H 6.21 was attached to the olefinic carbon δ_C 141.6 (C5). Using this proton resonance as a starting point for assigning the gross ring structure, HMBC correlations (**Figure 3.3.6**) were seen for δ_C 133.8 (C4) and the methyl group carbon at δ_C 11.0 (C14). This suggested that the carbon at δ_C 133.8 (C4) was the olefinic partner of the carbon bearing the distinctive proton (δ_H 6.21 (H5)). In addition, the methyl group protons at δ_H 1.83 (H14) correlated into δ_C 133.8 (C4), such that this olefinic carbon would be substituted by this methyl group. A three-bond correlation between δ_H 1.83 (H14) and δ_C 172.3 (C3) indicated that δ_C 133.8 (C4) was in all likelihood bonded to δ_C 172.3 (C3).

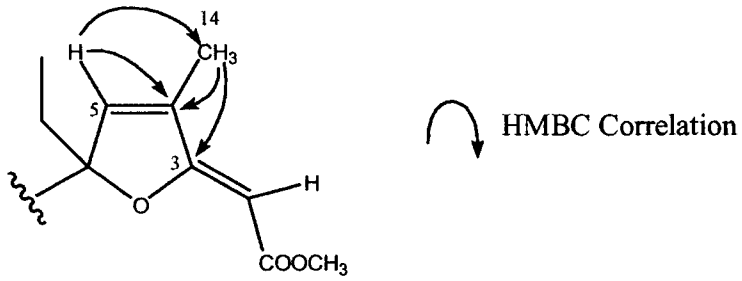

Figure 3.3.6 Selected HMBC Correlations for Compound **37**: Fragment **A**

Once again, by HSQC correlations, the other characteristic proton singlet at δ_H 4.79 was shown to be attached to a carbon with a chemical shift of δ_C 84.0 (C2). As shown in **Figure 3.3.7**, this proton had HMBC correlations to the carbons bearing chemical shifts of δ_C 172.3 (C3) and δ_C 166.9 (C1). Furthermore, the methyl ester was characterized by a strong HMBC correlation of the methyl protons at δ_H 3.67 into the carbon at δ_C 166.9 (C1). Given the C5/C4/C3 order had already been ascertained, and the carbon at δ_C 166.9 (C1) is an ester, it was apparent that the carbon with δ_C 84.0 (C2) would most likely be positioned between

the carbons at δ_C 172.3 (C3) and δ_C 166.9 (C1). Looking back at the carbon with a chemical shift of δ_C 141.6 (C5) it was indirectly shown to be connected to the quaternary carbon at δ_C 98.1(C6) by HMBC correlations from the methylene protons (δ_H 1.70(H15), 1.82(H15')) of an ethyl group attached to δ_C 98.1(C6). Thus, the core carbon connectivity of the ring, C1 through C6, was established.

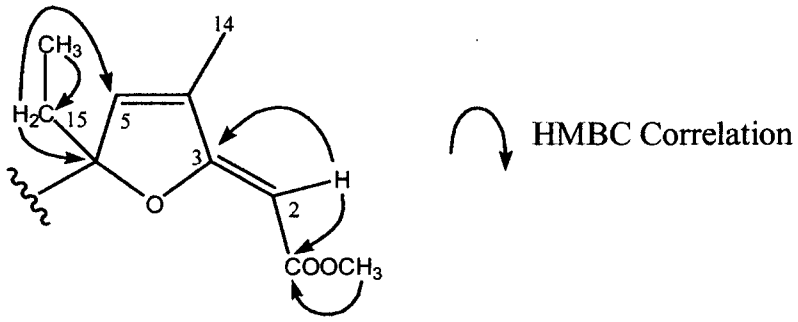

Figure 3.3.7 Selected HMBC Correlations for Compound **37**: Fragment **A**

The stereochemistry of the C2-C3 double bond was determined to be Z based upon a selective 1-D gradient NOESY spectrum (**Figure 3.3.8**). By pulsing the proton at 4.79 ppm (H2) a nuclear overhauser enhancement was seen for the methyl protons at 1.83 ppm (H14) indicating that they were on the same side of the double bond.

The five-membered ring was formed by placing an ether-type linkage between the quarternary carbon, δ_C 98.1(C6), and the olefinic carbon, δ_C 172.3 (C3). The quarternary carbon at δ_C 98.1(C6) would be consistent with an oxygen bearing quartnerary carbon bonded to an olefin. Interestingly, at 172.3 ppm, C3 was downfield of the carbonyl carbon, δ_C 166.9 (C1). As can be seen in **Figure 3.3.9**, there are three resonance contributors to the proposed ring system. Resonance structure **I** is thought to be the major resonance contributor as it would place a positive charge on C3, accounting for the deshielding of this carbon.

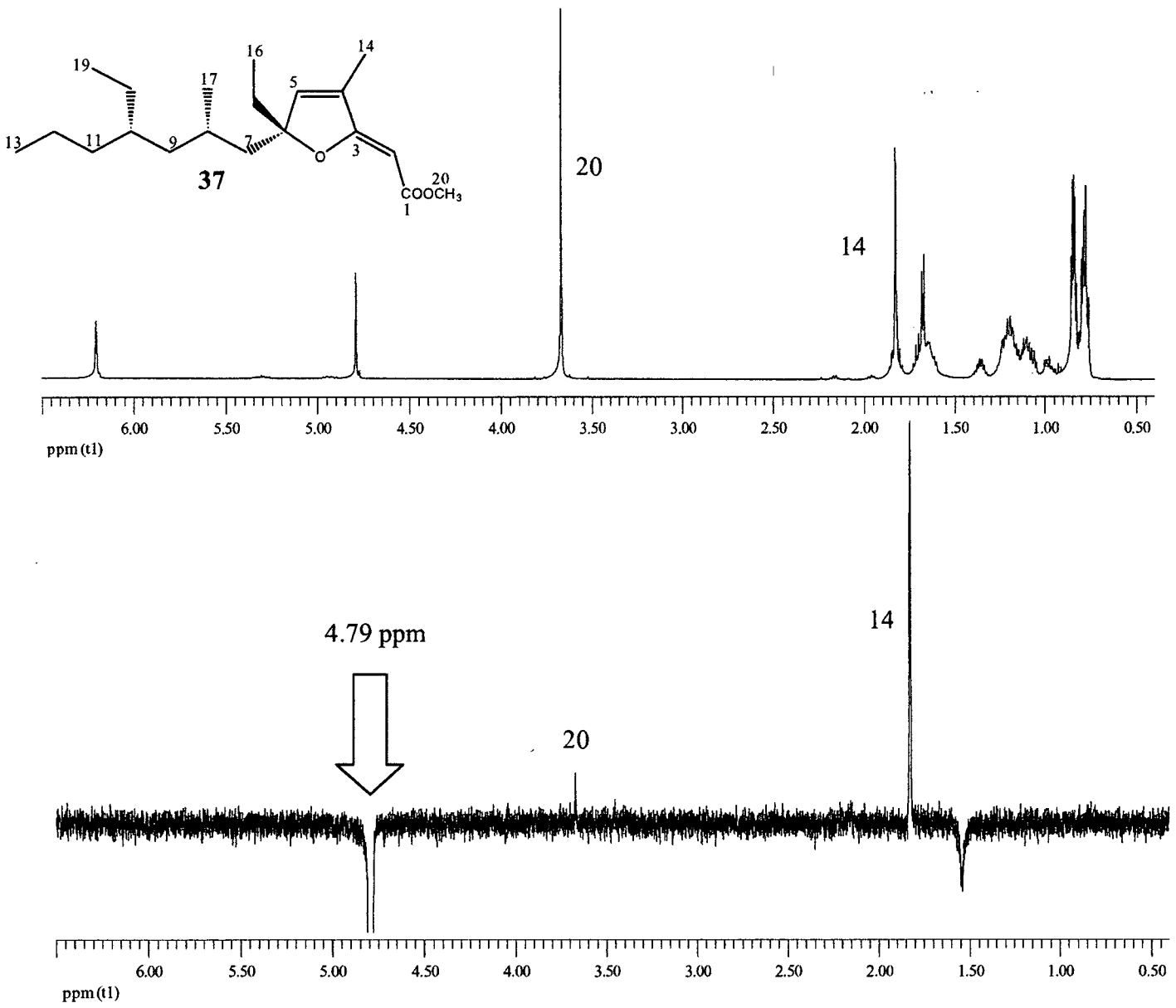

Figure 3.3.8 Selective Gradient 1-D NOE (400 MHz, $CDCl_3$) of **37**

Furthermore, resonance structure **I** would be the most stable possessing a tertiary carbon bearing a positive charge stabilized by an adjacent anionic oxygen. By comparison, resonance structure **III** has greater charge separation and the positive charge is located on a secondary carbon, C5, which causes **III** to be less energetically favourable than **I**. Resonance structure **II** places a positive charge on the oxygen attached to C3. Theoretically this positively charged oxygen could be stabilized by the adjacent negatively charged oxygen attached to C2. This would result in an inductive effect that would destabilize the positive charge at C3. However, given the fact that the carbon chemical shift of C3 is well downfield at 172.3 ppm, the empirical data does not support resonance structure **II** as a major contributor. Thus, the rationale for the deshielding at C3 is based upon the electron withdrawing effects of the adjacent oxygen and the partial positive charge of C3, as shown by resonance structure **I**.

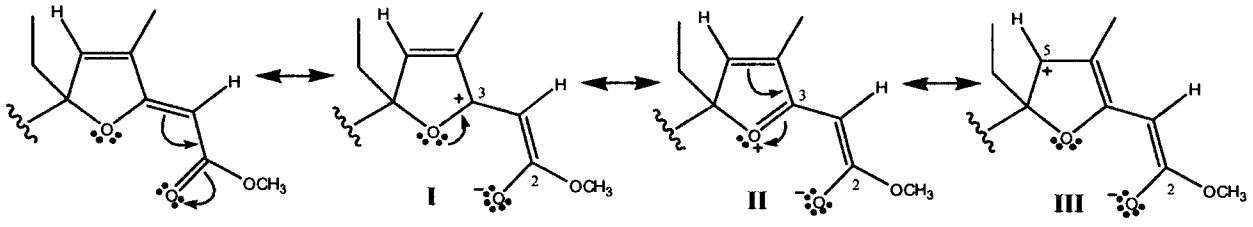

Figure 3.3.9 Resonance structures for Fragment A (**37**)

The existence of the two double bonds, one carbonyl, and the heterocycle in Fragment A satisfied the four degrees of unsaturation. From the mass spectrometry data it was obvious that ten carbons and twenty-one hydrogens remained to construct a saturated hydrocarbon chain (Fragment B). As with the cyclic peroxide polyketide chains from

Chapter 2, the key to elucidating the carbon chain for **37** lies in the strong HMBC correlations of the terminal methyls. Two triplets at δ_H 0.79 (δ_C 10.7 (C19)) and δ_H 0.84 (δ_C 14.6 (C13)), and one doublet at δ_H 0.84 (δ_C 21.7 (C17)) indicated the main chain must possess one methyl group and one ethyl group branch. HMBC correlations (**Figure 3.3.10**) from δ_H 0.79 (H19) to the methylene carbon at δ_C 26.3 (C18) and the methinic carbon at δ_C 36.0 (C10) established the ethyl branch carbons as δ_C 10.7 (C19), 26.3 (C18) extending from the main chain at δ_C 36.0 (C10). The methyl branch protons δ_H 0.84 (H17) showed HMBC correlations into the methine carbon at δ_C 26.1 (C8) and two methylene carbons at δ_C 43.0 (C8) and δ_C 45.1 (C7). Furthermore, the remaining methyl carbon, δ_C 14.6 (C13), corresponded to the terminus of the main carbon chain. These terminal methyl protons, δ_H 0.84 (H13), had HMBC correlations into to methylene carbons δ_C 19.5 (C12) and δ_C 35.4 (C13). These correlations accounted for all the carbons and hydrogens remaining, giving three pieces to be put together.

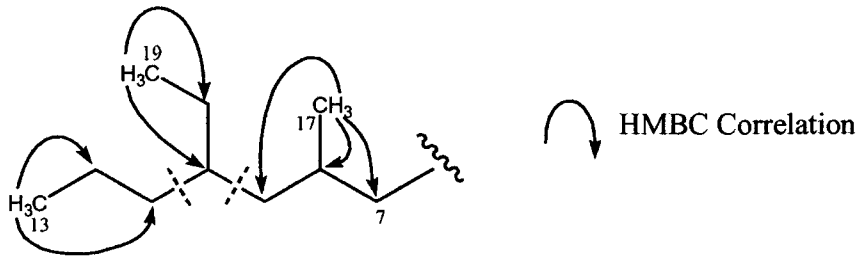

Figure 3.3.10 Methyl HMBC Correlations for Compound **37**: Fragment **B**

The three sub-fragments were attached based upon HMBC correlations (**Figure 3.3.11**) into the central methine carbon at δ_C 36.0 (C10). The geminally coupled methylene protons δ_H 0.97, 1.07 (H9, H9') showed two-bond correlations into the methine carbon at δ_C 36.0 (C10). In addition, the methylene protons at δ_H 1.11 (H11) had an HMBC correlation

into the methine carbon at δ_C 36.0 (C10) and they had a three-bond COSY correlation to the methine proton at δ_H 1.19 (H10). These correlations were important as they clarified the ordering of the carbons of the main chain as δ_C 45.1 (C7), δ_C 26.1 (C8), δ_C 43.0 (C9), δ_C 36.0 (C10), δ_C 35.4 (C11), δ_C 19.5 (C12), and δ_C 14.6 (C13).

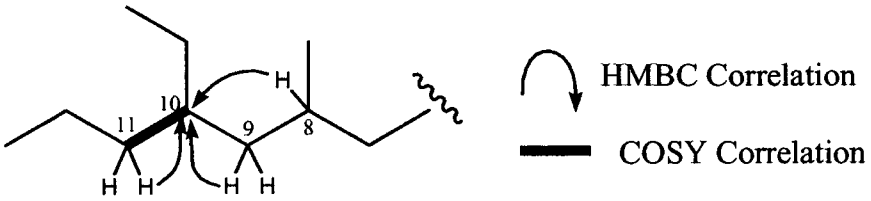

Figure 3.3.11 Selected HMBC and COSY Correlations for Compound **37**: Fragment **B**

Fragment A and fragment B could only be joined by a covalent bond between the carbon at δ_C 98.1 (C6) and δ_C 45.1 (C7). In support of this connectivity are two HMBC correlations (**Figure 3.3.12**). The methine proton δ_H 1.36 (H8) correlates to the carbon δ_C 98.1 (C6). In addition, the methylene protons δ_H 1.68 (H7) correlate to the carbon δ_C 32.0 (C15). Hence, the gross structure of **37** was established.

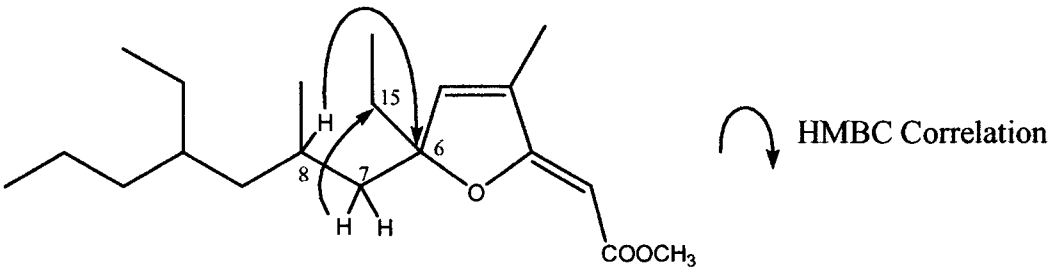

Figure 3.3.12 Selected HMBC Correlations for Compound **37**

3.4 Structure Elucidation of Glánvillic Acid B (38)

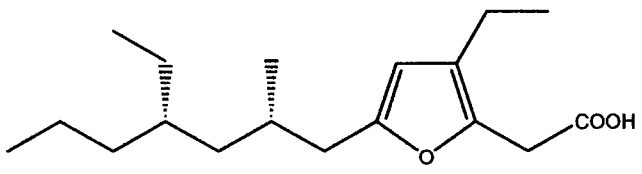

38

Compound **38** was isolated as an optically active, clear oil, that gave a negative mode HRESIMS $[M-H]^-$ peak at m/z 293.2121 appropriate for a molecular formula of $C_{18}H_{30}O_3$ (calc'd 293.2117 for $C_{18}H_{29}O_3$). Accordingly, **38** had four degrees of unsaturation. The ^{13}C NMR (**Figure 3.4.1**), ^1H NMR (**Figure 3.4.2**), and HSQC (**Figure 3.4.3**) spectra revealed four methyl carbons, six methylene carbons, two methine carbons (δ_C 30.0, 36.0) and one olefinic carbon (δ_C 107.7). By HMBC data three additional olefinic (δ_C 124.5, 139.5, 154.5) carbons and one carbonyl carbon (δ_C 172.2) were seen. Two fragments, a furan ring and a carbon chain, were constructed and connected based upon COSY (**Figure 3.4.4**) and HMBC (**Figure 3.4.5**) spectra to provide the gross structure of compound **38**. A detailed summary of the 1- and 2-D NMR spectroscopic data is listed in **Table 3.4.1**.

Table 3.4.1 ^{13}C and ^{1}H NMR Data for **38**

C#	^{13}C δ, ppm[a]	^{1}H δ, ppm (Int., m, J(Hz))[b]	COSY	HMBC
1	172.2[c]			H2
2	31.6[c]	3.60 (2, br s)	H5	
3	139.5[c]			H2, H5, H14
4	124.5[c]			H2, H5, H14, H15
5	107.7	5.85 (1, br s)	H2	H7, H7', H14
6	154.5[c]			H7, H7'
7	35.9	2.50 (1, dd, 14.8, 5.7)	H7'	H9, H9', H16
7'		2.32 (1, m)	H7	
8	30.0	1.82 (1, m)	H7, H7', H9, H9' H16	H7, H7', H9, H9', H16
9	41.0	1.16 (1, m)	H8, H9'	H7, H7', H16
9'		1.04 (1, m)	H8, H9	
10	36.0	1.31 (1, m)		H9, H9', H18
11	35.4	1.17 (2, m)		H13
12	19.4	1.22 (2, m)	H13	H13
13	14.5	0.85 (3, t, 6.9)	H12	
14	18.0	2.32 (2, q, 7.5)	H15	H15
15	14.7	1.11 (3, t, 7.5)	H14	H14
16	20.1	0.85 (3, d, 6.6)	H8	H7, H7'
17	26.4	1.27 (2, m)	H18	H9, H9', H18
18	10.8	0.81 (3, t, 7.3)	H17	

[a]Recorded at 100 MHz, calibrated to the $CDCl_3$ ^{13}C δ of 77.0 ppm
[b]Recorded at 500 MHz, calibrated to the $CDCl_3$ ^{1}H δ of 7.24 ppm
[c]^{13}C δ recorded from HSQC and HMBC data

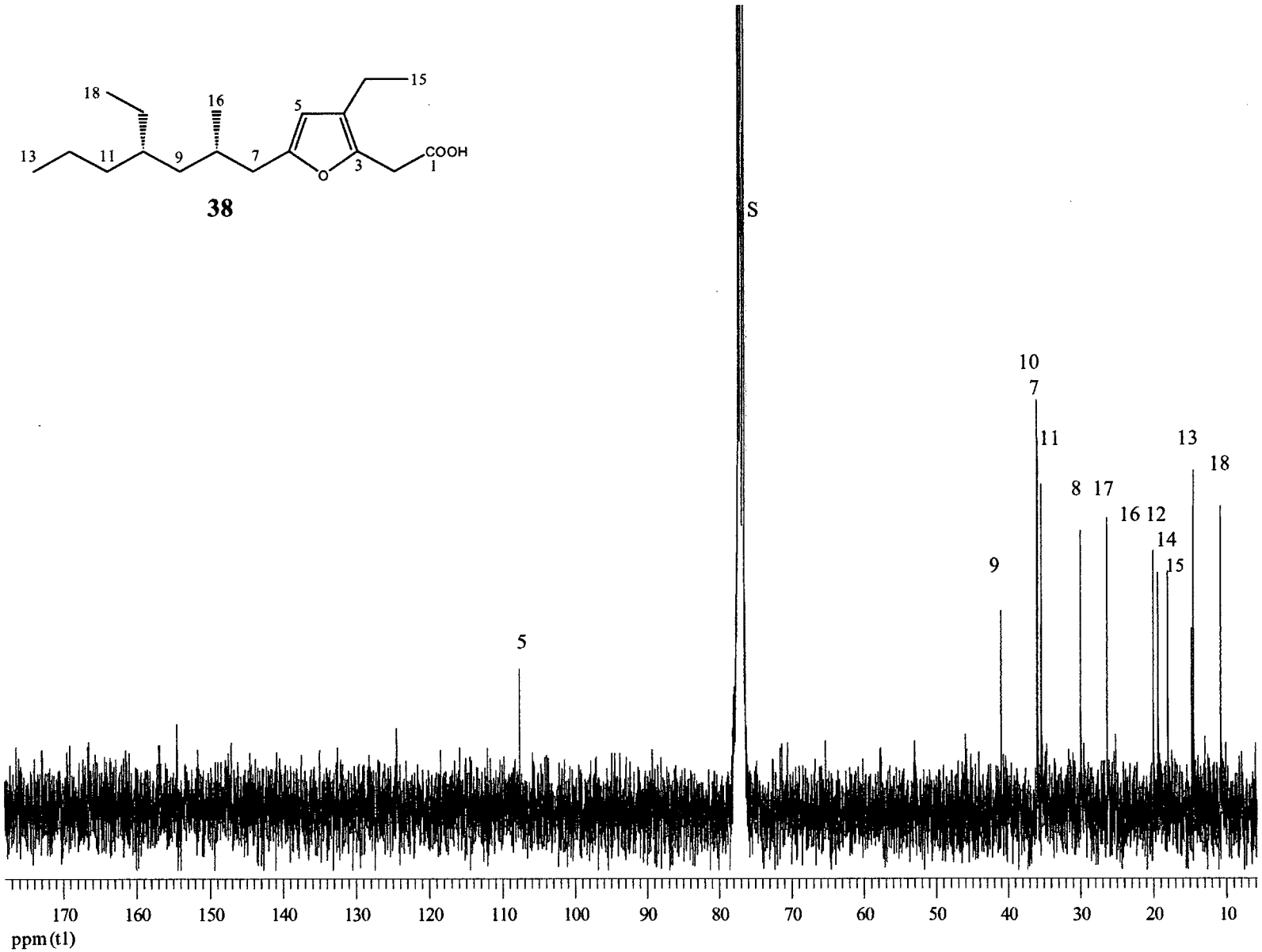

Figure 3.4.1 ^{13}C Spectrum (100 MHz, $CDCl_3$) of **38**

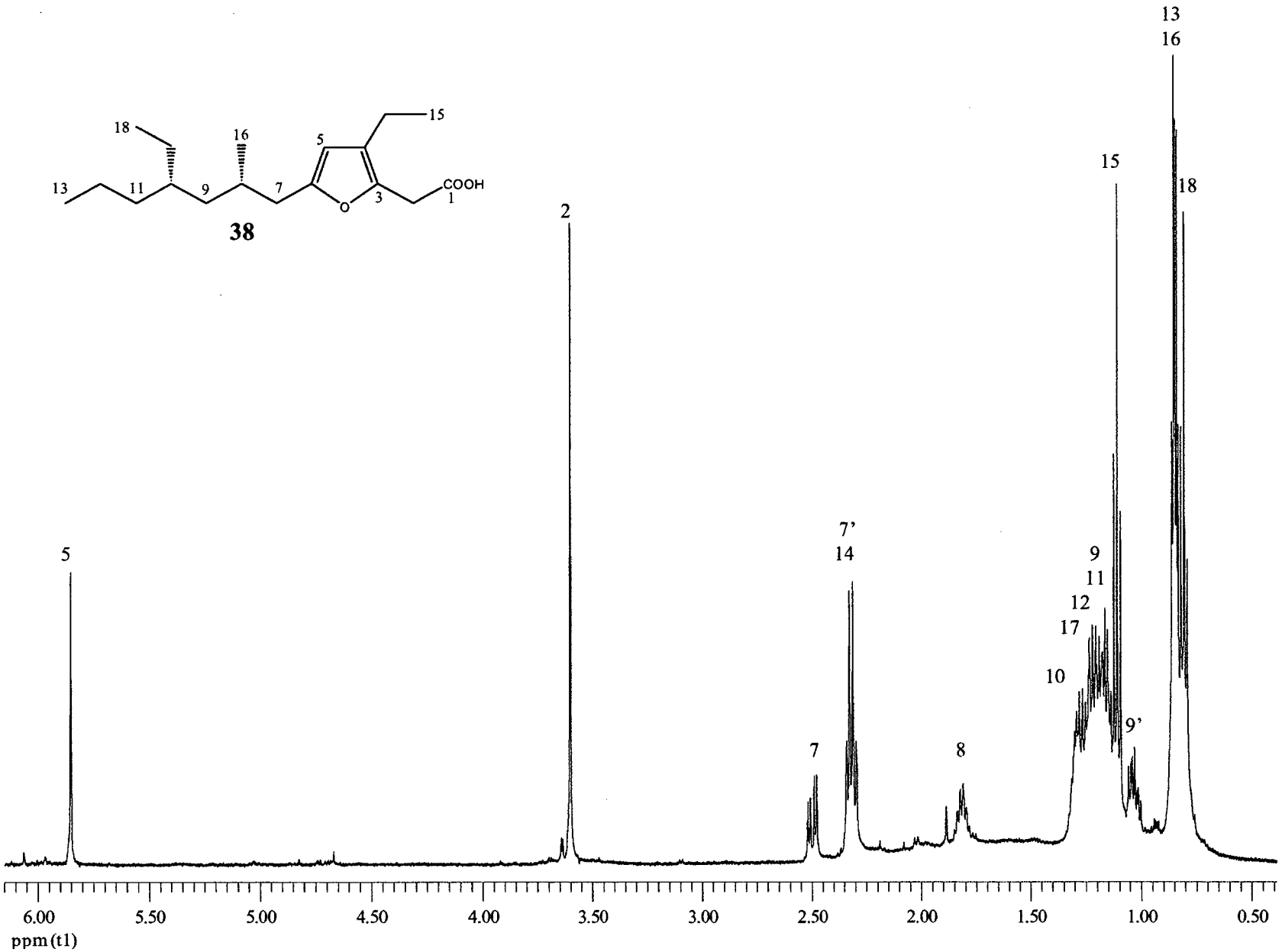

Figure 3.4.2 ^{1}H Spectrum (500 MHz, $CDCl_3$) of **38**

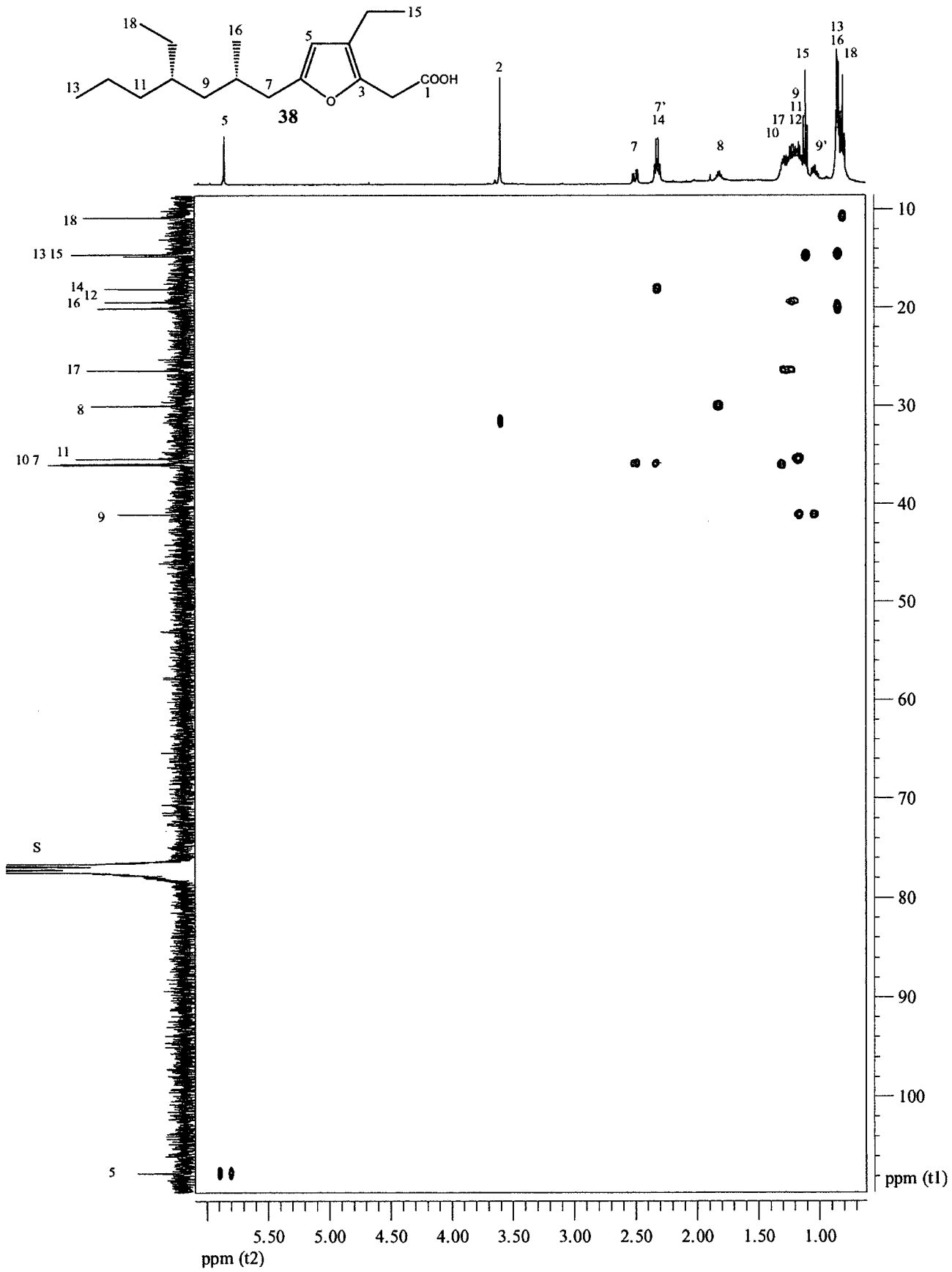

Figure 3.4.3 HSQC Spectrum (400 MHz, $CDCl_3$) of **38**

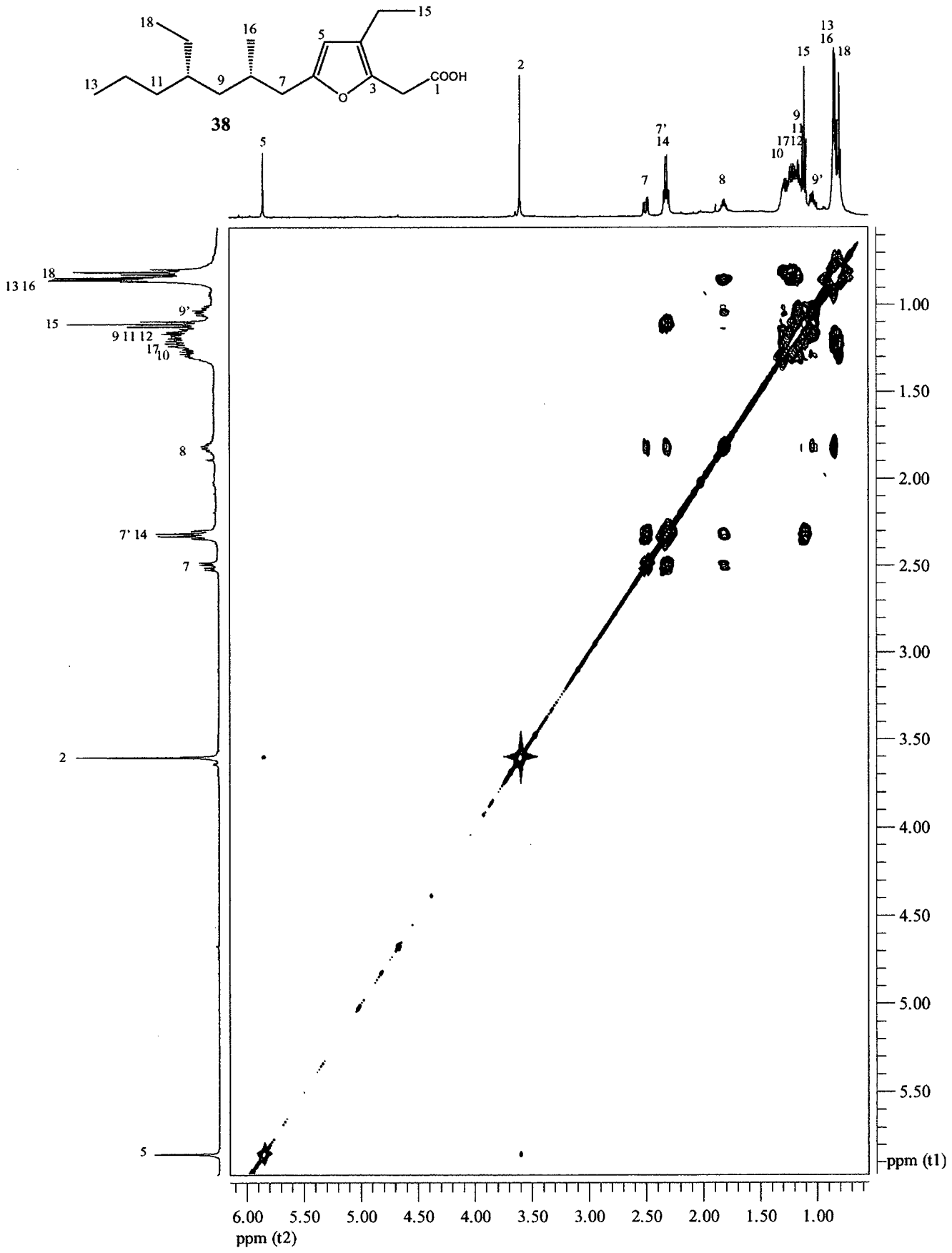

Figure 3.4.4 COSY Spectrum (500 MHz, $CDCl_3$) of **38**

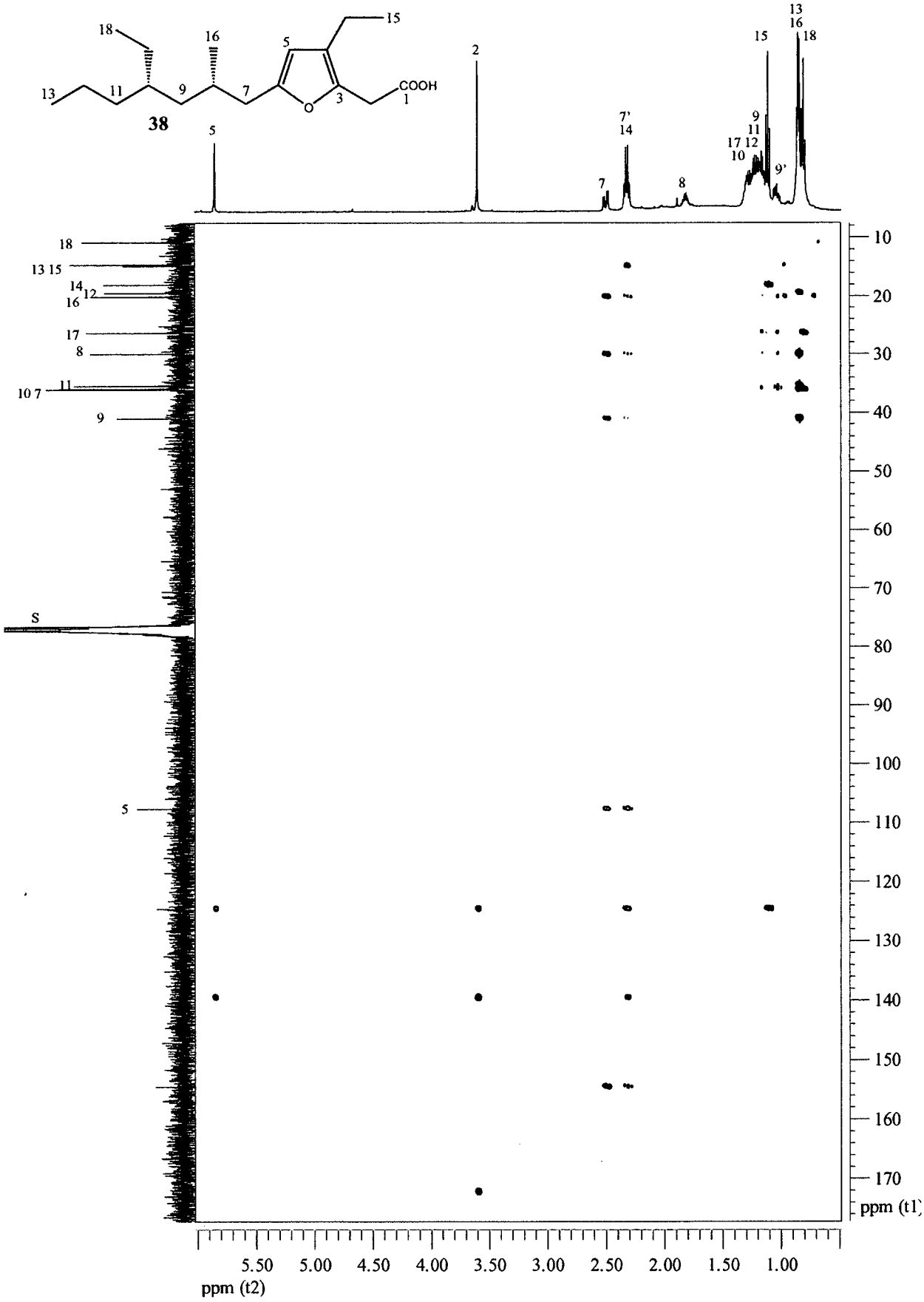

Figure 3.4.5 HMBC Spectrum (500 MHz, $CDCl_3$) of **38**

Due to the limited amount of material, not all of the carbons displayed signals in the ^{13}C spectrum, presumably as a result of low isotopic abundance and long relaxation times. Consequently, five carbon chemical shifts (δ_C 31.6, 124.5, 139.5, 154.5, 172.2) could only be assigned based upon HMBC correlations. The ring moiety, Fragment A, was completely assigned based upon the HMBC data collected (**Figure 3.4.6**). Starting with the broad singlet resonance at δ_H 5.85 (δ_C 107.7 (C5)), HMBC correlations were seen for olefinic carbons at δ_C 124.5 (C4) and 139.5 (C3). By further inspection of the HMBC spectrum, an ethyl branch was found to be substituted at δ_C 124.5 (C4) and an acyl group was attached to δ_C 139.5 (C3). The question remained which of the carbons of δ_C 124.5 (C4) and 139.5 (C3) was bonded directly to δ_C 107.7 (C5). An HMBC correlation between δ_H 2.32 (H14) and δ_C 107.7 (C5) indicated that the carbon bearing the ethyl group, δ_C 124.5 (C4), was directly bonded to δ_C 107.7 (C5). Additional correlations of the methylene protons 2.50 (H7), δ_H 2.32 (H7') (δ_C 35.9 (C7)) into δ_C 107.7 (C5) and 154.5 (C6) established the final carbons of the ring C3-C6. A 2,3,5-trisubstituted furan ring could then be formed.

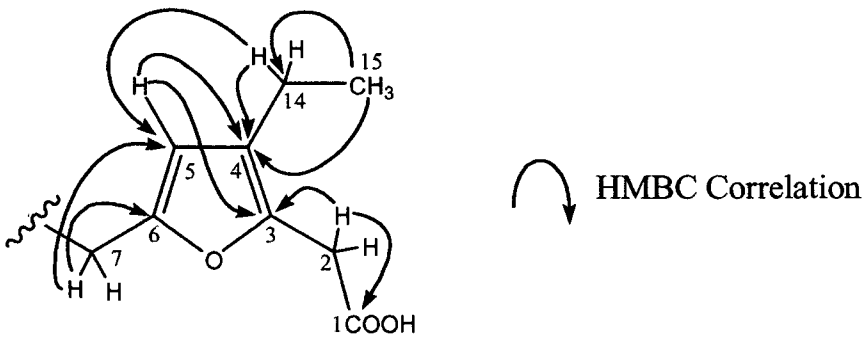

Figure 3.4.6 Selected HMBC Correlations for Compound **38**: Fragment A

Having satisfied all four degrees of unsaturation, a fully saturated chain (Fragment B) was constructed, beginning with the methylene carbon (δ_C 35.9 (C7)) attached directly to the ring moiety. As can be seen in **Figure 3.4.7**, two HMBC correlations for each of the geminal protons at 2.50 (H7) and δ_H 2.32 (H7') into the methinic carbon at δ_C 30.0 (C8) and the methylene carbon at δ_C 41.0 (C9). Further HMBC correlations from the methyl protons at δ_H 0.85 (C16) into the carbon at δ_C 35.9 (C7) indicated that the methine carbon, δ_C 30.0 (C8), must be bonded directly to the methyl and to the carbon with the chemical shift of δ_C 35.9 (C7). This clarified the ordering as C7/C8/C9, with a methyl branch as C16 from C8.

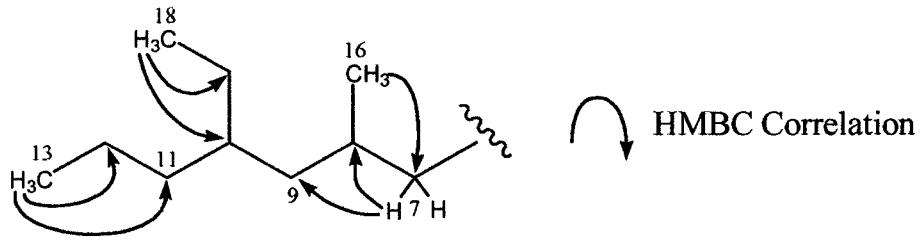

Figure 3.4.7 Selected HMBC Correlations for Compound **38**: Fragment B

The methyl carbon at δ_C 14.5 (C13) showed HMBC correlations into two methylene carbons (δ_C 19.4 (C12) and δ_C 35.4 (C11)), whereas the methyl carbon at δ_C 10.8 (C18) showed HMBC correlations into a methylene carbon (δ_C 26.4 (C17)) and a methine carbon at δ_C 36.0 (C10). By a COSY correlation between δ_H 0.81 (H18) and δ_H 1.27 (H17) it was decided that the methyl at δ_C 10.8 (C18) was part of an ethyl group which branched from the main chain at the methine carbon δ_C 36.0 (C10).

This resulted in a carbon chain that possesses the same connectivity as the saturated hydrocarbon chains seen in compounds **32** and **37**. As no HMBC or COSY correlations could

aid in assigning the order of the two methylene carbons, C11 and C12, near the terminus of the main chain, it was necessary to compare the carbon chemical shifts. By comparison of the chemical shift data, the order of the methylene carbons was found to be δ_C 35.4 at C11 and δ_C 19.4 at C12. This was consistent with the previous analysis of spectroscopic data for compounds **32** and **37**, but inconsistent with the ordering of these two compounds for the previous isolation of methyl glánvillate B. In the characterization of methyl glánvillate B, C11 was assigned a shift of δ_C 19.5 and C12 was given a chemical shift of δ_C 35.5, opposite to the current assignment. No mention of the rationale for the assignment of these carbons was given in the paper. Running a ^{13}C NMR simulation for **38** with ACD/CNMR Predictor® software (v.7.05) gave chemical shifts of δ_C 35.5 for C11 and δ_C 19.5 for C12. Based upon this result and in keeping with the assignments of compounds **32** and **37**, C11 was assigned as δ_C 35.4 and C12 as δ_C 19.4. Thus, the full assignment of compound **38** was completed.

3.5 Proposed Stereochemistry and Biosynthesis of Structures 37 and 38

As previously mentioned in the General Introduction, *Plakortis* furano polyketides are thought to be derived from cyclic peroxide polyketides. Both Faulkner *et al.*[42] and Fattorusso *et al.*[53] have biosynthetically rationalized the stereochemistry of furan polyketides based upon the stereochemistry of their parent cyclic peroxide polyketides. In a similar fashion, the current study proposes the stereochemistry of the furano polyketides, **37** and **38,** based upon their hypothetical cyclic peroxides precursors. The cyclic peroxide precursors of **37** and **38**, shown in **Scheme 3.5.1**, would follow the same biosynthetic pathway as cyclic peroxides **32** and **33** discussed in section **2.5**. Hence, it is reasonable to assume the stereochemistry of the cyclic peroxide precursors for **37** and **38** would be the same as **32** and

33. In **Scheme 3.5.1** two cyclic peroxides are shown, the methyl ester as precursory to **37** and the free acid as precursory to **38**. Possibly the methyl ester is formed by the action S-adenosyl methionine upon the free acid. In both cases, abstraction of an α-proton from the cyclic peroxide opens the ring and forms an epoxide intermediate. Intramolecular attack on

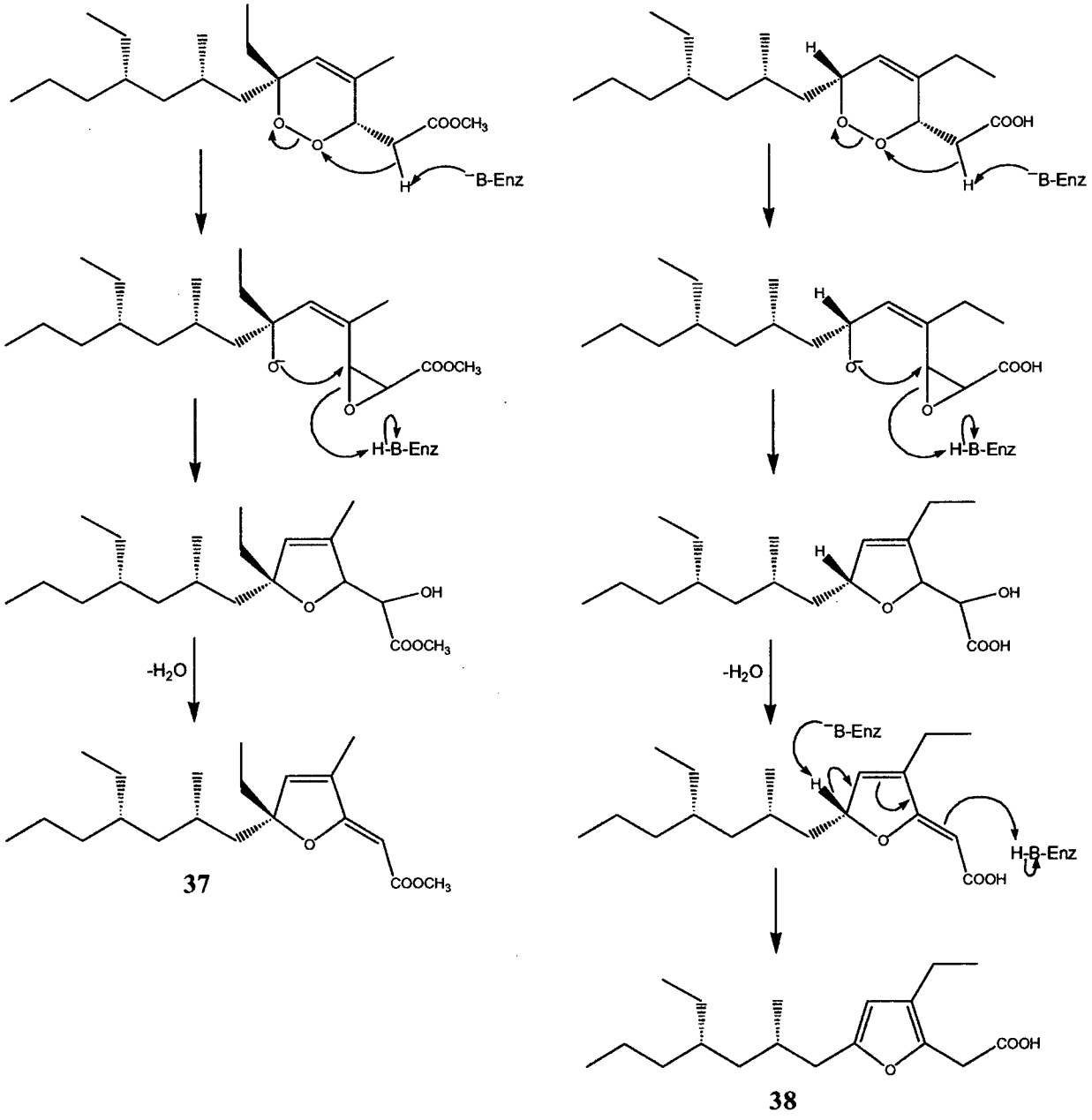

Scheme 3.5.1 Proposed Biosynthesis of Compounds **37** and **38** from Cyclic Peroxides

the epoxide by the anionic oxygen would form the furano type ring system. Loss of H_2O would produce the final conjugated structure of the furano polyketide, **37**. Addition of a proton at position two and abstraction of the proton at position six produces the furan ring in compound **38**. In this manner, it is proposed that the two furan polyketides are methyl (2Z,6R,8S,10S)-6,10-diethyl-4,8-dimethyl-3,6-epoxytrideca-2,4-dienoate (**37**) and (8S,10S)-4,10-diethyl-3,6-epoxy-8-methyltrideca-3,5-dienoic acid (**38**, glánvillic acid B).

3.6 Conclusion

At the time of this study, only five other compounds have been isolated with a similar α,β-unsaturated furano ester ring system like compound **37**. None of these related compounds possess a methyl group attached to the ring at position four nor do they bear the same carbon chain. Glánvillic acid B (**38**) was previously isolated in its methyl ester form via synthetic modification. This study represents the first time glánvillic acid B was isolated in its free acid form. Only glánvillic acid A, which has one degree of unsaturation in its carbon chain, shares the same 2,3,5-trisubstituted furan structure. In addition, glánvillic acids A & B were originally isolated from the Dominican sponge, *Plakortis halichondrioides*, which is of different species than *Plakortis angulospiculatus,* the sponge from which glánvillic acid B (**38**) was isolated in the current study.

Interestingly, compounds **37** and **38** possess identical carbon chains, in terms of their connectivity, as compounds **32** and **33**. It is very likely that the methyl and ethyl substituents on the carbon chains of compounds **37** and **38** are in a *syn* orientation, as was proposed for compounds **32** and **33**. Further stereochemical investigations would need to be conducted to fully prove the absolute configuration of compounds **37** and **38**.

CHAPTER 4 General Discussion

4.1 Comparison of the Polyketide Biosynthesis for Compounds 32, 33, 37, and 38

The rich structural diversity of polyketides stems from slight differences in the assembly of small carbon units by the polyketide synthases and further modifications to the resulting carbon chain. Different combinations of acetate, propionate, and butyrate units, along with variations in the starter unit, produce linear carbon chains that are released from the PKS complex of enzymes. Post-polyketide synthase modifications allow for the introduction of many structural features, including rings and functional groups. This structural diversity results in a wide range of potent biological activities that has led to important drugs, such as the previously mentioned antifungal drug, amphotericin B.

As can be seen with the structures of **32**, **33**, **37**, and **38** (**Scheme 4.1.1**), differences in the ordering of acetate, propionate, and butyrate units leads to structural diversity. Compounds **32**, **37**, and **38** share a similarly branched carbon chain. Accordingly, the first three units assembled by the PKS would be propionate-butyrate-propionate for **32**, **37**, and **38**. The extension by one extra carbon in the chain of **33** would be consistent with a butyrate starter unit, instead of a propionate residue. Structures **32** and **33** have an identical ordering of units after their respective starter units. The ethyl branch attached to the quaternary carbon of the ring in compounds **32**, **33**, and **37** is derived from a butyrate placed as the fourth residue. By comparison, structure **38** has an acetate residue where the other three compounds have butyrates. The ethyl branch attached to the double bond of the rings in compounds **32**, **33**, and **38** is derived from a butyrate placed as the fifth residue. By comparison, structure **37**

has a propionate unit as the fifth residue, giving a methyl branch. All of the compounds terminate with an acetate residue.

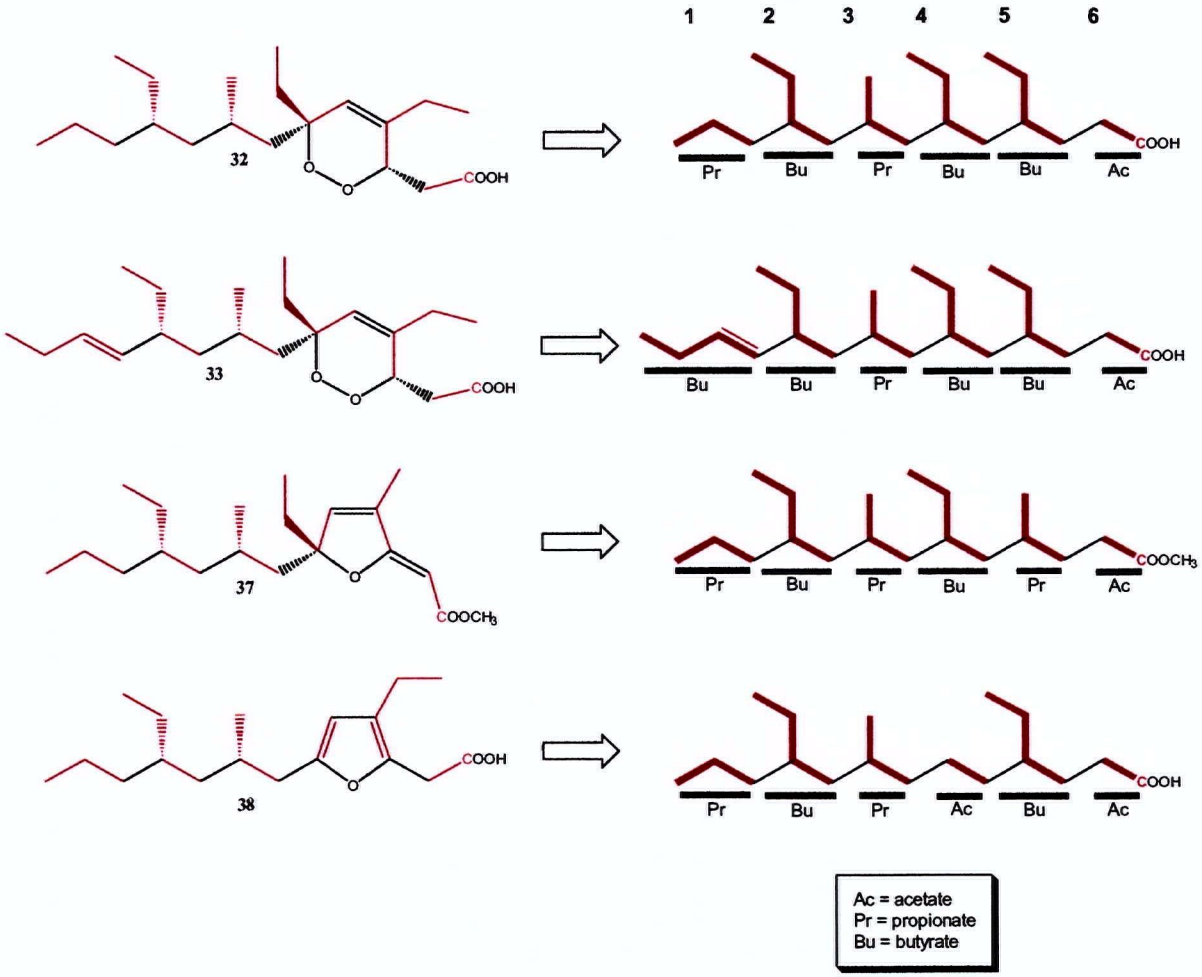

Scheme 4.1.1 Polyketide Linear Chain Representations for **32, 33, 37,** and **38**

It is proposed that all the structures shown are converted into cyclic peroxides as either their final structure or as a transitory intermediate (**Scheme 4.1.2**). Compounds **32** and **33** would be converted directly into their final cyclic peroxide forms via the enzymatic incorporation of oxygen, as shown previously in **Scheme 2.5.2** (pg. 52). Compound **37** would go one step further, by conversion of its six-membered peroxide ring into a furano structure according to **Scheme 3.5.1** (pg. 77). With formation of a methyl ester, possibly through the

action of S-adenosyl methionine, compound **38** would be converted from a furano to its furan form by abstraction of the proton from the methinic carbon of the ring, as according to **Scheme 3.5.1** (pg. 77). The comparison of these compounds highlights some of the structural differences that arise in polyketide biogenesis. It is from this structural variance of polyketides that results in a great diversity of biological activity.

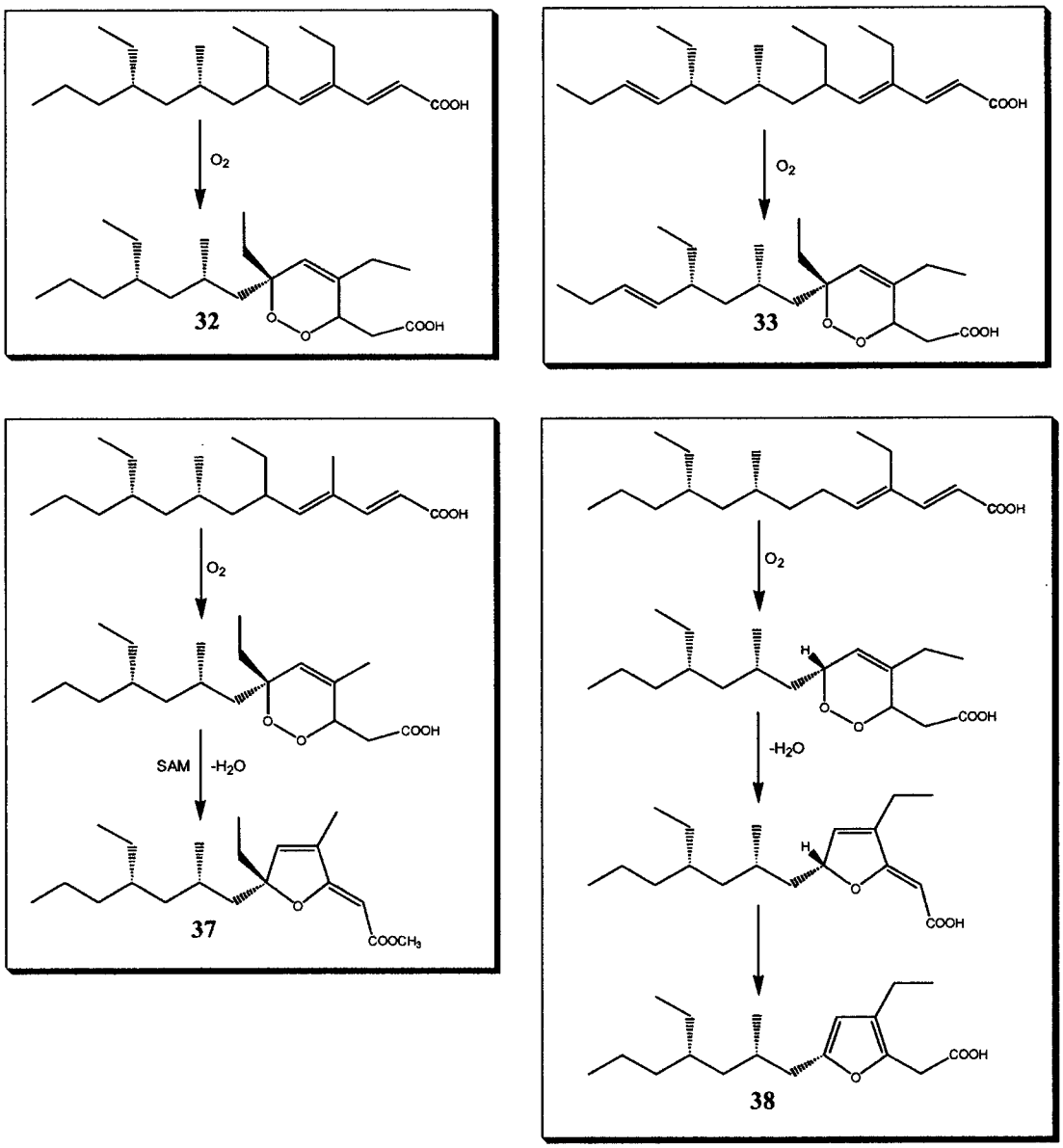

Scheme 4.1.2 Proposed Biosynthetic Schemes for Compounds **32, 33, 37,** and **38**

4.2 Chemical Genetic Profiling of Marine Invertebrate Extracts

The cluster plot, shown in **Figure 4.2.1**, displays the haploid mutant, chemical-genetic profiles for 17 compounds of known action, two compounds of unknown action, and the crude extracts of five marine invertebrates. Dr. Charlie Boone's lab (U of T) tested ~4500 yeast haploid deletion mutants strains in parallel for sensitivity or resistance to particular compounds. Compounds and extracts are clustered on the horizontal axis of this fitness test profile based upon the similarity of their signatures. Yeast strains that are sensitive to the compound or extract are represented in red, those that are resistant are represented in green, and those with no significant change are represented in black.

Table 4.2.1 Drugs in Fitness Test Profile

Abbreviation	Full Name	Mode of Action
Clot	Clotrimazole	ERG11 inhibitor (ergosterol biosynthesis)
FLC	Fluconazole	ERG11 inhibitor (ergosterol biosynthesis)
Gelda	Geldanamycin	Hsp90 inhibitor (chaperone)
Nocod	Nocodazole	Microtubule depolymerizing agent
Tuni	Tunicamycin	Alg7 inhibitor (protein glycosylation)
Thia	Thialysine	
SMM	Sulfometuron methyl	amino acid biosynthesis inhibitor
FK506	FK506	calcineurin inhibitor
Cyh	Cycloheximide	inhibits protein synthesis
Agel E	Agelasine E	unknown
Cyto	Cytochalasin A	Actin depolymerizing agent
BFA	Brefeldin A	inhibits secretion
CPT	Camptothecin	topoisomerase I inhibitor
MitoC	Mitomycin C	
Wort	Wortmannin	phosphatidyl inositol inhibitor
MMS	Methylmethane sulfonate	DNA damaging agent
CAS	Caspofungin	inhibits cell wall biosynthesis
Pap B	Papuamide B	unknown
Rapa	Rapamycin	inhibits protein translation and more

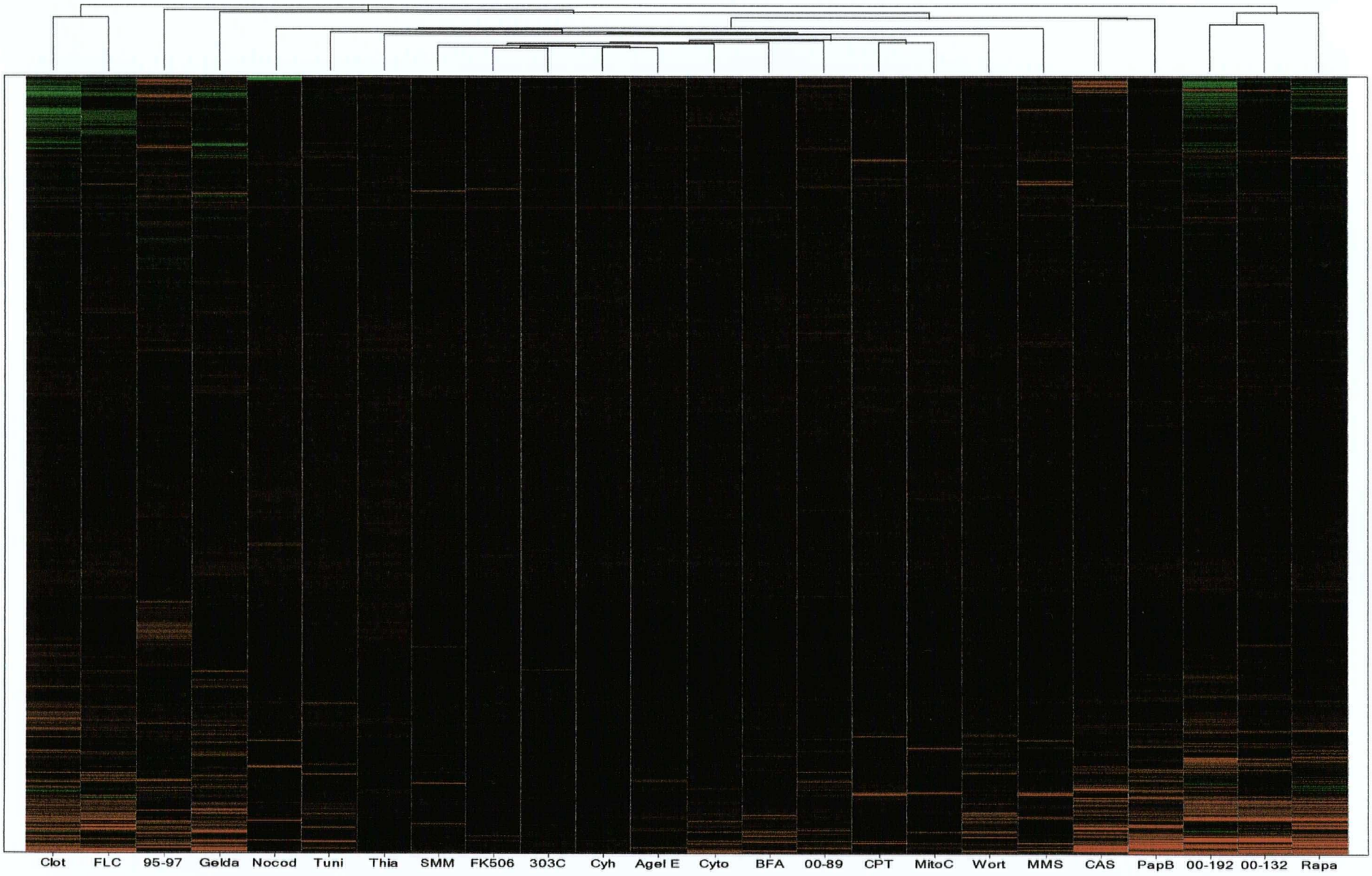

Figure 4.2.1 Haploid Deletion Mutant Fitness Test Profile

Table 4.2.2 Marine Invertebrate Extracts in Fitness Test Profile

Extract/Compound	Organism	Collection Location
00-303 (303C)	Sponge	Dominica
95-57	Sponge	Papua New Guinea
00-89	Sponge	Indonesia
00-132	Sea Cucumber	Dominica
00-192	Sponge	Indonesia

The profiles of fluconazole (FLC) and clotrimazole (Clot) cluster together (see tree dendrogram atop **Figure 4.2.1**). This is expected given that they target the same protein, in that both inhibit the product of *ERG11*, an essential gene in the yeast ergosterol biosynthesis pathway. **Figure 4.2.2** displays a scatterplot and an expanded portion of the chemical genetic profile for fluconazole and clotrimazole. Each strain is represented by a blue box whose

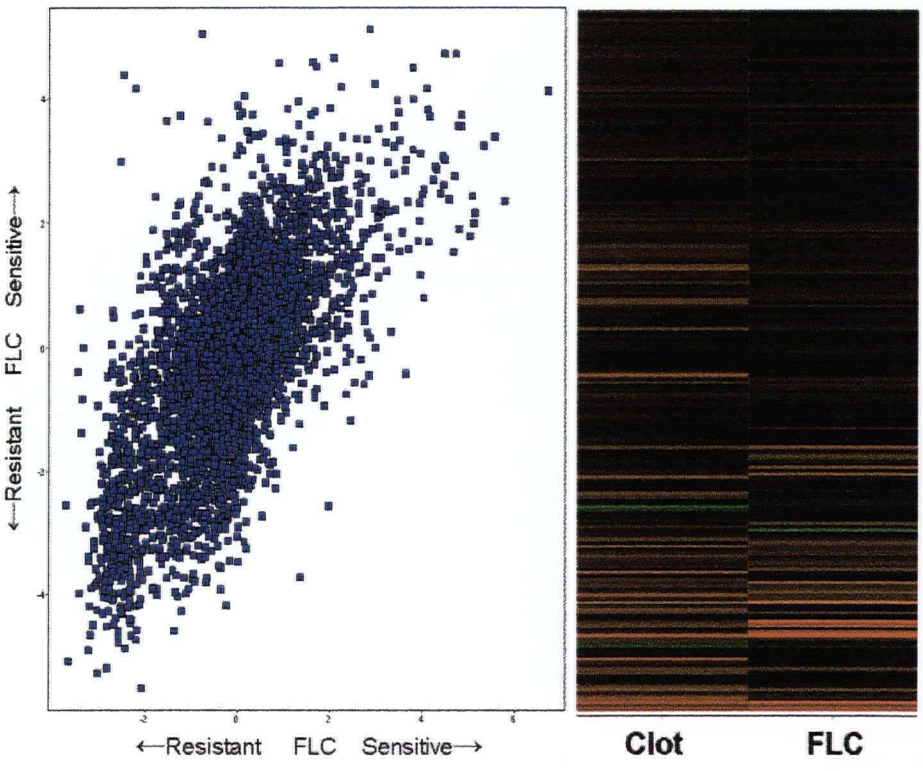

Figure 4.2.2 Scatterplot and Fitness Test Profile Expansion for Clotrimazole and Fluconazole

coordinates on the scatterplot are correlated with the degree to which each strain is resistant or sensitive to the two drugs. The majority of strains that showed no sensitivity or resistance are found together around the coordinates (0,0) on the scatterplot. These strains would be shown in black on the on the profile shown to the right of **Figure 4.2.2**. The upper right quadrant of the scatterplot shows the strains that are significantly sensitive to both drugs. Although the correlations in the chemical genetic profile aren't as obvious at first sight, statistical analysis of the scatterplot shows a significant correlation between the profiles of the two drugs. Based upon this correlation of sensitive strains it is deduced that clotrimazole and fluconazole inhibit similar pathways and have the same cellular target.

In the case of fluconazole and camptothecin (**Figure 4.2.3**), the lack of correlation between the profiles of fluconazole, an inhibitor of ergosterol biosynthesis, and the profile of

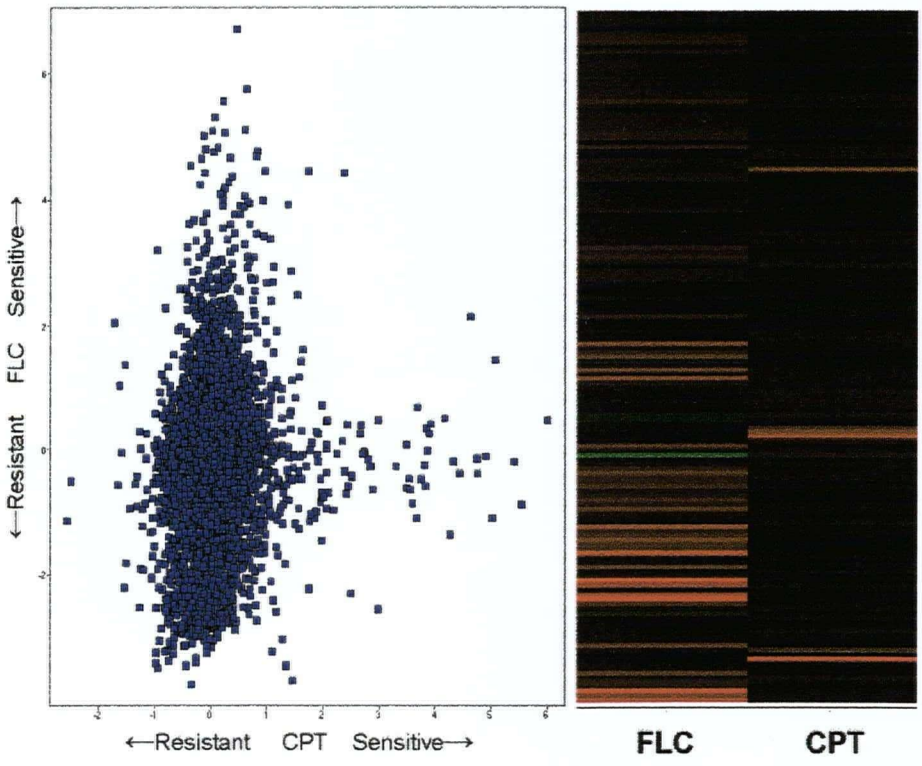

Figure 4.2.3 Scatterplot and Fitness Test Profile Expansion for Fluconazole and Camptothecin

camptothecin, a topoisomerase inhibitor, can clearly be seen. Both the scatterplot and the chemical genetic profile expansion show a lack of correlation. The scatterplot shows the most sensitive strains for either compound are not the same. This is echoed in the profile where the most intensely red bands (the most sensitive strains) do not correspond to one another.

The crude extract of from the sponge *Plakortis angulospiculatus* (00-303), albeit very potent against *C. albicans* and *S. cerevisiae*, gave a non-specific profile. Few yeast strains were shown to be sensitive in the fitness test profile (**Figure 4.2.1**) of the crude extract of 00-303. Those strains that were sensitive to the extract often showed general, non-specific drug sensitivity. In addition, the extract of 00-303 did not show any specificity in a haploinsufficiency assay. It was hoped that by testing the purified compound **33**, by excluding the other secondary metabolites in the extract, the profile might be cleared of "noise" and reveal a specific target or pathway. This had never been attempted before with the cyclic peroxide class of polyketide compounds. Unfortunately, the results for **33** showed a similar profile to that of the crude extract 00-303 in both the haploid and heterozygote deletion assays. Hence, the crude 00-303 and compound **33** seem to target generally drug-sensitive strains of *S. cerevisiae*. This is consistent with the diverse biological activity listed in the literature for *Plakortis* cyclic peroxide polyketides.

Due to timing considerations, the sponge extract 00-303 was selected as an isolation project and as an archetype for the chemical genetic analysis of marine invertebrate extracts. The crude 00-303 was selected based upon its potency against *C. albicans* and *S. cerevisiae*. Although the crude extract did not show a specific fitness test profile, the isolation part of the project had already begun. Providing the purification was underway and the biological activity data was very strong, the isolation of the active compounds **32** and **33** was

completed. Later, it was discovered that two marine invertebrate extracts 00-132, from an Indonesian sponge, and 00-192, from a Dominican Sea Cucumber, showed intriguing fitness test profiles. They both displayed profiles strongly sensitive for a number of yeast strains, indicative of some mode of specificity. Interestingly, the two crudes possessed similar profiles to one another and, in turn, both of their profiles were similar to rapamycin (**Figure 4.2.4**). Rapamycin is a polyketide that targets the TOR proteins in yeast which are involved in regulating protein translation, as well as many other cellular processes. The initial assays of the extracts of 00-132 and 00-192 showed comparable activity against *C.albicans*, but considerably less than the extract of 00-303. At the time of this thesis, both of these extracts are under study to isolate the compounds responsible for this activity.

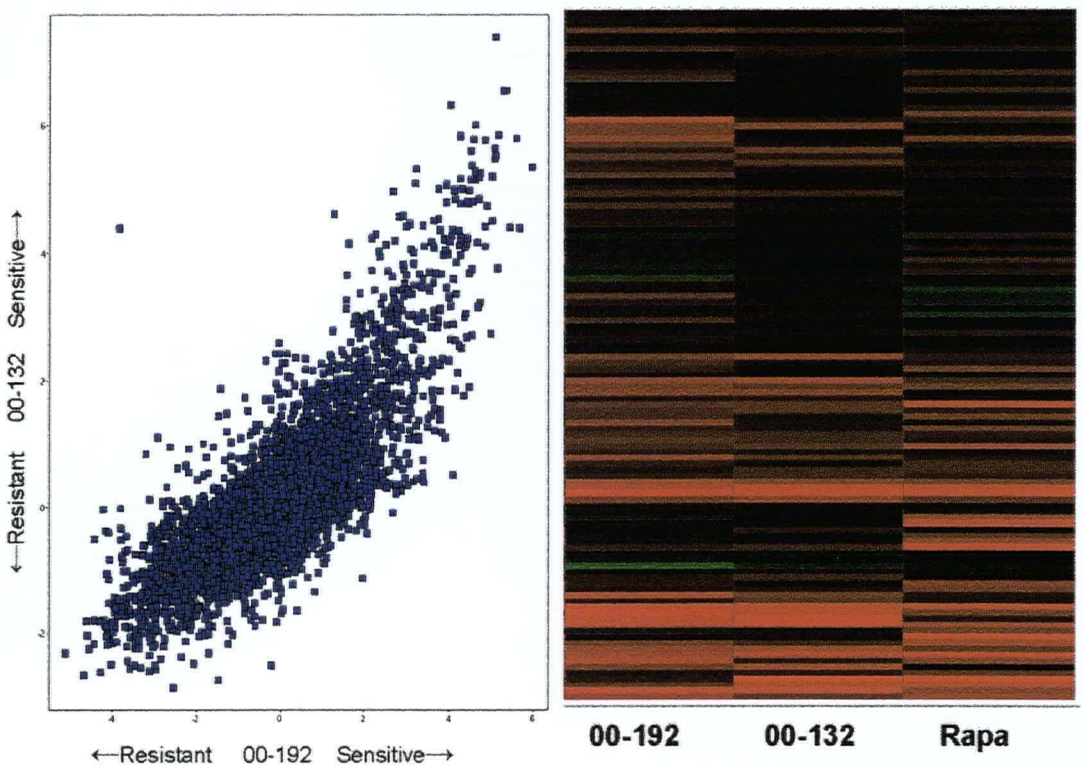

Figure 4.2.4 Scatterplot and Fitness Test Profile Expansion for Extracts 00-132 and 00-192

EXPERIMENTAL SECTION

General Experimental Procedures

One- and two-dimensional NMR spectra were recorded on either a 400 MHz Bruker Avance 400 spectrometer or a 500 MHz Bruker AMX-500, both housing a 5mm BBI-Z probe. One-dimensional ^{13}C spectra were recorded on a Bruker AM-400, with a normal 5mm probe, at 100 MHz. All samples were run in deuterated chloroform (99.96% isotopic purity) and NMR data was calibrated to the solvent signals of δ_H 7.24 ppm and δ_C 77.0 ppm. All NMR spectra were initially processed by XWIN-NMR® and, subsequently, processed on MestRe-C® (v.3.7.9) software for inclusion in this thesis. Electrospray ionization (ESI) mass spectrometry was run by staff in the UBC Mass Spectrometry Centre, Department of Chemistry, on a Bruker Esquire ion trap mass spectrometer.

All chromatography was performed using HPLC grade solvents, including doubly-distilled, 0.22 μm filtered H_20. Size exclusion chromatography used LH-20®, lipophilic sephadex, as a solid phase. Normal phase silica gel (230-400 mesh) was used in running flash columns. HPLC was performed using a Waters 2487 Dual λ Absorbance Detector and a Waters 1525 Binary HPLC Pump with Breeze® software. A CSC-Inertsil, 150A/ODS-2, 5μm reverse phase HPLC column was employed in the final purification of all compounds. Thin-layer chromatography (normal and reverse phase) was performed on commercial plates. Staining with 1% *p*-anisaldehyde, 2% H_2SO4 in acetic acid solution and visualization under UV light (254 nm) facilitated the identification of unknown compounds.

Biological testing against *Candida albicans* and bacterial pathogens was conducted in the department of Chemistry, UBC, by Helen Wright. Minimum inhibitory concentrations (MIC) were determined by an Alamar Blue® microdilution assay using Mueller-Hinton broth

with incubation at 37°C. Bioautographic assays were also done with the help of Helen Wright on 8 x 8 cm normal phase TLC plates, staining with MTT (thiazolyl blue). Haploinsufficiency profiling with *Saccharomyces cerevisiae* was performed by Ainslie Parsons in Dr. Charlie Boone's laboratory, Department of Biochemistry, University of Toronto.

Animal Material

The sponge *Plakortis angulospiculatus* (Carter, Homosclerophorida/Plakinidae) was collected by SCUBA, September 3, 2000, near Pennville, Dominica, 15° 37.4'N, 61°25.1'W. The sponge was found on vertical walls at a depth of 10 to 15 m and was described to be medium brown outside, tan inside. A voucher specimen has been deposited (museum # ZMAPOR 17723) in the Zoologisch Museum, University of Amsterdam.

Extraction of *P. angulospiculatus* and Isolation of Compounds 32, 33, 37, and 38

See Section 2.2 and 3.2 for isolation method.

32: clear oil; $[\alpha]^{23}_{D}$ = -37.8 (c 0.26, $CHCl_3$); ^{1}H NMR 0.81 (3, t), 0.86 (3, t), 0.87 (3, d), 0.88 (3, t), 1.00 (1, m), 1.07 (3, t), 1.08 (1, m), 1.15 (2, m), 1.23 (4, m), 1.40 (2, m), 1.52 (1, m), 1.63 (1, dq), 1.75 (1, dq), 2.01 (2, m), 2.61 (1, dd), 2.93 (1, dd), 4.57 (1, br d), 5.49 (1, br s); ^{13}C NMR 8.2, 10.8, 11.6, 14.6, 19.5, 22.4, 24.9, 26.0, 26.4, 31.0, 35.4, 36.1, 36.9, 42.9, 43.3, 76.2, 83.8, 125.3, 137.5, 175.2; positive ion HRESIMS $[M+Na]^+$ m/z 363.2505 (calc'd 363.2511 for $C_{20}H_{36}O_4Na$)

33: clear oil; $[\alpha]^{23}_{D}$ = -30.7 (c 0.25, $CHCl_3$); ^{1}H NMR 0.80 (3, t), 0.83 (3, d), 0.87 (3, t), 0.94 (3, t), 1.05 (1, m), 1.07 (3, t), 1.14 (1, m), 1.19 (1, m), 1.28 (1, m), 1.40 (2, m), 1.52 (1, m), 1.62 (1, dq), 1.73 (1, dq), 1.81 (1, m), 1.97 (2, m), 1.99 (2, m), 2.58 (1, dd), 2.92 (1, dd), 4.55(1, br d), 4.95(1, dd), 5.36(1, dt), 5.49(1, br s); ^{13}C NMR 8.1, 11.6, 11.7, 14.3, 21.3, 24.9, 25.7, 25.9, 28.9, 30.9, 36.8, 42.3, 43.3, 44.5, 76.3, 83.7, 125.3, 132.2, 133.2, 137.2, 175.4; positive ion HRESIMS $[M+Na]^+$ m/z 375.2502 (calc'd for375.2511 for $C_{21}H_{36}O_4Na$)

37: clear oil; $[\alpha]^{24}_{D}$ = - 104.2 (c 0.24, $CHCl_3$); ^{1}H NMR 0.78 (3, t), 0.79 (3, t), 0.84 (3, d), 0.84 (3, t), 0.97 (1, m), 1.07 (1, m), 1.11 (2, m), 1.19 (3, m), 1.21 (2, m), 1.36 (1, m), 1.68 (2, d), 1.70 (1, m), 1.82 (1, m), 1.83 (3, d), 3.67 (3, s), 4.79 (1, s), 6.21 (1, s); ^{13}C NMR 8.0, 10.7, 11.0, 14.6, 19.5, 21.7, 26.1, 26.3, 32.0, 35.4, 36.0, 43.0, 45.1, 50.5, 84.0, 98.1, 133.8, 141.6, 166.9, 172.3; positive ion HRESIMS $[M+Na]^+$ m/z 345.2415 (calc'd 345.2406 for $C_{20}H_{34}O_3Na$)

38: clear oil; ^{1}H NMR 0.81 (3, t), 0.85 (3, d), 0.85 (3, t), 1.04 (1, m), 1.11 (3, t), 1.16 (1, m), 1.17 (2, m), 1.22 (2, m), 1.27 (2, m), 1.31 (1, m), 1.82 (1, m), 2.32 (1, m), 2.32 (2, q), 2.50 (1, dd), 3.60 (2, br s), 5.85 (1, br s); ^{13}C NMR 10.8, 14.5, 14.7, 18.0, 19.4, 20.1, 26.4, 30.0, 31.6, 35.4, 35.9, 36.0, 41.0, 107.7, 124.5, 139.5, 154.5, 172.2; negative ion HRESIMS $[M-H]^-$ m/z 293.2121 (calc'd 293.2117 for $C_{18}H_{29}O_3$)

Bibliography

[1]Cannell, R.J.P. in *Methods in Biotechnology: Natural Products Isolation.* Ed. Cannell, R.J.P.. Human Press. Totowa, New Jersey. **1998**. ch. 1. p. 1-2.

[2]Faulkner, D.J. *Antonie van Leeuwenhoek* **2000**, 77, 135-145.

[3]a) Newmann, D.J.; Cragg, G.M.; Snader, K.M. *J. Nat. Prod.* **2003**, 66, 1022-1037.; b) Newman, D.J.; Cragg, G.M.; Snader, K.M. *Natural Products Reports* **2000**, *17*, 215-234.

[4]Tulp, M.; Bohlin, L. *Trends in Pharmacological Sciences* **2002**, *23*, 225-231.

[5]Wani, M.C.; Taylor, H.L.; Wall, M.E.; Coggon, P.; McPhail, A.T. *J. Am. Chem. Soc.* **1971**, 93, 2325-2327.

[6]Mann, J. *Nature Reviews: Cancer* **2002**, 2, 143-148.

[7]a) Andersen, R.J.; Williams, D.E. *Pharmaceuticals from the Sea* in *Issues in Environmental Science and Technology*, Vol. 13. Ed. Harrison, R.M.; Hester, R.E.. The Royal Society of Chemistry. Cambridge. **2000**. p. 55-79.; b) Brusca, R.C.; Brusca, G.J. Invertebrates. Sinauer Associates. Sunderland. MA. **1990**. p. 1-6.

[8]Lindel, T.; Jensen, P.R.; Fenical, W.; Long, B.H.; Casazza, A.M.; Carboni, J.; Fairchild, C.R. *J. Am. Chem. Soc.* **1997**, 119, 8744-8745.

[9] Pettit, G.R.; Herald, C.L.; Clardy, J.; Arnold, E.; Doubek, D.L.; Herald, D.L. *J. Am. Chem. Soc.* **1982**, 104, 6848.

[10]ter Haar, E.; Kowalski, R.J.; Hamel, E.; Lin, C.M.; Longley, R.E.; Gunasekera, S.P.; Rosenkranz, H.S.; Day, B.W. *Biochemistry* **1996**, 35, 243.

[11]a) Gupte, M.; Kulkarni, P.; Ganguli, B.N. *Appl. Microbiol. Biotechnol.* **2002**, 58, 46-57. b) Dasgupta, F. *Antifungal agents – past, present, future prospect.* Ed. Varma, R.S.; Khan, I.K.; Singh, A.P.. National Academy of Chemistry and Biology. Lucknow. **1998**. p. 29-54.

[12]Jiang, B.; Bussey, H.; Roemer, T. *Current Opinion in Microbiology* **2002**, 5, 466-471.

[13]Odds, F.C.; Brown, A.J.P.; Gow, N.A.R. *TRENDS in Microbiology* **2003**, 11, 272-279.

[14]a) Abbanat, D.; Leighton, M.; Maiese, W.; Jones, E.B.G.; Pearce, C.; Greenstein, M. *Journal of Antibiotics* **1998**, 51, 296-302.; b) Schlingmann, G.; Milne, Lisa; Williams, D.R.; Carter, G.T. *Journal of Antibiotics* **1998**, 51, 303-316.; c) Albaugh, D.; Albert, G.; Bradford, P.; Cotter, V.; Froyd, J.; Gaughran, J.; Kirsch, D.R.; Lai, M.; Rehnig, A.; Sieverding, E.; Silverman, S. *Journal of Antibiotics* **1998**, 51, 317-322.

[15]Pettit, G.R.; Cichacz, Z.A.; Herald, C.L.; Boyd, M.R.; Schmidt, J.M.; Hooper, J.N.A. *J.Org. Chem.* **1993**, 58, 1302-1304.

[16]Pettit, R.K.; McAllister, S.C.; Pettit, G.R.; Herald, C.L.; Johnson, J.M.; Cichacz, Z.A. *Int. J. Antimicrobial Agents* **1998**, 9, 147-152.

[17]Ovechkina, Y.Y.; Pettit, R.K.; Cichacz, Z.A.; Pettit, G.R.; Oakley, B.R. *Antimicrobial Agents and Chemotherapy* **1999**, 43, 1993-1999.

[18]Shreiber, S.L. *Bioorg.Med.Chem* **1998**, 6, 1127-1152.

[19]Tan, D.S.; Foley, M.A.; Stockwell, B.R.; Shair, M.D.; Schreiber, S.L. *J.Am.Chem.Soc.* **1999**, 121, 9073-9087.

[20]Stockwell, B.R. *Trends in Biotechnology* **2000**, 18, 449-455.

[21]Mayer, T.U. *Trends in Cell Biology* **2003**, 13, 270-277.

[22]Drews, J. *Nat.Biotech.* **1996**, 14, 1516-1518.;

[23]a)Bassett, D.E. *Nature: Genetics* **1997**, 15, 339-344.; b) Bostein, D.; Chervitz, S.A.; Cherry, J.M. Science 1997, 277, 1259-1260.

[24]Bach, T.J.; Lichtenhaler, H.K. *Z. Naturforsch* **1983**, 38, 212-219.

[25]Hughes, T.R. *Funct. Integr. Genomics* **2002**, 2, 199-211.

[26]a) Hughes, T.; Andrews, B.; Boone, C. *Cell* **2004**, 116, 5-7.; b) Lum, P.Y.; Armour, C.D.; Stepaniants, S.B. et al. *Cell* **2004**, 116, 121-137.; c) Giaever, G.; Flaherty, P.; Kumm, J.; Proctor, M.; Nislow, C.; Jaramillo, D.F.; Chu, A.M.; Jordan, M.I.; Arkin, A.P.; Davis, R.W. *Proc. Nat. Acad. Sci.* **2004**, 101, 793-798.

[27]a)Tong, A.H.Y.; Evangelista, M.; Parsons, A.B.; Xu, H.; Bader, G.D.; Page, N.; Robinson, M.; Raghibizadeh, S.; Hogue, C.W.V.; Bussey, H.; Andrews, B.; Tyers, M.; Boone, C. *Science* **2001**, 294, 2364-2368. b) Marton, M.J.; DeRisi, J.L.; Bennett, H.A.;Iyer, V.R.; Meyer, M.R.; Roberts, C.J.; Stoughton, R.; Burchard, J.; Slade, D.; Dai, H.; Bassett, D.E.; Hartwell, L.H.; Brown, P.O.; Friend, S.H. *Nature Medicine* **1998**, 4, 1293-1301.

[28]Parsons, A.B.; Brost, R.L.; Ding, H.; Li, Z.; Zhang, C.; Sheikh, B.; Brown, G.W.; Kane, P.M.; Hughes, T.R.; Boone, C *Nature Biotechnology* **2004**, 22, 62-69.

[29]a) Lokey, R.S. *Curr.Op.Chem.Bio.* **2003**, 7, 91-96.; b) Salomon, C.E.; Magarvey, N.A.; Sherman, D.H. *Nat. Prod. Rep.* **2004**, 21, 105-121.

[30]Staunton, J.; Weissman, K.*J. Nat. Prod. Rep.* **2001**, 18, 380-416.

[31]McNamara, C.M.; Box, S.; Crawforth, J.M.; Hickman, B.S.; Norwood, T.J.; Rawlings, B.J. *J. Chem. Soc., Perkin Trans.* 1 **1998**, 83-87.

[32]Jimenez, M.S.; Garzon, S.P.; Rodriguez, A.D. *J. Nat. Prod.* **2003**, 66. 655-661.

[33]Takada, N.; Wantabe, M.; Yamada, A.; Suenaga, KI.; Yamada, K.; Ueda, K.; Uemura, D. *J. Nat. Prod.* **2001**, 64. 356-359.

[34]Rudi, A.; Talpir, R.; Kashman, Y.; Benayahu, Y.; Schleyer, M. *J. Nat. Prod.* **1993**, 56, 2178-2182.

[35]Patil, A.D.; Freyer, A.J.; Bean, M.F.; Carte, B.K.; Westley, J.W.; Johnson, R.K.; Lahouratate, P. *Tet.* **1996**, 52, 377-394.

[36]Davidson, B.S. *J. Org. Chem.* **1991**, 56, 6722-6724.

[37]a)Gustafson, K.; Andersen, R.J. *J. Org. Chem.* **1982**, 47, 2167-2169.; b)Graziani, E.I.; Andersen, R.J. *Chem. Comm.* **1996**, 2377-2378.; c)Kubanek, J.; Andersen, R.J. *Tet. Lett.* **1997**, 38, 6327-6330.

[38] Yanai, M.; Ohta, S.; Ohta, E.; Hirata, T.; Ikegami, S. *Bioorg. Med. Chem.* **2003**, 11, 1715-1721.

[39]Ovenden, S.P.B.; Capon, R.J. *J. Nat. Prod.* **1999**, 62, 214-218.

[40]Williams, D.E.; Allen, T.M.; Soest, R.V.; Behrisch, H.W.; Andersen, R.J. *J. Nat. Prod.* **2001**, 64, 281-285.

[41]Stierle, D.B.; Faulkner, D.J. *J. Org. Chem.* **1980**, 45, 3396-3401.

[42]Compagnone, R.S.; Pina, I.C.; Rangel, H.R.; Dagger, F.; Suarez, A.I.; Reddy, M.V.R; Faulkner, D.J. *Tet.* **1998**, 54, 3057-3068.

[43]a)Patil, A.D.; Freyer, A.J.; Bean, M.F.; Carte, B.K.; Westley, J.W.; Johnson, R.K.; Lahouratate, P. *Tet.* **1996**, 52, 377-394.; b) Hayes, P.Y.; Kitching, W. *J. Am. Chem. Soc.* **2002**, 124, 9718-9719.

[44]Ravi, B.N.; Armstrong, R.W.; Faulkner, D.J. *J. Org. Chem.* **1979**, 44, 3109-3113.

[45]Rudi, A.; Afanii, R.; Gravalos, L.G.; Aknin, M.; Gaydou, E.; Vacelet, J.; Kashman, Y *J. Nat. Prod.* **2003**, 66, 682-285.

[46]Campagnuolo, C.; Fattorusso, E.; Taglialatela-Scafati, O.; Ianaro, A.; Pisano, B. *Eur. J. Org. Chem.* **2002**, 1, 61-69.

[47]Qureshi, A.; Stevenson, C.S.; Albert, C.L.; Jacobs, R.S.; Faulkner, D.J. *J. Nat. Prod.* **1999**, 62, 1205-1207.

[48]Huang, X.H.; van Soest, R.; Roberge, M.; Andersen, R.J. *Org. Lett.* **2004**, 6, 75-78.

[49]Gunasekera, S.P.; Gunasekera, MM.; Gunawardana, G.P.; McCarthy, P.; Burres, N. *J. Nat. Prod.* **1990**, 53, 669-674.

[50]Supporting Information for Reference 51 available via the Internet: http://pubs.acs.org/subscribe/journals/orlef7/suppinfo/4/i04/ol016943y/ol016943y_s1.pdf

[51]Yao, G.; Steliou, K. *Org. Lett.* **2002**, 4, 485-488.

[52]Capon, R.J.; Macleod, J.K. *Tetrahedron* **1985**, 41, 3391-3404.

[53]Cafieri, F.; Fattorusso, E.; Taglialatela-Scafati, O.; Ianaro, A. *Tet.* **1999**, 7045-7056.